ISSN 0735-1348

Ancient TL

A periodical devoted to Luminescence and ESR dating

Department of Physics, East Carolina University, 1000 East 5th Street, Greenville, NC 27858, USA
http://www.ecu.edu/cs-cas/physics/ancient-timeline/

June 2017, Volume 35 No.1

An improved multiple-aliquot regenerative-dose (MAR) procedure for post-IR IRSL dating of K-feldspar 1
Bo Li, Zenobia Jacobs and Richard G. Roberts

Defining minimum reporting requirements for ESR dating of optically bleached quartz grains 11
Mathieu Duval, Jean-Jacques Bahain, Melanie Bartz, Christophe Falguères Verónica Guilarte, Davinia Moreno, Hélène Tissoux, Miren del Val, Pierre Voinchet and Lee J. Arnold

Always remain suspicious: a case study on tracking down a technical artefact while measuring IR-RF 20
Sebastian Kreutzer, Madhav Krishna Murari, Marine Frouin, Markus Fuchs and Norbert Mercier

Thesis abstracts 31
Bibliography 35
Announcements 52

Ancient TL

Started by the late David Zimmerman in 1977

EDITOR

Regina DeWitt, Department of Physics, East Carolina University, Howell Science Complex, 1000 E. 5th Street Greenville, NC 27858, USA; Tel: +252-328-4980; Fax: +252-328-0753 (dewittr@ecu.edu)

EDITORIAL BOARD

Ian K. Bailiff, Luminescence Dating Laboratory, Univ. of Durham, Durham, UK (ian.bailiff@durham.ac.uk)
Geoff A.T. Duller, Institute of Geography and Earth Sciences, Aberystwyth University, Ceredigion, Wales, UK (ggd@aber.ac.uk)
Sheng-Hua Li, Department of Earth Sciences, The University of Hong Kong, Hong Kong, China (shli@hku.hk)
Shannon Mahan, U.S. Geological Survey, Denver Federal Center, Denver, CO, USA (smahan@usgs.gov)
Richard G. Roberts, School of Earth and Environmental Sciences, University of Wollongong, Australia (rgrob@uow.edu.au)

REVIEWERS PANEL

Richard M. Bailey
Oxford, UK
richard.bailey@ouce.ox.ac.uk

James Feathers
Seattle, WA, USA
jimf@uw.edu

Rainer Grün
Canberra, Australia
rainer.grun@anu.edu.au

David J. Huntley
Burnaby B.C., Canada
huntley@sfu.ca

Sebastian Kreutzer
Bordeaux, France
sebastian.kreutzer@u-bordeaux-montaigne.fr

Michel Lamothe
Montréal, Québec, Canada
lamothe.michel@uqam.ca

Norbert Mercier
Bordeaux, France
norbert.mercier@u-bordeaux-montaigne.fr

Didier Miallier
Aubière, France
miallier@clermont.in2p3.fr

Andrew S. Murray
Roskilde, Denmark
anmu@dtu.dk

Vasilis Pagonis
Westminster, MD, USA
vpagonis@mcdaniel.edu

Naomi Porat
Jerusalem, Israel
naomi.porat@gsi.gov.il

Daniel Richter
Leipzig, Germany
drichter@eva.mpg.de

David C.W. Sanderson
East Kilbride, UK
David.Sanderson@glasgow.ac.uk

Andre Sawakuchi
São Paulo, SP, Brazil
andreos@usp.br

Ashok K. Singhvi
Ahmedabad, India
singhvi@prl.res.in

Kristina J. Thomsen
Roskilde, Denmark
krth@dtu.dk

Web coordinators: Joel DeWitt, Regina DeWitt
Article layout and typesetting: Sebastian Kreutzer, Nathan Brown, Regina DeWitt
Bibliography: Sebastien Huot

Ancient TL

An improved multiple-aliquot regenerative-dose (MAR) procedure for post-IR IRSL dating of K-feldspar

Bo Li[1*], Zenobia Jacobs[1,2], Richard G. Roberts[1,2]

[1] Centre for Archaeological Science, School of Earth and Environmental Sciences
University of Wollongong, New South Wales, Australia
[2]ARC Centre of Excellence for Australian Biodiversity and Heritage, University of Wollongong,
Wollongong, NSW 2522, Australia

*Corresponding Author: bli@uow.edu.au
Received: March 19, 2017; in final form: May 7, 2017

Abstract

In optical dating, multiple-aliquot dating methods have been considered inferior to single-aliquot methods, due to difficulties inherent to in between-aliquot normalisation. In this study, we propose an improved multiple-aliquot regenerative-dose (MAR) procedure for the multiple-elevated-temperature post-IR IRSL (MET-pIRIR) signals from K-feldspar grains. This method is based on observations that a common, or standardised, growth curve (SGC) exists between different aliquots from the same and different samples, and that between-aliquot variation can be largely eliminated by application of regenerative-dose ('re-normalisation') or least squares (LS) normalisation procedures. We find that this improved MAR procedure significantly increases the accuracy and precision of D_e determinations. We tested this method using several sediment samples from Marathousa, a Middle Pleistocene archaeological site in Greece, and demonstrate that, for the K-feldspar grains from these samples, the proposed MAR method overcomes problems associated with inappropriate sensitivity correction of the natural (L_n) and test dose (T_n) signals at low stimulation temperatures (50 – 150 °C) more effectively than the SAR method. The MAR method can also reduce instrument time for measurement of older samples.

Keywords: K-feldspar, IRSL, post-IR IRSL, multiple aliquot, single aliquot

1. Introduction

In optical dating, both the optically stimulated luminescence (OSL) signal from quartz and infrared stimulated luminescence (IRSL) signal from potassium-rich (K) feldspar grains can be measured to determine the radiation ('burial') dose received by mineral grains after their last exposure to sunlight (Aitken, 1998). To obtain useful information regarding the burial time of quartz and K-feldspar grains, the OSL or IRSL signals must be converted into a reliable estimate of equivalent dose (D_e). The D_e is estimated by comparing the natural OSL or IRSL signals against a series of known-dose laboratory signals that form a dose response curve (DRC); regenerative-dose methods are preferred over additive-dose methods, because the D_e is obtained by interpolation, rather than by extrapolation, of the DRC (e.g., Lian & Roberts, 2006). Two kinds of regenerative-dose methods have been developed for D_e determination—multiple-aliquot regenerative-dose (MAR) procedures (Wintle, 1993; Aitken, 1998) and single-aliquot regenerative-dose (SAR) procedures (Murray & Roberts, 1998; Galbraith et al., 1999; Murray & Wintle, 2000). Emphasis has shifted from the development and use of MAR procedures to SAR procedures to exploit the many inherent advantages of the latter (e.g., Duller, 2008; Wintle, 2014).

Some studies, however, have demonstrated that the SAR method is not always suitable, and that there may be merit in revisiting the MAR procedure in specific cases. For example, for quartz samples from the Chinese Loess Plateau, Lu et al. (2007) showed that the build-up of OSL signal during repeated SAR measurement cycles resulted in underestimation of the D_e. They proposed a sensitivity-corrected MAR method, in which the test dose signal (T_x) is used to normalise between aliquots, following the suggestion by

Roberts & Duller (2004) that T_x not only corrects for sensitivity change but can also be used for between-aliquot normalisation. In the MAR procedure of Lu et al. (2007), the sensitivity-corrected natural signal (L_n/T_n) was projected on to the dose response curve established using the sensitivity-corrected regenerative-dose signal (L_x/T_x) from multiple aliquots.

For feldspar IRSL signals, it has been suggested that a large sensitivity change may occur during measurement of L_n, resulting in a significant difference between the luminescence efficiency of the natural dose and subsequent test dose (T_n), and between L_n/T_n and L_x/T_x, when using SAR (e.g., Chen et al., 2013; Li et al., 2013a; Chen et al., 2015; Guo et al., 2015; Van den Bergh et al., 2016). This would cause the sensitivity correction of L_n to be inappropriate, giving rise to erroneous D_e estimates. Li et al. (2013a) were the first to apply a MAR procedure based on sensitivity-corrected signals (L_n/T_n and L_x/T_x) to pIRIR dating of K-feldspar grains. In their study, the sample was divided into different groups of aliquots: one group was used to measure the natural signals, and the other groups were bleached using a solar simulator for several hours before being given different regenerative doses. The IRSL and MET-pIRIR L_x and T_x signals were then measured to establish a dose response curve, and the D_e estimated from the L_n/T_n signals. A similar approach was adopted by Chen et al. (2015) and Guo et al. (2015). This method, however, is only suitable for samples that exhibit homogeneous behaviours among different aliquots, and is not applicable to samples with L_x/T_x signals that are highly variable among different grains or aliquots (e.g., Li et al., 2014b, 2015b).

A key objective of any MAR procedure, therefore, should be to reduce any between-aliquot variability. This can be achieved through the application of an appropriate normalisation procedure. Li et al. (2015a, 2016) proposed the regenerative-dose normalisation ('re-normalisation') and least squares (LS) normalisation methods to reduce the between-aliquot differences in DRC shapes for single aliquots of quartz and K-feldspar. When these methods were applied to samples from a variety of geological provenances, environmental settings and depositional ages, the OSL and MET-pIRIR signals had significantly reduced between-aliquot scatter and similar DRCs. As a result, a 'global standardised growth curve' (gSGC) could be established for quartz (Li et al., 2015a, 2016) and K-feldspar (Li et al., 2015b).

In this study, we aim to investigate the feasibility of incorporating the re-normalisation method into a MAR procedure, and examine the advantages and disadvantages of the new MAR procedure compared to conventional MAR and SAR procedures. We demonstrate that the new MAR method overcomes the difficulty in normalising for between-aliquot scatter in samples from a site in Greece, and allows for the construction of a standardised growth curve for these samples. This method has the potential to be used for D_e determination of K-feldspars from other sites and geographical locations.

2. Sample descriptions

Samples were collected from Marathousa I, a newly discovered Lower Palaeolithic archaeological site located in the Megalopolis basin in southern Greece (Panagopoulou et al., 2015). The sedimentary deposits are of Middle Pleistocene age and are composed of lacustrine clay, silt and sand beds, alternating with lignite seams, representing a former lake environment (Vinken, 1965; Van Vugt et al., 2000). Here, we present results for four samples: MAR-01, MAR-R1, MAR-R2 and MAR-R5. MAR-01, MAR-R2 and MAR-R5 were collected from sandier units underlying the archaeological level, while MAR-R1 was collected from a lignite seam overlying the archaeological level.

3. Experimental procedures

All samples were prepared for IRSL analysis using routine procedures (Aitken, 1998). Samples were treated with solutions of HCl acid and H_2O_2 to remove carbonates and organic matter, respectively, and then dried and sieved to obtain grains of 180 – 212 μm in diameter. The K-feldspar grains were separated from quartz and heavy minerals using a solution of sodium polytungstate with a density of 2.58 g/cm^3. The separated K-feldspar grains were immersed in 10 % HF acid for 40 min to etch the surfaces of the grains and remove the outer, alpha-irradiated portions; they were then rinsed in HCl acid to remove any precipitated fluorides. The dried and etched K-feldspar grains were mounted as a monolayer on stainless-steel discs of 9.8 mm diameter using "Silkospray" silicone oil as an adhesive. Grains covered the central ∼ 5 mm diameter portion of each disc, corresponding to several hundred grains per aliquot.

IRSL measurements were made on an automated Risø TL-DA-20 reader equipped with IR diodes for stimulation (870 △ 40 nm). The total IR power delivered to the sample position was ∼ 135 mW/cm^2 (Bøtter-Jensen et al.,

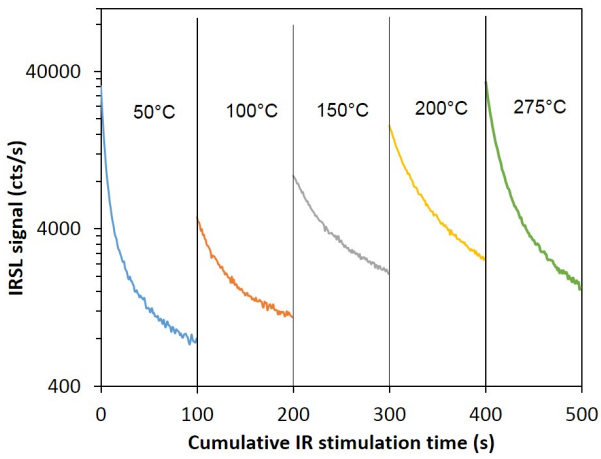

Figure 1. Representative IRSL (50 °C) and MET-pIRIR (100 – 275 °C) decay curves for a single aliquot of sample MAR-01, stimulated at different temperatures (shown above each curve).

Table 1. Single-aliquot (a) and multiple-aliquot (b) procedures for pMET-pIRIRmeasurements.

Step	Treatment		Observed
	(a) Single-aliquot	(b) Multiple-aliquot	
1	Give regenerative dose, D_i [a]	Give regenerative dose, D_i [a]	
2	Preheat at 320 °C for 60 s	Preheat at 320 °C for 60 s	
3	[b] IRSL measurement at 50 °C for 100 s	[b] IRSL measurement at 50 °C for 100 s	L_x (50 °C)
4	[b] IRSL measurement at 100 °C for 100 s	[b] IRSL measurement at 100 °C for 100 s	L_x (100 °C)
5	[b] IRSL measurement at 150 °C for 100 s	[b] IRSL measurement at 150 °C for 100 s	L_x (150 °C)
6	[b] IRSL measurement at 200 °C for 100 s	[b] IRSL measurement at 200 °C for 100 s	L_x (200 °C)
7	[b] IRSL measurement at 275 °C for 100 s	[b] IRSL measurement at 275 °C for 100 s	L_x (275 °C)
8	Give test dose, 60 Gy	Give test dose, 60 Gy	
9	Preheat at 320 °C for 60 s	Preheat at 320 °C for 60 s	
10	[b] IRSL measurement at 50 °C for 100 s	[b] IRSL measurement at 50 °C for 100 s	T_x (50 °C)
11	[b] IRSL measurement at 100 °C for 100 s	[b] IRSL measurement at 100 °C for 100 s	T_x (100 °C)
12	[b] IRSL measurement at 150 °C for 100 s	[b] IRSL measurement at 150 °C for 100 s	T_x (150 °C)
13	[b] IRSL measurement at 200 °C for 100 s	[b] IRSL measurement at 200 °C for 100 s	T_x (200 °C)
14	[b] IRSL measurement at 275 °C for 100 s	[b] IRSL measurement at 275 °C for 100 s	T_x (275 °C)
15	**Solar simulator bleach for 4 hrs**	**Solar simulator bleach for 4 hrs**	
16	Repeat step 1–15 for different D_i	Give normalisation dose, D_r [b]	
17		Preheat at 320 °C for 60 s	
18		[b] IRSL measurement at 50 °C for 100 s	L_r (50 °C)
19		[b] IRSL measurement at 100 °C for 100 s	L_r (100 °C)
20		[b] IRSL measurement at 150 °C for 100 s	L_r (150 °C)
21		[b] IRSL measurement at 200 °C for 100 s	L_r (200 °C)
22		[b] IRSL measurement at 275 °C for 100 s	L_r (275 °C)
23		Give test dose, 60 Gy	
24		Preheat at 320 °C for 60 s	
25		[b] IRSL measurement at 50 °C for 100 s	T_r (50 °C)
26		[b] IRSL measurement at 100 °C for 100 s	T_r (100 °C)
27		[b] IRSL measurement at 150 °C for 100 s	T_r (150 °C)
28		[b] IRSL measurement at 200 °C for 100 s	T_r (200 °C)
29		[b] IRSL measurement at 275 °C for 100 s	T_r (275 °C)

[(a)] For the natural sample, the given dose $D_i = 0$ Gy

[(b)] The same D_r ($\sim$ 400 Gy) is applied to all aliquots from the different groups.

2000). Laboratory irradiations were carried out on the reader using a calibrated $^{90}Sr/^{90}Y$ beta source. IRSL signals were detected by an Electron Tubes Ltd. 9235B photomultiplier tube fitted with Schott BG-39 and Corning 7-59 filters to restrict transmission to 320 – 480 nm. Each IRSL measurement was made for 100 s, and the resulting signal was calculated as the sum of counts over the initial 10 s of optical stimulation, with 'late light' subtraction (Aitken, 1998) of the background count rate over the final 10 s of optical stimulation. For each IRSL measurement, an 'IR-off' period of up to 50 s prior to stimulation was applied to monitor and minimise the isothermal decay signal (Fu et al., 2012).

4. Results

4.1. A single-aliquot LS-normalisation procedure and standardised growth curve

We tested whether the LS-normalisation method is applicable to the samples from Greece, using a total of 18 single aliquots of K-feldspar from sample MAR-01. Each aliquot was measured using the SAR pMET-pIRIR procedure (Table 1a), in which the aliquots were bleached for $\sim$ 4 hrs in a solar simulator at the end of each SAR cycle (Li et al., 2014b). Two to four regenerative doses, ranging from 0 to $\sim$ 1900 Gy, were given to each aliquot and the signals measured, together with the signals arising from the test dose of $\sim$ 60 Gy applied to each aliquot. Fig. 1 shows representative natural IRSL (50 °C) and MET-pIRIR (100 – 275 °C) decay curves for an aliquot of sample MAR-01. The intensities of the MET-pIRIR signals are on the order of a few hundred to several tens of thousands of counts per second. The L_n/T_n and L_x/T_x signals observed for different aliquots of this sample, measured at different stimulation temperatures, are compared in Fig. 2a – e. Large between-aliquot scatter can be observed: for example, the relative standard deviation (RSD) of the L_x/T_x ratios at a fixed dose are about 5 – 10 %. This finding is similar to that made by Li et al. (2015b), who suggested that T_x cannot fully correct for the differences between aliquots.

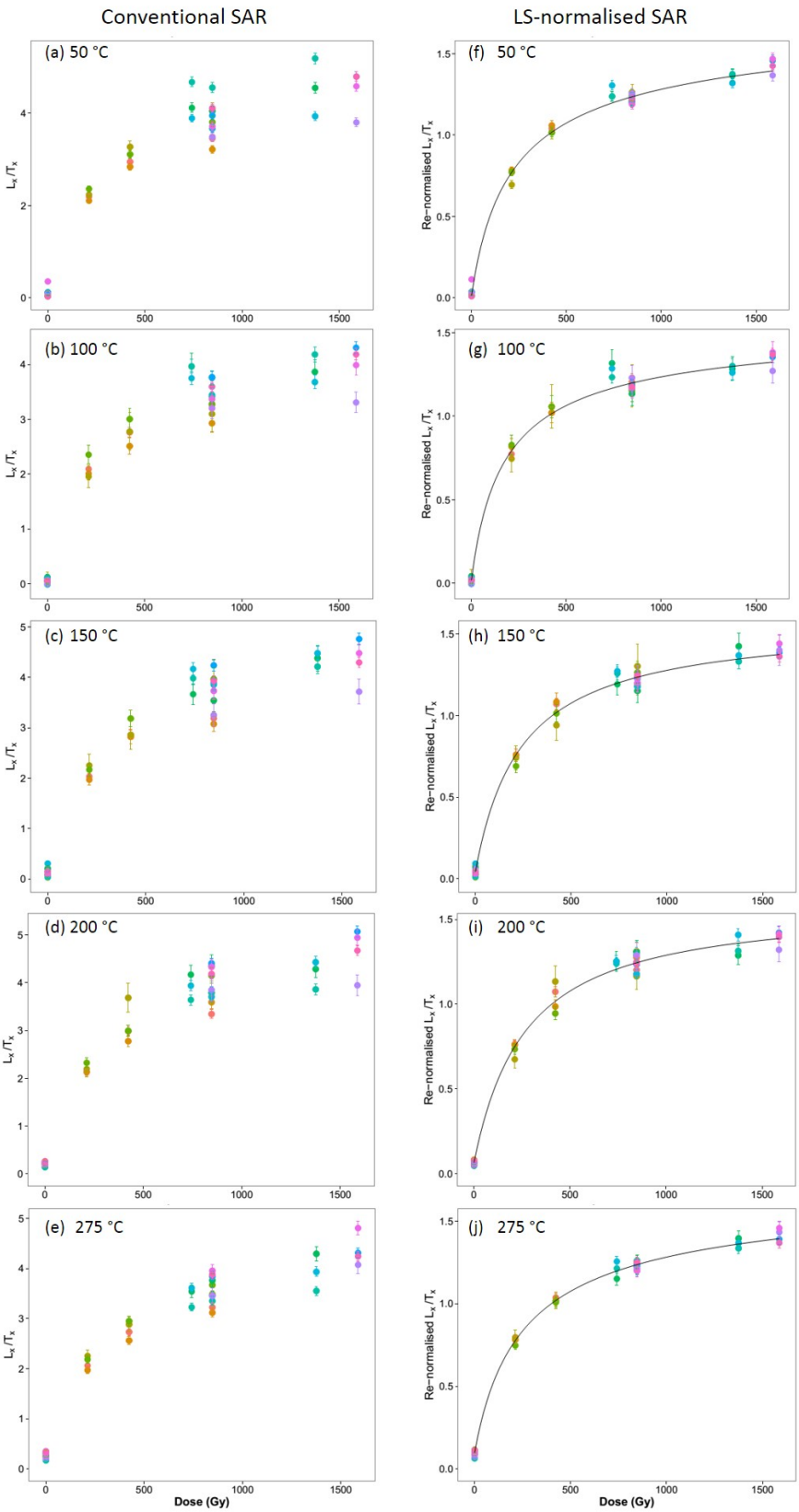

Figure 2. SAR L_x/T_x ratios (a – e) and re-normalised L_x/T_x ratios (f – j) for sample MAR-01, plotted as a function of laboratory dose. Different aliquots are represented by different colours. Aliquots were measured using the SAR pMET-pIRIR listed in Table 1a. The data shown in panels (f) – (j) for the different aliquots were fitted using a general-order kinetic function (full lines). The DRCs have been normalised to unity at a dose of 400 Gy, to facilitate direct comparison with the multiple-aliquot DRCs (section 4.3).

To test whether different aliquots of the same sample have similar growth curve shapes, we applied the LS-normalisation procedure of Li et al. (2016). This procedure comprises the following steps: (1) L_x/T_x signals from all aliquots are fitted using a best-fit model; (2) L_x/T_x values from each aliquot are re-scaled using scaling factors determined through an optimisation procedure that minimises the sum of squared residuals between the re-scaled signals and the curve of best fit; and (3) the fitting (step 1) and re-scaling (step 2) procedures are repeated iteratively until there is negligible change in the LS-normalised regenerative-dose signals. The LS-normalisation procedure was achieved using the built-in function 'lsNORM()' provided in the **R**-package 'numOSL' (Peng et al., 2013; R Core Team, 2016). A general-order kinetic (GOK) function (Guralnik et al., 2015) of the form $f(x) = a[1-(1+bcx)^{(-1/c)}]+d$, where x is the dose and the parameters a, b, c and d are constants, was used to fit the DRCs; a denotes the maximum signal level, b is the reciprocal of the saturation dose D_0, c is a kinetic order modifier, and d is an offset accounting for potential recuperation effects. For $c \to 0$, the GOK function reduces to a single saturating exponential. As c increases, the GOK function progressively deviates from first-order behaviour and approximates a double saturating exponential or a saturating exponential plus linear function; see Guralnik et al. (2015) for details.

The LS-normalised DRCs are shown in Fig. 2f – j, where it can be seen that the between-aliquot scatter for the L_x/T_x ratios is greatly reduced (e.g., the RSD for the L_x/T_x signals at a fixed dose is reduced to about 1 – 4 %). These results suggest that different aliquots measured using the SAR pMET-pIRIR procedure share similar DRCs, provided the L_x/T_x signals are normalised appropriately.

4.2. A multiple-aliquot LS-normalisation procedure and standardised growth curve

We propose that the MAR procedure can also be improved and optimised using this LS-normalisation method. The two most critical prerequisites of a multiple-aliquot procedure are that: 1) different aliquots share the same DRCs; and 2) between-aliquot differences in luminescence signals are normalised appropriately. For the former, we have demonstrated that the pMET-pIRIR signals from feldspars may share similar DRCs (Li et al., 2015b), and this is confirmed for our samples (section 4.1). For between-aliquot normalisation, we applied the pMET-pIRIR procedure of Li et al. (2013a, 2014b) to all four Greek samples. A total of 55 aliquots (4 from MAR-01, 15 from MAR-R1, 22 from MAR-R2 and 14 from MAR-R5) were bleached in the solar simulator for $\sim$ 8 hrs. These aliquots were then given different regenerative doses, ranging from 0 to $\sim$ 2000 Gy, and were measured using the procedure listed in Table 1b. The IRSL signals for the regenerative and test doses were measured successively at 50, 100, 150, 200 and 275 °C, following a preheat at 320 °C for 60 s. At the end of each test dose IRSL measurement, the aliquots were bleached for $\sim$ 4 hrs in a solar simulator. An identical regenerative dose (D_r) was then given to the bleached aliquots, followed by measurement of the regenerative and corresponding test dose signals (L_r and T_r, respectively), as before.

The L_x/T_x ratios measured at different stimulation temperatures are shown in Fig.3a – e for different aliquots, plotted against their corresponding regenerative doses. Two features of these data are noteworthy. First, there are large between-sample variations in the L_x/T_x ratios at a dose. Second, there is also substantial between-aliquot scatter for some of these samples. As a result, a reliable DRC cannot be constructed from the multiple-aliquot L_x/T_x ratios. Fig.3f – j shows the re-normalised ratios ($\frac{L_x/T_x}{L_r/T_r}$), plotted as a function of regenerative dose at the different stimulation temperatures. The L_x/T_x ratios were normalised by dividing the corresponding L_r/T_r ratios obtained by giving each aliquot an additional regenerative dose, D_r (Table 1b). Peng et al. (2016) conducted numerical simulations comparing the SGCs obtained using different re-normalisation doses and found little difference in accuracy or precision for a range of re-normalisation doses; we used a re-normalisation dose of 400 Gy for our samples. It can be seen that the between-aliquot scatter is reduced and, more importantly, the normalisation procedure appears to bring the DRCs of the different samples into much closer alignment. This result supports our proposition that the re-normalisation procedure can help improve the MAR results, to the extent that there is potential to construct reliable SGCs for multiple-aliquot MET-pIRIR signals.

4.3. Comparing LS-normalised SAR and MAR SGCs

The fitted SAR SGCs shown in Fig. 2f – j are shown as red dashed lines in Fig. 3f – j, to facilitate comparison with the MAR SGCs, shown as solid lines. Both the SAR and MAR SGCs were normalised using the signal induced by a regenerative dose of 400 Gy, so their shapes are directly comparable. The SAR SGCs differ from the MAR SGCs at low stimulation temperatures (i.e., 50, 100 and 150 °C); they exhibit a much steeper growth at low doses and reach a slightly higher saturation level (Fig. 3f – h). The difference is most significant for the 50 °C IRSL signal (Fig. 3f) and decreases as the stimulation temperature is increased. Only a slight difference in DRC shape and saturation intensity is observed at a stimulation temperature of 275°C (Fig. 3j). We propose that the difference between the SAR and MAR SGCs at the lower temperatures is a result of progressive sensitivity change (luminescence efficiency) between the measurement of L_x and T_x, possibly extending over several measurement cycles for different IR stimulation temperatures. A prediction of this outcome is that the D_e values determined using the SAR and MAR SGCs are likely also to be different, especially for the signals measured using low-temperature stimulations.

4.4. D_e estimation based on SAR and MAR SGCs

We calculated D_e values based on the SAR SGCs for each stimulation temperature (Fig. 2f – j), following the method

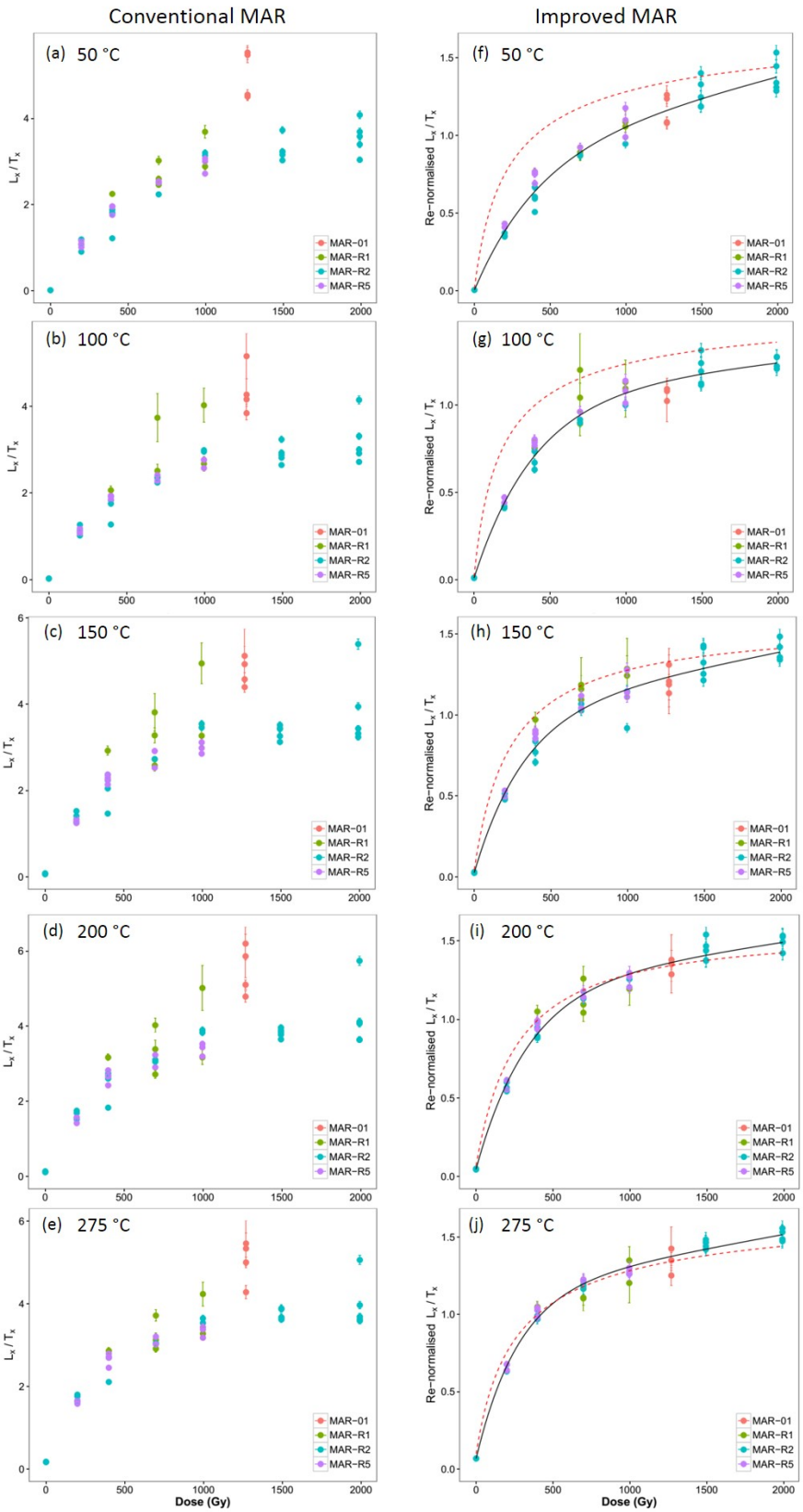

Figure 3. MAR L_x/T_x ratios (a – e) and re-normalised MAR L_x/T_x ratios (f – j) for the four Greek samples, plotted as a function of laboratory dose. Each data point corresponds to one aliquot, with different colours representing the different samples. The data shown in panels (f) – (j) were fitted using a general-order kinetic function, shown by black lines; the dashed lines are the best-fit SGCs obtained from the SAR data for sample MAR-01 (Fig.2f – j).

and equation presented in Li et al. (2015a):

$$f(D_e) = \frac{L_n}{T_n} \times \frac{f(D_r)}{\frac{L_r}{T_r}}$$

where $f(D_e)$ denotes the SAR SGCs established by LS-normalisation, and D_r and L_r/T_r denote the additional regenerative dose and the ratio for the corresponding sensitivity-corrected signal, respectively. Li et al. (2015a) provide a worked example of how to calculate SGC D_e values using this function.

We also calculated D_e values based on the MAR SCGs at each stimulation temperature (Fig. 3f – j) for three of the samples — MAR-01 (6 aliquots), MAR-R2 (9 aliquots) and MAR-R5 (10 aliquots) — using the pMET-pIRIR procedure listed in Table 1b. After measuring the L_n and T_n signals, each aliquot was bleached for $\sim$ 4 hrs in the solar simulator and then given a regenerative dose of 400 Gy and a subsequent test dose of 60 Gy, the same as used to establish the MAR SGCs. The L_n/T_n ratios were then re-normalised using the corresonding (L_r/T_r) ratios, and the re-normalised ratios ($\frac{L_n/T_n}{L_r/T_r}$) were projected on to the MAR SGCs (solid lines in Figs. 3f – j) to estimate the D_e values.

The D_e values determined at each stimulation temperature were combined using the central age model (Galbraith et al., 1999; Galbraith & Roberts, 2012) (to obtain weighted-mean D_e values for the single- and multiple-aliquot data sets, for comparison. The weighted-mean D_e values are plotted as a function of stimulation temperature in Fig. 4a – c (D_e-T plots) for samplesMAR-01, MAR-R2 and MAR-R5. The MAR D_e values (circles) differ negligibly with stimulation temperature, whereas the SAR D_e values (triangles) increase systematically with stimulation temperature, resulting in statistically significant differences between the SAR and MAR weighted-mean D_e values for all three samples at stimulation temperatures of 50, 100 and 150 °C. The SAR and MAR weighted-mean D_e values are statistically indistinguishable at stimulation temperatures of 200 and 275 °C.

Low-temperature (<200 °C) IRSL signals are commonly thought to suffer from anomalous fading, giving rise to underestimation of the measured D_e values (Li et al., 2014a). The D_e-T plot is often used in support of this influence (Li & Li, 2011), based on observations of an increase D_e with an increase in stimulation temperature until a D_e 'plateau' is reached at higher temperatures; the latter is interpreted as indicating negligible fading of the IRSL signal at stimulation temperatures above 200 °C (Li & Li, 2011) or above 250 °C for older samples (Li & Li, 2012). The SAR D_e-T plots exhibit patterns for the Greek samples consistent with those reported previously for other samples (i.e., an increase in D_e with stimulation temperature), which might be attributed to anomalous fading causing underestimation of the measured D_e values at low stimulation temperatures. However, the MAR D_e-T plots show negligible change in D_e with an increase in stimulation temperature, which implies no difference in fading rate of the signals measured at the various stimulation temperatures.

To explicitly test for the effect of fading on D_e values,

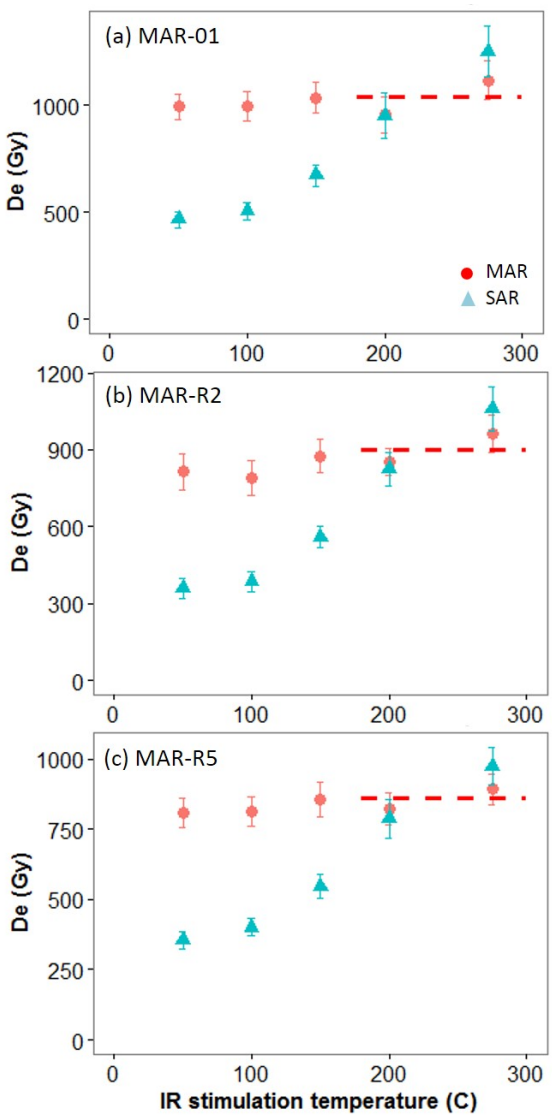

Figure 4. D_e values obtained based on SAR SGCs (blue triangles) and MAR SGCs (red circles), plotted as a function of IR stimulation temperature for samples MAR-01 (a), MAR-R2 (b) and MAR-R5 (c). The horizontal dashed lines represent the weighted-mean SAR and MAR D_e values obtained at IR stimulation temperatures of 200 and 275 °C.

we conducted anomalous fading tests on samples MAR-R2 and MAR-R5, using a single-aliquot measurement procedure similar to that described in Auclair et al. (2003), but based on the MET-pIRIR procedure. The corresponding anomalous fading rates (g-values) are displayed in Fig. 5a for the IRSL and MET-pIRIR signals measured at the different stimulation temperatures. There is little difference between the fading rates for the various signals, and all g-values are statistically consistent with zero at 2σ. This pattern differs from those reported for samples from other regions, as presented in previous studies, which typically exhibit the highest anomalous fading rate for the 50 °C IRSL signal and lower rates for the signals measured at higher stimulation temperatures (e.g., Li

& Li, 2011, 2012). Given the absence of significant fading in samples MAR-R2 and MAR-R5, therefore, the D_e values should be consistent regardless of stimulation temperature, and this is confirmed by the MAR D_e results.

Furthermore, the fading test results indicate that the pattern seen in the SAR D_e results is not a result of varying degrees of anomalous fading at the different stimulation temperatures. Instead, we suggest that this pattern indicates that the extents of sensitivity changes occurring during measurement of L_n, prior to measurement of T_n, are different from those occurring between L_x and T_x, so that the sensitivity-correction method in SAR does not adequately compensate for these changes. This proposition is supported by the SAR dose recovery data for sample MAR-01 (Fig. 5b), which display the same pattern of increasing D_e with increasing stimulation temperature as seen with the natural samples (Fig. 4a – c), i.e., there are significant underestimation in the recovered ratio for the low-temperature (50 – 100 °C) signals. Given anomalous fading is not a factor in dose recovery experiments, the underestimation in the low-temperature (50 – 100 °C) signals confirms that the pattern seen in the SAR D_e results is a result of different extents of sensitivity changes occurred during measurement of L_n, T_n, L_x and T_x.

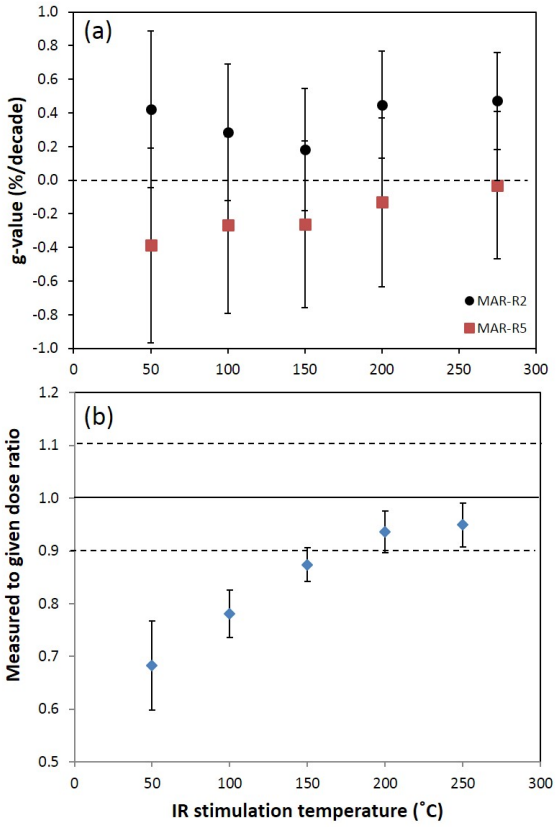

Figure 5. (a) Anomalous fading rates (expressed as the g-value) for samples MAR-R2 (black cirles) and MAR-R5 (red squares), plotted against IR stimulation temperature. (b) SAR dose recovery test results for sample MAR-01, obtained using the pMET-pIRIR procedure listed in Table 1a.

5. Discussion

The new LS-normalised pMET-pIRIR MAR method applied to K-feldspar offers several advantages over standard SAR procedures. Most importantly, it does not suffer from problems associated with inappropriate sensitivity correction between measurement of the L_n, T_n and L_x and T_x signals. Similar to previous studies (e.g., Chen et al., 2013; Li et al., 2013b; Chen et al., 2015; Guo et al., 2015; **?**), we find that erroneous results can be obtained using a SAR procedure if the relative change in sensitivity between L_n and T_n is significantly different from the changes between L_x and T_x. Our SGC (Fig. 3f – j), fading (Fig. 5a), dose recovery test (Fig. 5b) and D_e (Fig. 4) results demonstrate that the MAR method proposed here can circumvent this problem effectively. Additionally, the MAR method potentially requires less instrument time than the SAR method, especially for older samples that need more and larger regenerative doses to construct a robust DRC. A MAR SGC can be established using different samples from the same site (Fig. 3), so there is no need to measure the same regenerative doses for each sample, and a single MAR SGC can be used to estimate D_e values for samples spanning a range of ages from the same site. Furthermore, the results produced by this method should be more reliable, because a DRC established using more regenerative doses (or data points) will be more precise than a conventional SAR dose response curve and also more resistant to random errors caused by measurement uncertainties, which may result in significant changes to the shape of observed DRCs (Li et al., 2017). As with all DRCs, it is important to minimise any sources of possible systematic bias in the construction of SGCs.

6. Conclusions

We have proposed a LS-normalised MAR procedure to determine D_e values for K-feldspars using the pMET-pIRIR signal. Our method is built on the demonstration that a common growth curve, or SGC, exists for different pIRIR signals (Li et al., 2015b) and that between-aliquot variation can be largely eliminated by normalising the L_n/T_n and L_x/T_x ratios using the corresponding L_r/T_r ratios from an additional regenerative dose (Li et al., 2015b,b, 2016). By applying a re-normalisation procedure, the new MAR method can overcome the main drawback of conventional multiple-aliquot methods — the difficulty of normalising different aliquots — resulting in a significant improvement in the accuracy and precision of the DRC construction and D_e estimation. Problems associated with inappropriate sensitivity correction of the L_n signal using the T_n signal in the standard SAR procedure can also be avoided and, especially for older samples, instrument time can be saved.

Acknowledgments

This research was funded by the Australian Research Council through Future Fellowships to Li (FT140100384) and Jacobs (FT150100138), and an Australian Laureate Fellowship to Roberts (FL130100116). We thank Yasaman Jafari and Terry Lachlan for valuable support in the OSL dating laboratory, and Panagiotis Karkanas for advice and assistance in the field.

References

Aitken, M.J. *An Introduction to Optical Dating*. Oxford University Press, 1998.

Auclair, M., Lamothe, M., and Huot, S. *Measurement of anomalous fading for feldpsar IRSL using SAR*. Radiation Measurements, 37 (4-5): 487–492, 2003.

Bøtter-Jensen, L., Bulur, E., Duller, G.A.T., and Murray, A.S. *Advances in luminescence instrument systems*. Radiation Measurements, 32(56): 523–528, 2000.

Chen, Y.W., Li, S.H., and Li, B. *Residual doses and sensitivity change of post IR IRSL signals from potassium feldspar under different bleaching conditions*. Geochronometria, 40: 229–238, 2013.

Chen, Y.W., Li, S.H., Li, B., Hao, Q.Z., and Sun, J.M. *Maximum age limitation in luminescence dating of Chinese loess using the multiple-aliquot MET-pIRIR signals from K-feldspar*. Quaternary Geochronology, 30: 207–212, 2015.

Duller, G.A.T. *Single-grain optical dating of Quaternary sediments: why aliquot size matters in luminescence dating*. Boreas, 37: 589–612, 2008.

Fu, X., Li, B., and Li, S H. *Testing a multi-step post-IR IRSL dating method using polymineral fine grains from Chinese loess*. Quaternary Geochronology, 10: 8–15, 2012.

Galbraith, R.F. and Roberts, R.G. *Statistical aspects of equivalent dose and error calculation and display in OSL dating: An overview and some recommendations*. Quaternary Geochronology, 11: 1–27, 2012.

Galbraith, R.F., Roberts, R.G., Laslett, G.M., Yoshida, H., and Olley, J.M. *Optical dating of single and multiple grains of Quartz from Jinmium Rock Shelter, Northern Australia: Part I, Experimental design and statistical models*. Archaeometry, 41(2): 339–364, 1999.

Guo, Y.J., Li, B., Zhang, J.F., and Roberts, R.G. *Luminescence-based chronologies for Palaeolithic sites in the Nihewan Basin, northern China: First tests using newly developed optical dating procedures for potassium feldspar grains*. Journal of Archaeological Science: Reports, 3: 31–40, 2015.

Guralnik, B., Li, B., Jain, M., Chen, R., Paris, R.B., Murray, A.S., Li, S.H., Pagonis, V., Valla, P.G., and Herman, F. *Radiation-induced growth and isothermal decay of infrared-stimulated luminescence from feldspar*. Radiation Measurements, 81: 224–231, 2015.

Li, B. and Li, S.H. *Luminescence dating of K-feldspar from sediments: A protocol without anomalous fading correction*. Quaternary Geochronology, 6(5): 468–479, 2011.

Li, B. and Li, S.H. *Luminescence dating of Chinese loess beyond 130 ka using the non-fading signal from K-feldspar*. Quaternary Geochronology, 10: 24–31, 2012.

Li, B., Jacobs, Z., Roberts, R.G., and Li, S.H. *Extending the age limit of luminescence dating using the dose-dependent sensitivity of MET-pIRIR signals from K-feldspar*. Quaternary Geochronology, 17: 55–67, 2013a.

Li, B., Roberts, R.G., and Jacobs, Z. *On the dose dependency of the bleachable and non-bleachable components of IRSL from K-feldspar: Improved procedures for luminescence dating of Quaternary sediments*. Quaternary Geochronology, 17: 1–13, 2013b.

Li, B., Jacobs, Z., Roberts, R., and Li, S.H. *Review and assessment of the potential of post-IR IRSL dating methods to circumvent the problem of anomalous fading in feldspar luminescence*. Geochronometria, 41(3): 178–201, 2014a.

Li, B., Roberts, R.G., Jacobs, Z., and Li, S.H. *A single-aliquot luminescence dating procedure for K-feldspar based on the dose-dependent MET-pIRIR signal sensitivity*. Quaternary Geochronology, 20: 51–64, 2014b.

Li, B., Roberts, R.G., Jacobs, Z., and Li, S.H. *Potential of establishing a 'global standardised growth curve' (gSGC) for optical dating of quartz from sediments*. Quaternary Geochronology, 27: 94–104, 2015a.

Li, B., Roberts, R.G., Jacobs, Z., Li, S.H., and Guo, Y J. *Construction of a 'global standardised growth curve' (gSGC) for infrared stimulated luminescence dating of K-feldspar*. Quaternary Geochronology, 27: 119–130, 2015b.

Li, B., Jacobs, Z., and Roberts, R. *Investigation of the applicability of standardised growth curves for OSL dating of quartz from Haua Fteah cave, Libya*. Quaternary Geochronology, 35: 1–15, 2016.

Li, B., Jacobs, Z., Roberts, R.G., Galbraith, R., and Peng, J. *Variability in quartz OSL signals caused by measurement uncertainties: problems and solutions*. Quaternary Geochronology, 41: 11–25, 2017.

Lian, O.B. and Roberts, R.G. *Dating the Quaternary: progress in luminescence dating of sediments*. Quaternary Science Reviews, 25: 2449–2468, 2006.

Lu, Y.C., Wang, X.L., and Wintle, A.G. *A new OSL chronology for dust accumulation in the last 130,000 yr for the Chinese Loess Plateau*. Quaternary Research, 67: 152–160, 2007.

Murray, A.S. and Roberts, R.G. *Measurement of the equivalent dose in quartz using a regenerative-dose single-aliquot protocol*. Radiation Measurements, 29: 503–515, 1998.

Murray, A.S. and Wintle, A.G. *Luminescence dating of quartz using an improved single-aliquot regenerative-dose protocol*. Radiation Measurements, 32(1): 57–73, 2000.

Panagopoulou, E., Tourloukis, V., Thompson, N., Athanassiou, A., Tsartsidou, G., Konidaris, G.E., Giusti, D., Karkanas, P., and Harvati, K. *Marathousa 1: A new Middle Pleistocene archaeological site from Greece*. Antiquity Project Gallery, 89(343), 2015.

Peng, J., Dong, Z.B., Han, F.Q., Long, H., and Liu, X.J. *R package numOSL: numeric routines for optically stimulated luminescence dating*. Ancient TL, 31: 41–48, 2013.

Peng, J., Pagonis, V., and Li, B. *On the intrinsic accuracy and precision of the standardised growth curve (SGC) and global-SGC (gSGC) methods for equivalent dose determination: A simulation study*. Radiation Measurements, 94: 53–64, 2016.

R Core Team. *R: A Language and Environment for Statistical Computing*. R Foundation for Statistical Computing, 2016. URL https://www.R-project.org/.

Roberts, H.M. and Duller, G.A.T. *Standardised growth curves for optical dating of sediment using multiple-grain aliquots*. Radiation Measurements, 38: 241–252, 2004.

Van den Bergh, G.D., Li, B., Brumm, A., Grün, R., Yurnaldi, D., Moore, M.W., Kurniawan, I., Setiawan, R., Aziz, F., Roberts, R.G., Suyono, S.M., Setiabudi, E., and Morwood, M.J. *Earliest hominin occupation of Sulawesi, Indonesia*. Nature, 529: 208–211, 2016.

Van Vugt, N., De Bruijn, H., Van Kolfschoten, T., and Langereis, C.G. *Magneto- and cyclostratigraphy and mammal-faunas of the Pleistocene lacustrine Megalopolis Basin, Peloponnesos, Greece*. Geologica Ultrajectina, 189: 69–92, 2000.

Vinken, R. *Stratigraphie und Tektonik des Beckens von Megalopolis (Peloponnes, Griechenland)*. Geologisches Jahrbuch, 83: 97–148, 1965.

Wintle, A.G. *Recent developments in optical dating of sediments*. Radiation Protection Dosimetry, 47: 627–635, 1993.

Wintle, A.G. *Luminescence dating methods*. In Holland, H D and Turekian, K K (eds.), *Treatise on Geochemistry*, pp. 17–35. Elsevier, Oxford, 2nd edition, 2014.

Reviewer

Vasilis Pagonis

Ancient TL

Defining minimum reporting requirements for ESR dating of optically bleached quartz grains

Mathieu Duval,[1*] Jean-Jacques Bahain,[2] Melanie Bartz,[3] Christophe Falguères,[2] Verónica Guilarte,[4] Davinia Moreno,[4] Hélène Tissoux,[2,5] Miren del Val,[6] Pierre Voinchet,[2] Lee J. Arnold[7]

[1]Australian Research Centre for Human Evolution (ARCHE), Environmental Futures Research Institute, Griffith University, Nathan QLD 4111, Australia.

[2]Département de Préhistoire, Muséum National d'Histoire Naturelle, UMR 7194, Paris, France.

[3]Institute of Geography, University of Cologne, Albertus-Magnus-Platz, 50923 Cologne, Germany.

[4]Centro Nacional de Investigación Sobre Evolución Humana (CENIEH), Paseo de la Sierra de Atapuerca 3, 09002 Burgos, Spain.

[5]Service Géologique National - BRGM. 45060 Orléans Cedex 2, France.

[6]Department of Mineralogy and Petrology, UPV/EHU University of the Basque Country, B Sarriena, s/n, 48940 Leioa, Spain.

[7]School of Physical Sciences, Institute for Photonics and Advanced Sensing (IPAS) and Environment Institute, University of Adelaide, North Terrace Campus, Adelaide, SA 5005, Australia.

*Corresponding Author: m.duval@griffith.edu.au

Received: February 28, 2017; in final form: May 29, 2017

Abstract

More than 30 years after the first Electron Spin Resonance (ESR) dating application to optically bleached quartz grains by Yokoyama et al. (1985), the absence of standardization for reporting methodology and age results remains an obstacle for the development and recognition of the ESR dating method within the Quaternary scientific community. To overcome this issue, the present work proposes some basic guidelines which should hopefully be useful not only for the ESR dating community, but also for any potential reviewers who may not be familiar with the specificities of this field.

Keywords: Electron Spin Resonance (ESR) dating; Quartz grains; Aluminium centre; Titanium centre; Equivalent Dose; Dose rate

1. Introduction

In any scientific paper, regardless of the field considered, the section dedicated to the description of the method is by definition of crucial importance: it must contain the minimum information about experimental conditions to provide the reader a clear and precise understanding of the analytical procedure that has been followed. This is a necessary requisite for not only evaluating the reliability and validity of the methodology that has been employed, but also to open the possibility to replicate the experiment under similar conditions (e.g. Azevedo et al., 2011; Kallet, 2004).

In geochronology studies this section is especially important, and minimum information should be reported with enough details so that the reader can correctly assess the reliability and interpret the meaning of the age estimates that have been produced. The data set provided should also be detailed enough to permit independent age re-assessments, in light of methodological advances that will be progressively made in the future (Duller, 2008). The importance of

standardizing the reporting of methodology and age results has already been carefully considered for many Quaternary dating techniques, such as radiocarbon (e.g. Millard, 2014, and references therein), Ar-Ar (Renne et al., 2009), U-series (Dutton et al., 2017) and luminescence dating (Forman et al., 2000; Duller, 2008). This is, however, somewhat contrasting with the situation in ESR dating.

Four decades after the first use of ESR spectroscopy for dating purpose (Ikeya, 1975), and 30 years after the first applications to optically bleached quartz grains (Yokoyama et al., 1985), the absence of a minimum standardization for reporting research in this field is a concern. It remains an obstacle for the development and recognition of the ESR dating method within the Quaternary scientific community. So far, the only attempt in this direction was made by Grün (1992) who produced some general recommendations for most of the materials that were then usually dated by ESR (mainly tooth enamel and carbonates).

More than 20 years later, one may observe an increasing number of ESR dating studies based on optically bleached quartz grains, using aluminum (Al), titanium (Ti) or germanium (Ge) paramagnetic centres, but the information reported varies greatly among papers. As with luminescence dating, an ESR age estimate based on optically bleached quartz grains is basically derived from the determination of two main parameters: the equivalent dose (D_E), which is the laboratory estimate of the palaeodose, i.e. the total dose absorbed by the sample since the ESR signal has been last reset to zero by sunlight exposure, and the dose rate ($\dot{D}$), which is an estimation of the mean dose annually absorbed by the sample. However, there are several ways to evaluate these two parameters, and so far there is no standardization of analytical procedures within the ESR dating community to determine the D_E or $\dot{D}$ term (notations from Grün (1992)). For this reason, providing only these two values in a scientific publication is not sufficient for the reader to gain a clear idea of the meaning and implications of the age results that have been obtained. It is frequently the case that the information presented in publications is not sufficient for external critical assessment. Given this situation, it now seems timely to define some minimum requirements for reporting methodology and ESR age estimates based on quartz grains.

2. Reporting ESR methodology

The standard ESR dating analytical procedure is usually made by five main steps: (i) sample collection, (ii) sample preparation, (iii) ESR dose response curve reconstruction and D_E determination, (iv) dose rate estimation and (v) age calculation. The following sub-sections 2.1 to 2.5 describe step by step the minimum information that should be reported, while an overview is given in Table 1.

2.1. Sample collection

The most crucial information to report here is any basic details regarding the position of the samples within the stratigraphic sequence, their depth, as well as the geographic location of the sampling locality (including altitude). It may also be mentioned whether additional sediment samples were collected for water content or additional laboratory analyses. Lastly, in cases where *in situ* dosimetry measurements have been carried out on site, the following should be briefly specified: (i) the relative position of the *in situ* measurement with respect to the ESR samples, (ii) the technique that has been used (e.g., thermoluminescence (TL) or optically stimulated luminescence (OSL) dosimeter, gamma spectrometry), (iii) how the calibration, if applicable, was performed, (iv) and how the data were extracted and converted to dose rate values (e.g., "energy windows," "threshold"). For points (iii) and (iv), referencing of previous work that already details the required information would be sufficient. Note that it may be more convenient to include points (ii) to (v) in the methods section dedicated to dose rate evaluation.

In particular, special emphasis should be given to the stratigraphic relationship between the dating event of interest and the sample being dated, i.e., whether the sample provides a direct, indirect, minimum, maximum or equivalent age estimate for the event/artefact/object/fossil under consideration. Additionally, the physical proximity (distance) of the sample to the event/artefact/object/fossil under consideration should be stated. Often this information is overlooked but it is critical to interpret the meaning of the final age estimate.

Additional information may be especially useful for the reader, like the sampling conditions (e.g., PVC tubes, blocks) and the precautions taken to minimize exposure to sunlight, if any (e.g., night sampling, day sampling under an opaque plastic cover), as bleaching rates of the ESR signals are known to be slower than that of the OSL signals (e.g., Duval et al., 2017). Brief description of the sedimentary context and geological characteristics of the deposits such as their origin (e.g., volcanic) or grain size could be provided as well, as they may give some insights about bleaching conditions during sediment transport (e.g., Voinchet et al., 2015). Pictures of the samples in their sedimentary context could also be used to provide complementary information for the reader.

2.2. Sample preparation

The main objective of sample preparation is the extraction of pure quartz grains from the raw sedimentary matrix. This is usually carried out by combining wet sieving and subsequent chemical treatment in order to remove carbonates, organics and other minerals (e.g., feldspars, magnetic minerals). In particular, hydrofluoric acid (HF) is not only used to remove all the minerals except quartz, but also to etch the external layer of the quartz grains for eliminating (or at least minimizing) the external alpha particles contributions. As a result of this operation, the external beta particle contribution to the dose rate may also be significantly impacted. Reporting full details of the analytical procedure should probably not be considered as mandatory, as this information is not directly useful to evaluate data reliability. However, it will indirectly affect the results as the preparation impacts the purity of the prepared samples. Consequently, we would suggest

Table 1: Summary checklist detailing the minimum information that should be provided when reporting ESR dating methodology based on optically bleached quartz grains.

Step	Minimum information that should be reported	Additional useful information that may be reported
1. Fieldwork	• Stratigraphic (unit/level) position of the samples • Stratigraphic relationship between the dating event of interest and the sample being dated, i.e., whether the sample provides a direct, indirect, minimum, maximum, or equivalent age estimate for the event/artefact/object/fossil under consideration • Geographic location and altitude of the sampled outcrop/site • If *in situ* measurements were carried out: (i) theri position with respect to the ESR samples, (ii) the technique employed (e.g., TL dosimeter, gamma probe),[1] (iii) its calibration, and (iv) data reduction procedure to derive dose rate values (e.g., "energy windows," "threshold")[1]	• Geological context and origin of the quartz grains • GPS coordinates of the site • Additional sediment samples collected for water content or future laboratory analysis? • Pictures of the samples in their sedimentary context • Sampling conditions and precautions to minimize sunlight exposure
2. Sample preparation	• Initial grain size fraction selected • Conditions of HF etching (concentration and duration)	• Conditions of laboratory illumination during the preparation • Each step of the procedure, preferentially in chronological order (e.g., wet sieving, chemical reaction, magnetic separation, density separation) • Chemical products used (type and concentration)
3. D_E reconstruction	• Experimental conditions of the ESR measurements (experimental setup, acquisition parameters, number of repeated measurements, number of rotations in the cavity, temperature of the ESR measurements)[1] • For the Al centre: bleaching conditions for the evaluation of the residual ESR intensity (UV simulator and lamp details, duration of the bleaching experiment)[1] • Evaluation of the ESR signal intensity (peak-to-peak measurement, peak-to-baseline, deconvolution)[1,2] • Corrections of the ESR intensities (sample weight, temperature of the cavity, receiver gain value, number of scans, mean value derived from tube rotations, averaging of the repeated measurements) • Equation of the fitting function[1] • Data weighting used for the fitting • Fitting program and error evaluation • Error reporting nomenclature (whether errors are reported at 1 sigma or 2 sigma confidence levels)	
4. Dose rate evaluation	• Technique(s) used to determine either the concentration of the radioelements in the sediment or the total alpha, beta, and gamma dose rate values[1] • Origin (reference) of the conversion and correction factors that have been used: dose rate conversion factors, alpha and beta attenuation factors for spherical grains, water attenuations, alpha efficiency[1,3] • Thickness, measured or assumed, removed from the grains by HF etching[1] • Details about the cosmic dose rate calculation: depth (thickness of the sediment cover above the sample), altitude, GPS coordinates, water correction and reference(s) for the equation used. In case of caves/rock shelters, some detail should be provided about how additional partial/complete shielding of bedrock has been factored into the equations used.[1] • Water content (% dry or % wet weight) value used (measured or assumed? if measured, specify how? If assumed, provide details about how a suitable value has been derived)[1] • Whether equilibrium or disequilibrium in the U-238 and Th-232 series has been considered for dose rate calculation[1] • Error reporting nomenclature (whether errors are reported at 1 sigma or 2 sigma confidence levels)	
5. ESR age calculation	• Details about the age calculation program used and error evaluation[3] • Error reporting nomenclature (whether errors are reported at 1 sigma or 2 sigma confidence levels)	

[1]Some aspects of the analysis may be the same as previously published, so that referring to another study may be sufficient.

[2]This may be indicated in a figure showing the ESR signal that is analysed

[3]There is now an increasing number of software available to the community for dose rate and age calculations (e.g. AGE, DRAC, DRC). Consequently, it may be as simple as citing the corresponding publication for the software. In such cases, special care should be taken to ensure that the empirical water content term is expressed in the same terms used in the software (% dry or wet mass).

that each step of the procedure is briefly reported at least in supplementary material (e.g., conditions of laboratory illumination, information concerning the wet sieving, details of the chemical digestion, kind of magnetic and density separation, post-HF sieving), preferentially in chronological order. An example of a standard report for sample preparation may be found in Liu et al. (2010), Duval et al. (2015b), or Voinchet et al. (2007).

Instead, the basic minimum information that should be known here is the selected initial grain size fraction after sieving and the conditions of HF etching (concentration and the duration of the etching), as they have a direct impact on the final grain size of the grains (Bell & Zimmerman, 1978; Bell, 1979; Yokoyama et al., 1985; Porat et al., 2015; Duval et al., 2015a), and thus on the alpha and beta attenuation values (Bell, 1980; Mejdahl, 1979). Laboratory water content evaluation of the sediment (i.e., current water content and, if applicable, saturated water content) should also be described, either here or in the dose rate evaluation section.

It is worth emphasizing for non-ESR dating specialists that the relative slow, wavelength-dependent optical bleaching properties of quartz ESR signals essentially preclude the need for strict laboratory lighting protocols during sample preparation. Both the Al and Ti centre ESR signals are apparently mostly depleted by UV wavelengths, primarily UVA and UVB (Tissoux et al., 2007), although mechanical resetting processes might also play a role in sedimentary settings (Liu & Grün, 2011). Laboratory bleaching experiments undertaken using sunlight simulators have shown that the Al signal reaches a minimum intensity after several hundreds of hours of bleaching, while the Ti-Li signal is fully reset in $<$50 h. In comparison, $<$4 h are required to zero the ESR signal of the Ti-H centre (see Figure 1 in Duval et al., 2017). However, it should be noted that these bleaching rates may vary greatly (albeit within the same order of magnitude) depending on the sample analysed and the experimental setup. A complete discussion of ESR signal bleaching may be found in Duval et al. (2017) and references therein. It is clear from existing experimental datasets that quartz ESR bleaching rates are significantly slower than those of quartz OSL signals (see comparison in Duval et al., 2017), and that short exposure of a few minutes to natural light, or several hours to UV-depleted laboratory lights, will have no measurable impact on the ESR signals. For this reason, ESR lighting condition requirements are not as strict as those employed for luminescence dating, although some basic precautions should nevertheless be taken (see some recommendations for sampling in Moreno et al., Accepted). Until further evidence demonstrating the opposite emerges, it is not considered essential to detail sample preparation lighting conditions in ESR papers.

2.3. ESR dose reconstruction

Acronyms usually employed in luminescence dating may also be used for ESR, depending on whether Single or Multiple Aliquot(s) and Additive or Regenerative dose methods have been employed (e.g. MAA, MAR, SAR, SARA, MARA, SAA). It could also be specified whether single grain or multiple grain analyses have been carried out, even if the former remains experimental in ESR dating (Beerten & Stesmans, 2005).

In most cases, ESR dose reconstructions of quartz grains are performed using a Multiple Aliquots Additive (MAA) dose approach, which means that the D_E value is obtained by back extrapolation of the fitting function to the abscissa axis. It is thus crucial to specify the number and the distribution of the irradiation dose steps (see discussions in Grün & Rhodes, 1991, 1992), as well as some basic information about the type and dose rate of the irradiation source (e.g., in Gy/h or Gy/s) that has been employed. Independently of whether ESR measurements have been performed at room temperature (for the Ge centre) or close to liquid nitrogen temperature (for Al and Ti centres), the following basic details about D_E measurement conditions should be specified:

- Experimental setup (type of spectrometer, ESR resonator, temperature control system).
- Acquisition parameters (microwave power, resolution, sweep width, modulation frequency, modulation amplitude, conversion time, time constant, number of scans, measurement temperature; see Grün (1992)).
- Number of rotations of the tube in the cavity for each aliquot and/or number of repeated measurements for each sample that have been carried out in order to evaluate the angular dependence of the signals due to grain heterogeneity and the repeatability/precision of the ESR data set.

Among the three main centres commonly used for dating purpose, the Al centre is unique in having an unbleachable component that gives rise to a residual ESR signal intensity. This residual signal must therefore be evaluated in order to avoid major D_E overestimation (Voinchet et al., 2003). Consequently, it is important to describe how this residual ESR intensity has been determined in the laboratory. For instance, quartz samples are sometimes simply directly exposed to natural sunlight to assess the unbleachable signal component. However, most of the time UV sunlight simulators are used to artificially bleach one aliquot: in this case, the type of simulator and lamps (electromagnetic spectrum covered), as well as the duration of the bleaching experiment should be specified.

The methods used to extract ESR intensities from the measured ESR spectra may vary from one centre to another. While there is apparent agreement in the scientific community regarding evaluation of the Al centre (Yokoyama et al., 1985; Toyoda & Falguères, 2003) or Ge centre (Falguéres et al., 1991; Walther & Zilles, 1994), evaluation of the Ti centres remains somewhat debated (see Duval & Guilarte, 2015 and reference therein). Consequently, it is important to explain how the ESR intensities were evaluated (e.g. peak-to-peak measurement, peak-to-baseline, deconvolution) and which peaks were used for D_E determination. This may be simply shown in a figure (see examples in Liu et al., 2010; Tissoux et al., 2007).

Finally, the data reduction and analysis procedures used for D_E evaluation should be briefly described:

- Whether ESR intensities from repeated measurements were averaged out and corrected (e.g., according to weight, temperature variations, number of scans, receiver gain).
- Whether (and how) the residual ESR intensity has been taken in consideration in the evaluation of the D_E value (for the Al centre only). This is usually done following the total bleach approach, as described in (Forman, 1989). A figure may simply be provided (see Figure 4 from Voinchet et al., 2003)
- Basic details about the fitting procedure: the function that has been used (including preferably the equation or at least citing a previous paper where this is specified, as there may be slight variations of a given function, e.g. Duval, 2012), the data weighting, the fitting program, error evaluation and whether errors are reported at 1 sigma or 2 sigma confidence levels.

This last point is of crucial importance. Indeed, because of the use of the additive dose method for ESR dose evaluation, the D_E value is obtained by extrapolation of the fitted function (unlike the regenerative dose method where the D_E value is obtained by interpolation instead; see Forman, 1989). Consequently, the value of the D_E estimate is directly and significantly dependent on the fitting function and options employed (see Duval, 2012 and Duval & Guilarte, 2015 and references therein).

2.4. Dose rate evaluation

Unlike fossil teeth for which uranium uptake in dental tissue has to be modeled (e.g., Grün, 2009a), the internal and external dose rate associated to quartz grains is usually assumed to remain constant over time. Consequently, the basic dose rate equation may be expressed as follows:

$$\dot{D} = \dot{D}_{int} + \dot{D}_{ext} + \dot{D}_{cosmic} \quad (1)$$

where $\dot{D}$, $\dot{D}_{int}$, $\dot{D}_{ext}$, and $\dot{D}_{cosmic}$ are the total, internal, external and cosmic dose rate components, respectively. ESR dating of quartz is mostly performed on grains whose diameter is between 60 and 300 μm, which means that the internal component, if existing, mainly comes from the alpha and beta particles contribution. Depending on the authors, the internal dose in quartz grains is usually either neglected, given the low concentrations of radioelements found in most quartz grains (e.g., Vandenberghe et al., 2008), or an assumed value is adopted (e.g., Duval et al., 2015a). Irrespective, the treatment of internal dose rate components should be clearly specified in the manuscript, particularly as it can constitute an important variable in environments with low external dose rates.

The external dose rate may be divided into several components as follows (detailed equations may be found in Grün, 1989):

$$\dot{D}_{ext} = \left[\dot{D}_\alpha + \dot{D}_\beta + \dot{D}_\gamma\right]_{ext.} + \dot{D}_{cosmic} \quad (2)$$

where $\dot{D}_{ext}$, $\dot{D}_\alpha$, $\dot{D}_\beta$, $\dot{D}_\gamma$, and $\dot{D}_{cosmic}$ are the alpha, beta and gamma dose rates, respectively. These components are directly calculated from the activities or concentrations of radioelements (mainly U-238, Th-232 and K-40) present in the quartz grains and surrounding environment. The technique used to obtain these values (ICP-MS and/or ICP-OES, High Resolution Gamma Spectrometry, alpha counting) should be specified, as they utilise very different amounts of material, and results obtained may be of variable representativeness for different components of the external dose rate. The measured radionuclide activities / concentrations are transformed into dose rate values using conversion factors that are specific to each element and the particle or ray emitted. The most commonly used are those published by Adamiec & Aiken (1998), recently updated by Guérin et al. (2011). It should be specified whether dose rate calculation has been performed by considering either secular equilibrium or disequilibrium in the U-238 and Th-232 series. If apparent disequilibrium is detected, then some discussion should also be provided about the possible effects on the final ages of assuming different time-dependent dose rate scenarios. As previously mentioned, the gamma dose rate may also be derived from *in situ* measurements: in that case, the comments made in Section 2.1 should be taken into consideration.

These external dose rate values are then corrected according to different factors related to the site history or to the sample preparation, such as water content or grain size. Water content correction is crucial for the alpha, beta and gamma dose rate components: it should be specified if the value is expressed as a % of wet sediment weight or a % of dry sediment weight, whether this water content of the sediment has been measured or assumed, and how this has been taken into consideration in the dose rate calculation. Further details about this issue may be found in Grün (1994) and references therein. The reason/justification for using a particular assumed water content value should also be clearly stated in any study, i.e., the authors should specify what factors have been considered in deriving a representative assumed long term water content. The initial and final (after HF etching) grain size fraction will determine the value of the attenuation factors for the internal and external alpha and beta components. If the grains are sufficiently etched, the external alpha dose rate component may be simply eliminated from the external dose rate calculation. It is not mandatory to indicate the values of these attenuations factors, since these can be derived independently using initial and post-etching grain sizes. It is, however, important to specify the source of the attenuation factors used in the study. The values from Brennan et al. (1991) and Brennan (2003) for spherical grains have been widely used over the last decades. Updated values have recently been presented by Nathan (2010) and Guérin et al. (2012), taking into account grain size, shape, density, and the radioelements that are involved. Finally, the alpha efficiency value used for correction of the external and/or internal alpha dose rate (if not null) should be specified.

For the cosmic dose rate, it should be specified whether this component has been measured or estimated via exist-

	Minimum information that should be reported
Summary Table 1	• Radioelement concentrations (ppm or %) or activities (Bq/kg) of the surrounding sediment used for the external dose rate calculation, depth below surface (in m), water content of the sediment (% dry or % wet weight)
Summary Table 2	• Value and associated error for each component of the dose rate (internal, external alpha, beta and gamma, cosmic), the total dose rate (in μGy/a or Gy/ka), the D_E (in Gy) and the calculated ESR age estimates (in ka or Ma) • When using the Al centre: the relative level of the residual ESR intensity in comparison with the natural ESR intensity (in %)
Figure 1	• Examples of the ESR signal that has been measured
Figure 2	• Some examples of dose response curves
	Additional information that may be reported
Table	• Numerical estimators to evaluate goodness-of-fit for each sample (e.g., adjusted r^2 value, least-square values, chi-square values). This information can also be included in Figure 2 of the main manuscript and/or the figure with the DRCs in supplementary material
Figure	• A stratigraphic column presenting the ESR age results in stratigraphic position
Supplementary material	• Figures showing all the dose response curves (ESR intensities vs. Dose + the fitting function) • Numerical data (ESR intensities vs. Dose) in a spreadsheet

Table 2: Summary checklist detailing: (i) the minimum information that should be provided when reporting ESR dating results based on optically bleached quartz grain; and (ii) additional useful information that may be reported.

ing tables. The latter is usually preferred, using the equation from Prescott & Hutton (1988). In addition, the corrections factors considered for the calculation such as altitude, latitude, depth, as well as the estimated ground density (Prescott & Hutton, 1994), or the water content (Readhead, 1987) should be mentioned. In the case of samples from caves/rock shelters, it is also useful to detail how additional partial/complete shielding by bedrock has been factored into the cosmic dose rate calculation.

Finally, the evaluation of the error on the dose rate should be briefly described. Some guidelines on this issue may be found in Aitken (1985) and Grün (1992). Error reporting nomenclature should be specified, i.e. whether errors are reported at 1 sigma or 2 sigma confidence levels.

2.5. Age calculation

ESR age calculation is quite straightforward when the dose rate is assumed to be constant over time. In such cases, an age is simply derived from the division of the D_E value by the total dose rate. However, details should be given about how the errors have been calculated and propagated to the final age values. There is now a range of dose rate and age calculation software available to the community (among others, AGE, DRAC and DRC; see Grün, 2009b, Durcan et al., 2015, and Tsakalos et al., 2016, respectively). Although most of these have been designed for luminescence dating, they may easily be adapted to the specificities of ESR dating. Consequently, the age calculation process may simply require citing the corresponding publications where basic information (error calculations, dose rate conversion factors, correction factors) about the software is presented. Error reporting nomenclature should be specified, i.e., whether errors are reported at 1 sigma or 2 sigma confidence levels.

3. Reporting ESR results

ESR age estimates and associated results should be reported in several tables and figures (see a summary in Table 2). Usually, a series of summary tables including radioelement concentrations, and details of the dose rate and D_E components are sufficient.

In addition to these numerical data, several supporting figures should be provided. It is recommended to show at least one ESR spectrum for the signal that has been analysed, indicating how the signal intensity has been evaluated (e.g. see Toyoda & Falguères, 2003 for the Al centre, Walther & Zilles, 1994 for the Ge centre, and Beerten et al., 2008 for the Ti centres) as debate remains over this issue within the community for some paramagnetic centres. Alternatively, it may be possible to refer to a previous study where appropriate details have been provided elsewhere. The most important figure to provide is undoubtedly related to the Dose Response Curves (DRCs). Because the reliability of the D_E values is

highly dependent on whether the function is well fitted or not through the experimental data points, some graphical examples of ESR DRCs must be presented in the main text (e.g. Duval et al., 2017). Ideally, all DRCs should be included in supplementary information (e.g., Duval et al., 2017) as this is the best way for the reader to evaluate the quality of the ESR data set and, thus, the reliability of the fitting results. In addition, it may be particularly useful to provide some numerical estimators (e.g., adjusted r^2 value, least square values, chi-square values) for the goodness-of-fit achieved for each sample, since this may be quite variable from one sample to another, even within a given site or section (e.g., Duval et al., 2017). Following on from these guidelines it may be worth discussing within the ESR dating community the interest of systematically providing the complete ESR data sets (i.e., ESR intensities and corresponding irradiation doses) in numerical format (spreadsheet).

4. Conclusion

To avoid misunderstandings it is worth mentioning here that the purpose of the present paper is not to standardise analytical procedures in the ESR dating community, or to provide recommendations for the most reliable analytical practices in ESR dating of quartz (see for example Moreno et al., Accepted for some fieldwork recommendations). We have instead aimed to provide some guidelines for reporting ESR methodology and results, in order to make sure that the basic minimum information is available for external critical assessment. A series of summary checklists are provided here in Tables 1 and 2. These recommendations are open to revision and should be considered as a starting point for further discussion. It is worth emphasizing that these recommendations may also be used as guidelines when peer-reviewing papers dealing with ESR dating results. In particular, they may be useful for potential reviewers who are not familiar with the specificities of this field.

It is common for ESR dating applications published by a given laboratory to employ the same analytical procedure, with very little variation from one study to another. Consequently, for some aspects of the ESR dating procedure it may be possible to refer to previous publications where the corresponding information has been detailed. This may be particularly useful if manuscript length is an issue. However, most journals now offer the possibility to include online supplementary information, which means that the restricted length of the main manuscript should no longer be a limitation for providing all the required information. This approach would ensure easy and direct access to the complete analytical procedure, and avoid the need to search through previous publications that may not be readily accessible.

Adhering to the suggested reporting requirements should enable more straightforward age and data re-assessments in light of progressive improvements in understanding of the ESR dating method. This may occur, for example, via the update of published parameters (e.g., dose rate conversion factors, alpha and beta attenuations) or the identification of more appropriate fitting functions, thereby enhancing the scientific vitality of the field.

Finally, it should also be emphasized that the recommendations discussed in the present work are only intended for ESR dating studies applied to optically bleached quartz grains. ESR dating applications involving other materials, such as fossil teeth, corals, carbonates, require the provision of different supporting information, as recommended by Grün (1992).

Acknowledgments

The authors would like to thank their colleagues geochronologists for sharing some useful information about their speciality, Lee Arnold (Adelaide University, Australia), Sébastien Nomade (LSCE, France) and Antoine Zazzo (MNHN, France) for Luminescence, Ar-Ar and Radiocarbon dating, respectively. MD's research is currently funded by an ARC Future Fellowship Grant (FT150100215). Finally, the thorough review by Lee Arnold has contributed to greatly improve the scientific content, and the English, of this work. This is why he has been invited by the leading author to co-author this study.

References

Adamiec, G. and Aiken, M. *Dose-rate conversion factors: update*. Ancient TL, 16(2): 37–50, 1998.

Aitken, M.J. *Thermoluminescence Dating*. Academic Press, London, 1985.

Azevedo, L.F., Canario-Almeida, F., Almeida Fonseca, J., Costa-Pereira, A., Winck, J.C., and Hespanhol, V. *How to write a scientific paper - Writing the methods section*. Revista Portuguesa de Pneumologia, 17(5): 232–238, 2011.

Beerten, K. and Stesmans, A. *Single quartz grain electron spin resonance (ESR) dating of a contemporary desert surface deposit, Eastern Desert, Egypt*. Quaternary Science Reviews, 24(1–2): 223–231, 2005.

Beerten, K., Rittner, S., Lomax, J., and Radtke, U. *Dose recovery tests using Ti-related ESR signals in quartz: First results*. Quaternary Geochronology, 3(1–2): 143–149, 2008.

Bell, W.T. *Attenuation factors for the absorbed radiation dose in quartz inclusions for thermoluminescence dating*. Ancient TL, 8: 2–13, 1979.

Bell, W.T. *Alpha dose attenuation in quartz grains for thermoluminescence dating*. Ancient TL, 12: 4–8, 1980.

Bell, W.T. and Zimmerman, D.W. *The effect of HF acid etching on morphology of quartz inclusions for thermoluminescence dating*. Archaeometry, 20: 63–65, 1978.

Brennan, B.J. *Beta doses to spherical grains*. Radiation Measurements, 37(4–5): 299–303, 2003.

Brennan, B.J., Lyons, R.G., and Phillips, S.W. *Attenuation of alpha particle track dose for spherical grains*. Nuclear Tracks and Radiation Measurements, 18(1–2): 249–253, 1991.

Duller, G.A.T. *Luminescence dating: Guidelines on using luminescence dating in archaeology*. English Heritage, Swindon, 2008.

Durcan, J.A., King, G.E., and Duller, G.A T. *DRAC: Dose Rate and Age Calculator for trapped charge dating*. Quaternary Geochronology, 28: 54–61, 2015.

Dutton, A., Rubin, K., McLean, N., Bowring, J., Bard, E., Edwards, R.L., Henderson, G.M., Reid, M.R., Richards, D.A., Sims, K.W.W., Walker, J.D., and Yokoyama, Y. *Data reporting standards for publication of U-series data for geochronology and timescale assessment in the earth sciences*. Quaternary Geochronology, 39: 142–149, 2017.

Duval, M. *Dose response curve of the ESR signal of the Aluminum center in quartz grains extracted from sediment*. Ancient TL, 30 (2): 1–9, 2012.

Duval, M. and Guilarte, V. *ESR dosimetry of optically bleached quartz grains extracted from Plio-Quaternary sediment: evaluating some key aspects of the ESR signal associated to the Ti-center*. Radiation Measurements, 78: 28–41, 2015.

Duval, M., Campaña, I., Guilarte, V., Miguens, L., Iglesias, J., and González Sierra, S. *Assessing the uncertainty on particle size and shape: Implications for ESR and OSL dating of quartz and feldspar grains*. Radiation Measurements, 81: 116–122, 2015a.

Duval, M., Sancho, C., Calle, M., Guilarte, V., and Peña-Monné, J.L. *On the interest of using the multiple center approach in ESR dating of optically bleached quartz grains: Some examples from the Early Pleistocene terraces of the Alcanadre River (Ebro basin, Spain)*. Quaternary Geochronology, 29: 58–69, 2015b.

Duval, M., Arnold, L.J., Guilarte, V., Demuro, M., Santonja, M., and Pérez-González, A. *Electron spin resonance dating of optically bleached quartz grains from the Middle Paleolithic site of Cuesta de la Bajada (Spain) using the multiple centres approach*. Quaternary Geochronology, 37: 82–96, 2017.

Falguéres, C., Yokoyama, Y., and Miallier, D. *Stability of some centers in quartz*. Nuclear Tracks and Radiation Measurements, 18(1–2): 155–161, 1991.

Forman, S.L. *Applications and limitations of thermoluminescence to date Quaternary sediments*. Quaternary International, 1: 47–59, 1989.

Forman, S.L., Pierson, J., and Lepper, K. *Quaternary Geochronology: Methods and Applications*, chapter Luminescence Geochronology, pp. 157–176. American Geophysical Union, 2000.

Grün, R. *Electron Spin Resonance (ESR) Dating*. Quaternary International, 1: 65–109, 1989.

Grün, R. *Suggestions for minimum requirements for reporting ESR age estimates*. Ancient TL, 10(3): 37–41, 1992.

Grün, R. *A cautionary note: use of 'water content' and 'depth for cosmic ray dose rate' in AGE and DATA programs*. Ancient TL, 12(2): 50–51, 1994.

Grün, R. *The relevance of parametric U-uptake models in ESR age calculations*. Radiation Measurements, 44(5–6): 472–476, 2009a.

Grün, R. *The "AGE" program for the calculation of luminescence age estimates*. Ancient TL, 27(2): 45–46, 2009b.

Grün, R. and Rhodes, E.J. *On the selection of dose points for saturating exponential ESR/TL dose response curves*. Ancient TL, 9 (3): 40–46, 1991.

Grün, R. and Rhodes, E.J. *Simulations of saturating exponential ESR/TL dose response curves - weighting of intensity values by inverse variance*. Ancient TL, 10(3): 50–56, 1992.

Guérin, G., Mercier, N., and Adamiec, G. *Dose-rate conversion factors: update*. Ancient TL, 29(1): 5–8, 2011.

Guérin, G., Mercier, N., Nathan, R., Adamiec, G., and Lefrais, Y. *On the use of the infinite matrix assumption and associated concepts: A critical review*. Radiation Measurements, 47(9): 778–785, 2012.

Ikeya, M. *Dating a stalactite by electron paramagnetic resonance*. Nature, 255(5503): 48–50, 1975.

Kallet, R. *How to write the methods section of a research paper*. Respiratory Care, 49(10): 1229–1232, 2004.

Liu, C.R. and Grün, R. *Fluvio-mechanical resetting of the Al and Ti centers in quartz*. Radiation Measurements, 46: 1038–1042, 2011.

Liu, C.R., Yin, G.-M., Gao, L., Bahain, J.-J., Li, J.-P., Lin, M., and Chen, S.-M. *ESR dating of Pleistocene archaeological localities of the Nihewan Basin, North China - Preliminary results*. Quaternary Geochronology, 5(2–3): 385–390, 2010.

Mejdahl, V. *Thermoluminescence dating: beta-dose attenuation in quartz grains*. Archaeometry, 21: 61–72, 1979.

Millard, A.R. *Conventions for reporting radiocarbon determinations*. Radiocarbon, 56(2): 555–559, 2014.

Moreno, D., Richard, M., Bahain, J.-J., Duval, M., Falguéres, C., Tissoux, H., and Voinchet, P. *ESR dating of sedimentary quartz grains: some basic guidelines to ensure optimal sampling conditions*. Quaternaire, Accepted.

Nathan, R.P. *Numerical modelling of environmental dose rate and its application to trapped-charge dating*. PhD thesis, University of Oxford, 2010.

Porat, N., Faerstein, G., Medialdea, A., and Murray, A.S. *Re-examination of common extraction and purification methods of quartz and feldspar for luminescence dating*. Ancient TL, 33(1): 22–30, 2015.

Prescott, J.R. and Hutton, J.T. *Cosmic ray and gamma ray dosimetry for TL and ESR*. Nuclear Tracks and Radiation Measurements, 23(2–3): 497–500, 1988.

Prescott, J.R. and Hutton, J.T. *Cosmic ray contributions to dose rates for luminescence and ESR dating: Large depths and long-term time variations*. Radiation Measurements, 23: 497–500, 1994. ISSN 1350-4487.

Readhead, M.L. *Thermoluminescence dose rate data and dating equations for the case of disequilibrium in the decay series*. Nuclear Tracks and Radiation Measurements, 13: 197–207, 1987.

Renne, P.R., Deino, A.L., Hames, W.E., Heizler, M.T., Hemming, S.R., Hodges, K.V., Koppers, A.A.P., Mark, D.F., Morgan, L.E., Phillips, D., Singer, B.S., Turrin, B.D., Villa, I.M., Villeneuve, M., and Wijbrans, J.R. *Data reporting norms for 40Ar/39Ar geochronology*. Quaternary Geochronology, 4(5): 346–352, 2009.

Tissoux, H., Falguères, C., Voinchet, P., Toyoda, S., Bahain, J.-J., and Despriée, J. *Potential use of Ti-center in ESR dating of fluvial sediment*. Quaternary Geochronology, 2(1–4): 367–372, 2007.

Toyoda, S. and Falguères, C. *The method to represent the ESR signal intensity of the aluminum hole center in quartz for the purpose of dating*. Advances in ESR Applications, 20: 7–10, 2003.

Tsakalos, E., Christodoulakis, J., and Charalambous, L. *The Dose Rate Calculator (DRC) for luminescence and ESR dating - A Java application for dose rate and age determination*. Archaeometry, 58(2): 347–352, 2016.

Vandenberghe, D., De Corte, F., Buylaert, J.P., Kučera, J., and Van den haute, P. *On the internal radioactivity in quartz*. Radiation Measurements, 43(2–6): 771–775, 2008.

Voinchet, P., Falguères, C., Laurent, M., Toyoda, S., Bahain, J.-J., and Dolo, J.M. *Artificial optical bleaching of the Aluminium center in quartz implications to ESR dating of sediments*. Quaternary Science Reviews, 22(10–13): 1335–1338, 2003.

Voinchet, P., Falguères, C., Tissoux, H., Bahain, J.-J., Despriée, J., and Pirouelle, F. *ESR dating of fluvial quartz: Estimate of the minimal distance transport required for getting a maximum optical bleaching*. Quaternary Geochronology, 2(1–4): 363–368, 2007.

Voinchet, P., Toyoda, S., Falguères, C., Hernandez, M., Tissoux, H., Moreno, D., and Bahain, J.-J. *Evaluation of ESR residual dose in quartz modern samples, an investigation on environmental dependence*. Quaternary Geochronology, 30: 506–512, 2015.

Walther, R. and Zilles, D. *ESR studies on flint with a difference-spectrum method*. Quaternary Science Reviews, 13(5–7): 635–639, 1994.

Yokoyama, Y., Falguères, C., and Quaegebeur, J.P. *ESR dating of quartz from quaternary sediments: First attempt*. Nuclear Tracks and Radiation Measurements, 10(4–6): 921–928, 1985.

Reviewer

Lee Arnold

Editor's Note

The manuscript was reviewed by Lee Arnold. The authors decided that his review made significant contributions to the manuscript, which warranted his inclusion as co-author of the study. The Editor agreed to this change after the manuscript had been accepted.

Ancient TL

Always remain suspicious: a case study on tracking down a technical artefact while measuring IR-RF

Sebastian Kreutzer[1], Madhav Krishna Murari[2], Marine Frouin[3]
Markus Fuchs[2], Norbert Mercier[1]
[1]IRAMAT-CRP2A, Université Bordeaux Montaigne, Pessec Cedex, France
[2]Department of Geography, Justus-Liebig-University Giessen, Germany
[3]Research Laboratory for Archaeology and the History of Art, Oxford University, Oxford, United Kingdom

* Corresponding Author: sebastian.kreutzer@u-bordeaux-montaigne.fr
Received: March 22, 2017; in final form: June 13, 2017

Abstract

Identifying systematic errors that are introduced by the measurement equipment is a necessary prerequisite for reproducible measurements and reliable results. However, technical artefacts often remain unpublished. Here we report on a sudden change of luminescence intensity observed while measuring IR-RF signals from K-feldspar extracts. The measurements were carried out on a *lexsyg research* reader. A lateral movement of the sample carrier up to 0.5 mm relative to the photomultiplier tube and the irradiation source, causes a change in the sample geometry. This movement results in inter-aliquot scatter during the measurement of IR-RF. Two solutions are discussed to remove this effect: (I) data post-processing and (II) design change by the manufacturer. Our study so far is limited to IR-RF measurements on a single luminescence reader and suggests due caution in the identification of such systematic errors.

Keywords: Luminescence, Infrared Radiofluorescence, Instrumentation

1. Introduction

It is assumed that the measured data are free from systematic errors caused by the instrument design. To identify and quantify the potential sources of systematic errors, measurement equipment is often tested rigorously before its routine use (e.g., Lomax et al., 2014). However, several sources of systematic errors do not necessarily reveal themselves during routine measurements. Some require time-consuming tests (e.g., Bray et al., 2002; Adamiec et al., 2011; Schmidt et al., 2011; Kadereit & Kreutzer, 2013) and the magnitude of the error may depend on the technical design (Kreutzer et al., 2013). Such errors often result in scattered data which hampers their direct discovery. Besides, the scatter might make publication difficult; the issue remains unreported and thus might be repeated by other groups.

At the IRAMAT-CRP2A in Bordeaux (France) several studies on infrared radiofluorescence (IR-RF) of potassium-enriched feldspar (K-feldspar) extracts have been undertaken since 2012. The IR-RF signal of K-feldspar is believed to provide a promising alternative to the so far established luminescence dating approaches, e.g., quartz SAR protocol (Murray & Wintle, 2000) or post-IR IRSL on feldspar (Thomsen et al., 2008). The IR-RF technique was introduced by Trautmann et al. (1999) and Erfurt & Krbetschek (2003) and later successfully applied by, e.g., Wagner et al. (2010). In contrast, Buylaert et al. (2012) raised considerable doubts on the applicability of the method for age determinations. Re-investigation of the IR-RF signal characteristics at the IRAMAT-CRP2A recently led to an improved protocol that uses stimulation at a higher temperature (here 70 °C instead of room temperature) for recording the IR-RF signal (Frouin, 2014; Frouin et al., 2015; Huot et al., 2015; Frouin et al., 2017).

While conducting further methodological studies using fine grain (4-11 µm, gently crushed coarse grains) K-feldspar separates, we encountered an unexpected inter-aliquot scatter (Kreutzer, 2016). Such scatter was previously reported by Krbetschek et al. (2000) and later by Frouin et al. (2017) on coarse grains (100-200 µm) and has been interpreted as being due to variations in the properties of the individual grains and/or superposition of competing signals. When measuring the fine grain fraction (ca. 10^6 grains/cup) a low scatter is

expected due to signal averaging effects. However, to our surprise, we observed a high inter-aliquot scatter. The observation gave rise to the idea that the measurement device might cause this variation.

Here we report on a series of instrumental tests performed on a particular Freiberg Instruments *lexsyg research* reader (Richter et al., 2013) at the IRAMAT-CRP2A. We present a case study to track down a repetitive, unwanted effect on this device. Our contribution continues a discussion initiated at the German LED 2016 in Emmendingen (Kreutzer, 2016).

2. Measurement setup

Measurements were carried out on a Freiberg Instruments *lexsyg research* reader (Richter et al., 2013) at the IRAMAT-CRP2A, Bordeaux (reader id: 12-re-01-0007). The device is equipped with a ^{90}Sr/^{90}Y ring-source (Richter et al., 2012). For IR-RF signal detection a Chroma D850/40 interference filter was used in front of a Hamamatsu H7421-50 PMT. For bleaching, we used the built-in solar simulator (SLS). The SLS is equipped with LEDs comprising six different wavelengths (cf. Frouin et al., 2017). All bleaching and measurement settings followed the suggestions made by Frouin et al. (2017). Relevant protocol parameters are listed below.

The samples (BDX16646, BDX16650, BDX16651) used for the experiments originate from the Atlantic coast (Médoc) in the north-west of Bordeaux (France). Sample preparation was carried out using routine methods for preparing coarse grain feldspar samples (e.g., Preusser et al., 2008). The grain size of 100 200 µm was extracted by wet sieving. Chemical treatments comprised, HCl (10 %), H_2O_2 (30 %), LST heavy liquids (2.72 g cm^{-3}, 2.62 g cm^{-3}, 2.58 g cm^{-3}). The K-feldspar fraction was not further etched. The fine grain fraction (4-11 µm) was obtained by gentle crushing of the coarse grains with a mortar and applying the Stokes'law. Approximately 0.6 mg of sample material were settled on austenitic stainless steel cups[1] delivered by Freiberg Instruments. All measurements were done in air.

The data analysis was carried out using the **R** package 'Luminescence' (Kreutzer et al., 2012, 2017).

3. Identifying an artefact

In the following section, we describe two independent IR-RF experiments that raised our suspicions about the reliability of the measurement equipment.

3.1. Experiment I

Our measurement protocol, henceforth called RF_{70}, is based on the IRSAR protocol by Erfurt & Krbetschek (2003); further developed by Frouin et al. (2017). It was applied to the fine-grained K-feldspar (FG-KFS) fraction of sample BDX16646. The RF_{70} protocol consists of two IR-RF steps (natural: 3,600 s and regenerative: 10,000 s) separated by a

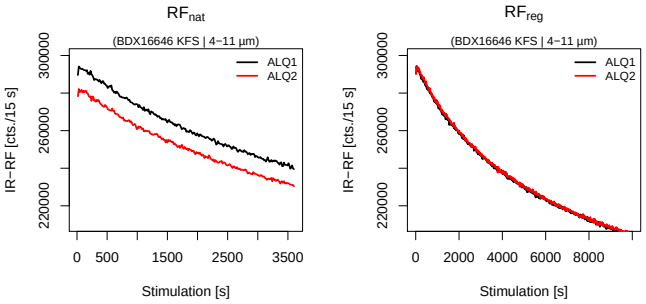

Figure 1. Results of RF_{70} measurements of sample BDX16646 after bleaching for 10,000 s. Two aliquots were measured. The left plot shows the natural IR-RF (RF_{nat}) curves, the right plot the regenerated IR-RF (RF_{reg}) curves. Please note that 'natural' here refers to the IRSAR and RF_{70} protocol nomenclature, indicating the first of the two measured IR-RF curves. For further details see main text.

bleaching (10,000 s) and a pause (3,600 s). Due to an artificial bleaching prior to the measurements (bleaching settings according to Frouin et al. 2017), the expected residual dose was supposed to be zero for both aliquots. The pause between the preceding artificial bleaching and the measurement was up to 2 days. The results of the measurements are shown in Fig. 1. Both regenerated IR-RF curves (RF_{reg}) are similar in shape and intensity (right plot). In contrast, the reset ('natural') IR-RF (RF_{nat}) curves (left plot), differ by ca. 4 % in their maximum intensity. Please note that, even the RF_{nat} was artificially bleached before measurement, we chose the term RF_{nat} for consistency with the published literature.

The equivalent doses (D_e) for the two aliquots were estimated with the horizontal sliding approach (Frouin et al. (2017)) and resulted in apparent doses of 0.9 {$Q_{2.5}$: -0.9 ; $Q_{97.5}$: 2.7} Gy (black curve) and 49.5 {$Q_{2.5}$: 45.0 ; $Q_{97.5}$: 54} Gy (red curves).[2] These results are unexpected for two reasons: (1) Due to the amount of grains (ca. 10^6) on each cup the inter-aliquot scatter was expected to be negligible and (2) the apparent dose should be approx. 0 Gy for both aliquots. In other words, the maximum RF_{nat} signal intensity difference of ca. 4 %, results in an apparent dose ca. 55 times higher for the second aliquot in comparison to the first aliquot.

Frouin et al. (2017) (supplement) showed that the relation between RF_{nat} and RF_{reg} can be written as

$$RF_{nat}(t) = RF_{reg}(t + t_n) + \varepsilon_t$$

where ε_t is the residual signal at time t within the co-domain $t \in \{t_{min}, ..., t_{nat_{max}}\}$. The simplification considers RF_{nat} to be an extract of RF_{reg}. Since the RF_{nat} curves in Fig. 1 (left) have different intensities, one would expect that they represent sections of the RF_{reg} curves in Fig. 1 (right). Hence, the red curve would have a flatter slope plotted than the normalised curve shows. Nevertheless, the normalised curves shown in Fig. 2 (left) reveal that both RF_{nat} curves have a similar shape leading to the speculation whether the determined dose is a measurement artefact.

[1] VA steal, quality: X15CrNiSi25-21, number: 1.4841, inner diameter: 7.95 mm, outer diameter: 9.95 mm, thickness bottom: 0.49 mm

[2] The terms $Q_{2.5}$ and $Q_{97.5}$ refer to the lower 2.5 % and the upper 97.5 % quantiles, respectively.

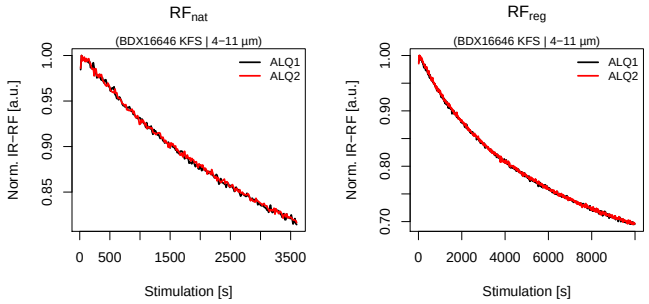

Figure 2. Similar as in Fig. 1, but with curves being normalised to the highest count value of each IR-RF curve.

3.2. Experiment II

The second experiment originally aimed at investigating potential short-time fading. The question whether the IR-RF suffers from anomalous fading (Wintle, 1973) is controversial and is discussed in the literature (e.g., Buylaert et al., 2012). However, so far no evidence for fading of the IR-RF signal has been presented. The sequence described in Table 1 aimed at detecting any short-term fading. The sequence consists of three steps: A pause of 3,600 s interspersed two IR-RF steps carried out at the SLS position (without bleaching).

Table 1. Measurement sequence used to investigate the short-term fading of the RF_{70} signal.

#	Step	Pos.	Obs.
1	Bleaching at 70 °C for 10,800 s	SLS	-
2	IR-RF measurements for 1,000 s at 70 °C after a stabilisation period of 900 s, channel resolution 15 s/channel	β-source	IR-RF
3	Pause for 3,600 s	SLS	-
4	Return to step 2	-	-

Four aliquots of the FG-KFS sample BDX16650 were measured. The sample was used in previous experiments with negligible sensitivity change. First, any residual signal was reset using the bleaching settings by Frouin et al. (2017) (Table 1, step 1). The full sequence was repeated three times for each aliquot.

The results for the four aliquots (represented by different colours) are shown in Fig. 3. Line styles indicate repeated cycles for the same aliquot. The pause of 3,600 s is indicated in the figure (please note the gap in the scale for the x-axis).

Figure 3 shows that (1) the IR-RF signals differ considerably between aliquots, which indicates that the observation made in Fig. 1 (similarity of the RF_{reg} of two aliquots) was coincidence, since this pattern could not be reproduced. (2) Although the general curve shapes appear similar, the intensities vary randomly with repetition. (3) The IR-RF signal after the pause is in two out of twelve cases higher (red circle) and for the remaining cases lower than the IR-RF signal before the pause. If the IR-RF signal of this particular sample did suffer from fading, the IR-RF signal after the pause would be higher in all cases. Nevertheless, the results of this experiment do not exclude a short-term IR-RF signal fading, but the experiment raised further questions about the reliability and reproducibility of the measurement system. Moreover, the IR-RF emission process cannot explain the observed differences in the IR-RF signal intensities.

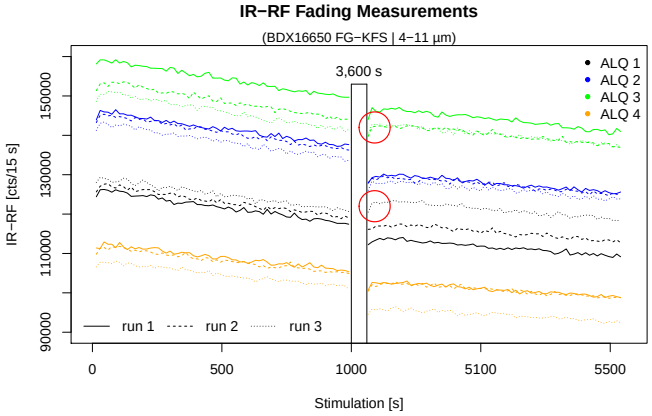

Figure 3. Fading measurements of the fine grain KFS fraction of sample BDX16650. IR-RF signals are recorded for 1000 s (ca. 60 Gy), with a pause of 3,600 s in between. The two red circles mark higher IR-RF signals after the pause. Colours code aliquots, line styles run numbers (repetitions). The solid lines represent the first series of measurements. The sample arm moved between each step. For further details see main text.

Therefore further experiments were carried out with the goal of discovering the reasons for the observed phenomenon.

4. Isolating instrument effects on results

4.1. Hypotheses

Assuming that a sudden change in the IR-RF intensity cannot be explained by the underlying physical IR-RF stimulation and emission processes, the observations need to be attributed to the used measurement system (software/hardware). Considering the design of the *lexsyg research* system (Richter et al., 2013), we hypothesised that the sudden change in the IR-RF sensitivity might have the following sources:

- A change in detection efficiency caused by the hardware (e.g., saturation effect in the PMT),
- a change in detection efficiency caused by the control software (e.g., buffer overflow),
- a change in the measurement geometry,
- a combination of reasons mentioned above.

We did not further investigate a change in detection efficiency caused by the control software since we did not have access to the source code of the *lexsyg research* control software. For the geometry change a further distinction can be made between (A) a drift of the sample carrier on the sample arm (cf. Appendix: Fig. 13 for a technical drawing showing

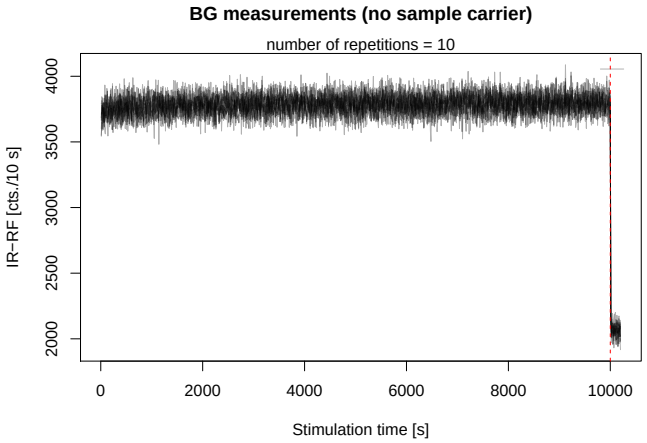

Figure 4. IR-RF background measurements without sample carrier and without load and unload step. The dashed red line indicates the closing of the shutter in front of the irradiation source.

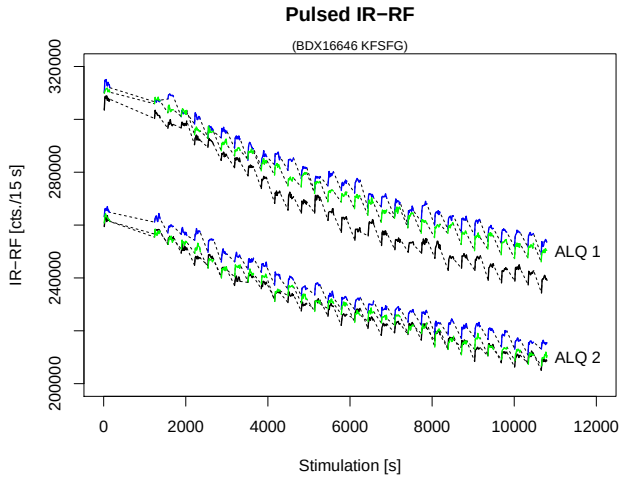

Figure 5. Pulsed IR-RF measurements. Colours indicate repetitions, the dashed line the applied real pause times.

the setup in the measurement chamber) and (B) an inaccurate sample arm positioning.

4.2. Background measurements

To test the overall reliability and reproducibility of the irradiation and the detection system, our first experiment aimed at repeatedly measuring the IR-RF background without a sample carrier on the sample arm and without a load and unload cycle in between. Therefore the sequence was modified manually after being created with the Freiberg Instruments *LexStudio2* software and consisted of the steps listed in Table 2.

Table 2. Background measurements without sample carrier and without load and unload step.

#	Step	Obs.
1	IR-RF for 10,100 s at room temperature, last 100 s: closed shutter	IR-RF
2	Pause of 60 s under the SLS position	-
3	Return to step 1	-

The last 100 s were recorded while the shutter in front of the β-source was closed (red dashed line). The measurements were repeated ten times. The results are shown in Fig. 4. Due to technical limitations, the pause of 60 s was not recorded and is not shown in the figure.

The measurements overlap and therefore cannot be distinguished in the figure. The results indicate a stable and reproducible IR-RF background with no sudden sensitivity change. This experiment was repeated with the following modified settings: (A) IR-RF for 1,000 s, 20 repetitions and (B) with an empty sample carrier and the sample arm under the source for 10 s, with load and unload cycle, 70 repetitions. All experiments gave consistent results and are not further reported. To summarise, the background measurements (with and without sample carrier) indicated no apparent technical problem, but showed a highly reliable and stable system.

4.3. Pulsed IR-RF measurements

Pulsed IR-RF measurements aimed at constructing a consecutively recorded presumed continuously decaying IR-RF curve, similar to the one shown, e.g., in Fig. 1. Except for the first channel (opening of the shutter), the combined pulsed IR-RF curve increments should result in a curve similar to a continuously recorded IR-RF curve. For the experiment, we used the previously measured FG-KFS sample (BDX16646). The sample was bleached before measuring using the internal SLS for 10,800 s, following the recommendations made by Frouin et al. (2017) (cf. Table 1, step 1). The sequence is listed in Table 3. 150 s of stimulation are followed by a pause of 1 s plus the time needed for the closing of the shutter located in front of the irradiation source. The stimulation-pause-cycle was repeated 30 times. Two aliquots were measured for one experiment, and the experiment was repeated three times. The results are shown in Fig. 5. The dashed lines indicate the applied pause under the irradiation source. No sample arm movement was assumed between the pause and the IR-RF measurements.

Table 3. Pulsed IR-RF sequence.

#	Step	Obs.
1	IR-RF measurements at 70 °C for 150 s, temperature stabilisation prior stimulation for 900 s	IR-RF
2	Pause of 1 s under β-source	-
3	IR-RF measurements at 70 °C for 150 s, no temperature stabilisation	IR-RF
4	Pause of 1 s under β-source	-
5	Return to step 3	-

The results reveal several unexpected effects.

- According to the sequence design the pause between each new IR-RF measurement should be 1 s. Instead, the time varied between 174 s and 179 s,

- the pause between the first and the second IR-RF signal appears to be even much longer,
- for all signals recorded during the 150 s intervals the intensity of the 1st channel was lower than for the 2nd one,
- the intensities recorded during the intervals show the expected decaying trend, but intensity levels vary considerably between subsequent intervals.

The long pause between the IR-RF measurements is the most striking observation. This pause is caused by a movement of the sample arm between each IR-RF step. After the pause of 1 s under the closed β-source, the sample arm moved to the SLS position and from there for an internal re-calibration to the calibration position (located between the maintenance position and TL-extra position, cf. Richter et al. (2013), before finally moving back to the irradiation position. Additionally, the photomultiplier tube (PMT) was switched off after each IR-RF measurement and restarted, including a temperature stabilisation phase, before any IR-RF signal detection (Andreas Richter, personal communication, March 2017). The time needed for the sample arm re-calibration and/or the temperature stabilisation of the PMT varies by a few seconds so that the effective pause between *all* IR-RF measurements varied between 174 s and 179 s. The pause between the first IR-RF measurement and the following one was attributed to a faulty set timestamp in the XSYG-file and thus is not real. The lower signal intensity of the first channel is attributed to the movement of the shutter in front of the irradiation source (approx. 100 ms; cf. supplement Frouin et al., 2017).

Further tests were carried out to determine whether the variation of the IR-RF signal intensity correlates with either the (A) on/off cycle of the PMT or (B) the sample arm movement itself.

4.3.1 Pulsed IR-RF - variation 1

To investigate the influence of the PMT run mode (on/off vs. continuous) and the sample arm movement (stopped vs. moving) on the IR-RF signal, the hardware control configuration file was modified manually. To consecutively exclude factors influencing the measurements, four different measurement modes were tested:

1. PMT mode: on/off | sample arm: moving
2. PMT mode: continuous | sample arm: stopped
3. PMT mode: on/off | sample arm: stopped
4. PMT mode: continuous | sample arm: moving

Setup #1 had already been tested in the previous experiments and was thus not repeated. Measurements with modes #2 to #4 were based on the pulsed IR-RF experiment described above (Table 3) using the same sample BDX16646 (FG-KFS). Before measuring the sample was reset using the internal SLS (similar bleaching settings as described above). The same aliquot was used for all experiments. The signal was not reset between each measurement. However, every new measurement mode required a reset of the reader hardware, i.e. every test was interrupted by a full system re-initialisation.

The results of the experiments are combined in Fig. 6, the dashed line indicates pause times. Green and red lines distinguish data measured without (#2 and #3) and with (#4) movement of the sample arm. Similar to Fig. 5 the time passed between the first and the second cycle is an artefact of the data format.

Figure 6 is divided into three areas, separating modes #2, #3 and #4. Figure 6-#2 shows data recorded with the PMT in continuous mode and without movement of the sample arm. Pauses between stimulation cycles were fixed at 5 s and only the shutter of the β-source was closed between cycles. The channel resolution was 15 s/channel, i.e. 10 data points were recorded during each 150 s interval and the pause of 5 s cannot be observed in Fig. 6-#2. The results do not reveal any sudden sensitivity change. Due to the off/on cycle of the PMT in mode #3, including temperature stabilisation, the recorded time between each cycle increased to 75 s. The IR-RF curves in Fig. 6-#3 show no considerable intensity change, indicating a high stabilisation and constant detection efficiency of the PMT. In contrast, mode #4 (Fig. 6-#4) included movement of the sample arm and the time between each IR-RF cycle increased to ca. 170 s. Our data show that for this experiment the IR-RF curves vary markedly for each cycle. Instead of an expected signal decrease of ca. 3 % from the 4th to 5th cycle, the IR-RF signal increases first by ca. 3 % (6th cycle) and by another 4 % for the 7th cycle. To increase the number of observations this experiment (setup #4) was repeated for 31 cycles, giving similar results (not shown).

These results indicate that the (1) on/off cycles of the PMT have no measurable influence on the signal intensity. The results also indicate that the unexpected IR-RF signal intensity changes are correlated with the movement of the sample arm and are caused by a change in the measurement geometry. Nevertheless, the results cannot reveal whether the geometry change is a product of an incorrect and varying sample arm positioning under the β-source or a movement of the sample carrier and/or the sample material itself triggered by the sample arm movement. To cancel out the one or the other possibility we performed another pulsed IR-RF experiment.

4.3.2 Pulsed IR-RF - variation 2

In the *lexsyg research* reader(s) operated at the IRAMAT-CRP2A the heating element is covered by a stainless steel plate, which is fixed by three screws (cf. Fig. 7). A custom made sample carrier ('teddy-bear' sample carrier), was mounted on the plate covering the heating element on the sample arm (Fig. 7) and fixed with two screws to prevent a movement of the sample carrier on the sample arm.[3]

The original experiment listed in Table 3 was repeated

[3] Please note the here described experiments are highly experimental, using non-automatised, manual settings. The manufacturer recommends none of these experiments, and wrong settings can seriously damage the measurement hardware.

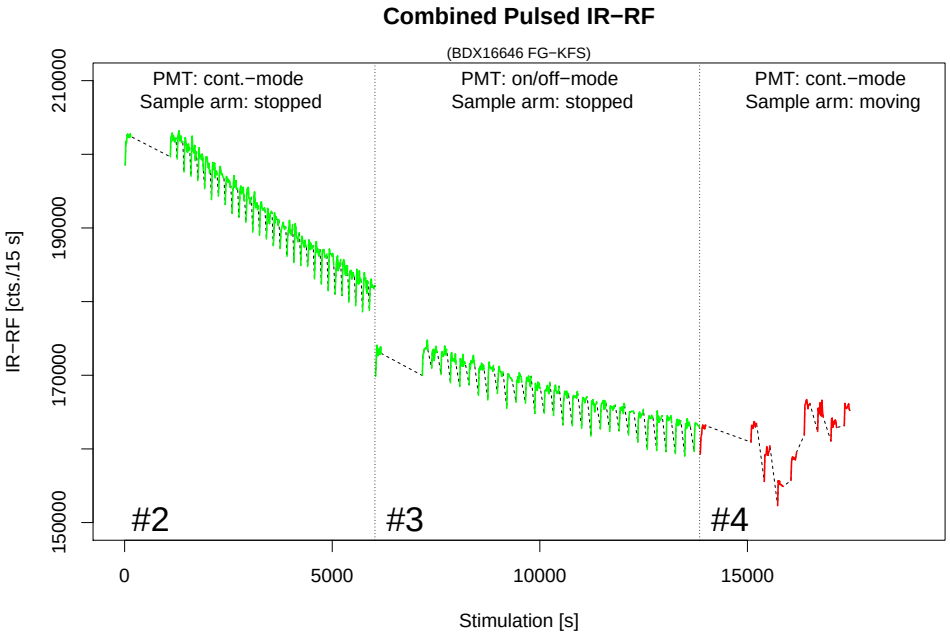

Figure 6. The figure shows a combination of three different pulsed IR-RF measurements. (#2) The PMT was operated in a continuous mode and the sample arm was not moving between each IR-RF cycle. (#3) The PMT was switched off and on between each shutter closing; the sample was not moving. (#4) The PMT was running in continuous mode, but the sample arm was allowed to move between each IR-RF simulation cycle. All measurements were carried out on one aliquot of the FG-KFS fraction of sample BDX16646. Dashed lines indicating passed time between each cycle. The dotted-dashed line separates the three different experiments. Colours emphasise the results. For further details see main text.

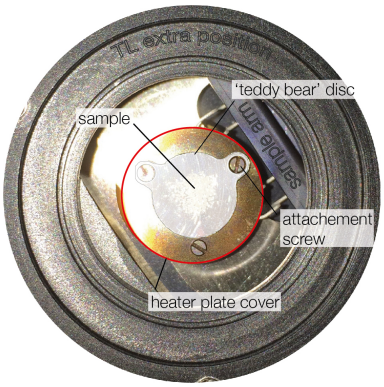

Figure 7. Photo of the sample arm with the heating plate and the special sample carrier ('teddy-bear' disc) fixed on the top. The picture was taken at the TL extra position Richter et al. (2013).

with this 'teddy-bear' disc. No other changes to the measurement settings were applied, i.e. the sample arm was allowed to move between each IR-RF cycle and the PMT automatically switched off and on. To be able to track individual grains, the natural coarse grain (100-200 µm) KFS fraction of sample BDX16646 was used instead of the bleached fine grain KFS fraction.

The grains were attached to the disc using silicon oil and a 4 mm mask. No SLS bleaching was applied. Results of this experiment are shown in Fig. 8. No unexpected IR-RF intensity change was observed during the IR-RF cycles. From this observation, we conclude that the believed geometry change is not related to a wrong positioning of the sample arm itself but a movement of the sample carrier on the sample arm. Photos of the sample carrier were taken before and after the experiment. No unwanted grain loss or grain movement on the disc is observed if silicon oil is used.

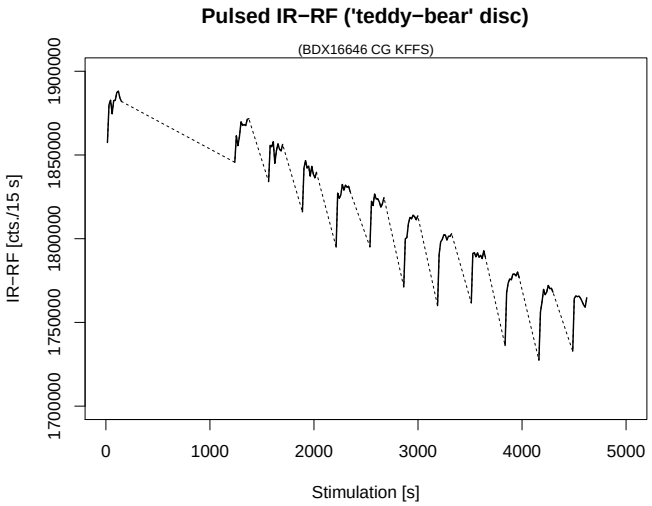

Figure 8. Results of pulsed IR-RF measurements on the coarse grain fraction of sample BDX16646 using a special sample carrier ('teddy-bear' disc). The disc was manually fixed on the stainless steel plate covering the heating element of the sample arm. The dashed lines indicate the real pause between each IR-RF measurement, except the first pause, which is data format artefact.

4.4. Varying heating temperature

Figures 5, 6 and 8 show that intensity of the first IR-RF cycle is always slightly lower than it would be expected from the overall trend of the signal decay. The first cycle differs from the others due to the additional temperature stabilisation over 900 s (Table 1) under the closed shutter of the β-source (administered dose due to Bremsstrahlung ca. 1 mGy). Such stabilisation was not carried out for the subsequent cycles, where the heating element was allowed to passively cool down before the temperature was increased again to 70 °C. Due to the high thermal inertia of the heating element, the measured temperature between the IR-RF curves was never lower than 60 °C.

To ensure that our conclusions were not biased by unwanted changes of the stimulation temperature, we conducted an experiment varying the applied measurement temperature. Therefore, the heating ramp was actively modulated allowing temperatures between 50 °C and 90 °C (cf. Fig. 9). The IR-RF signal of sample BDX16646 (fine grain, KFS) was recorded continuously. Prior to measurement, the sample was reset using the internal SLS.

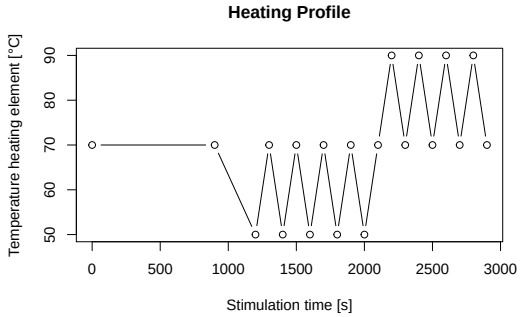

Figure 9. Preset heating profile as used for the 'varying heating temperature' experiment. After a stabilisation phase of 900 s the temperature is alternated between, (1) 70 °C and 50 °C and (2) between 70 °C and 90 °C.

Figure 10 (upper) shows the recorded IR-RF signal (black curve, 'NIR PMT'), the lower plot shows the temperature of the heating element recorded by the internal sensor in the heating element (red curve, 'Heating element'). The IR-RF detection started after a temperature stabilisation phase of 900 s (dashed line marked with '1'). Initially, the IR-RF signal remained stable even when the temperature was lowered to 50 °C, but dropped with a small delay while the temperature was increased again to 70 °C ('2'). The following IR-RF signals decrease sharply if the temperature is lowered and increase if the temperature is increased ('3', '4', '5'). The strongest decrease was observed after the temperature was first increased to 90 °C ('4') and then lowered to 70 °C ('5'). In contrast, for the experiments presented in Section 4.3 the maximum temperature was limited to 70 °C ('2'). The results show that temperature variations influence the IR-RF signal (e.g., Frouin, 2014). However, they cannot explain the observed light level changes, caused by the geometry change, but the chosen test sequence may have introduced an additional data scatter.

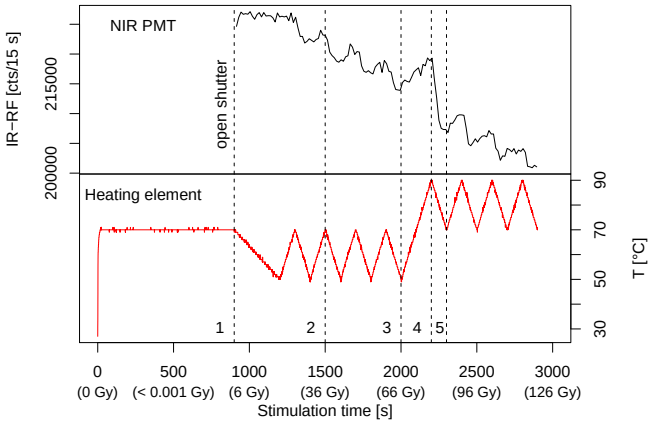

Figure 10. Results of the varying heating temperature experiment. The upper plot shows the recorded IF-RF signal and the lower plot the recorded temperature of the heating element (not the sample) using an internal sensor. Dashed lines and numbers in the plot label observations. The 2nd x-axis indicates the administered dose in Gy. For details see main text.

5. Discussion and further implications

Our findings demonstrate that the observed variation of the IR-RF signal intensity can be attributed to a change in the sample geometry. This geometry change appears to be induced by a movement of the sample carrier on the sample arm during its movement from one position in the reader to another. Krbetschek et al. (2000) considered the individual grain composition (non-emitting, less emitting grains) of each aliquot as the main factor for inter-aliquot scatter. Additionally, Erfurt (2003), Erfurt & Krbetschek (2003) and Erfurt et al. (2003) emphasised the general importance of a stable sample geometry. The original IRSAR protocol by Erfurt & Krbetschek (2003) explicitly demands a bleaching without geometry changes, but without giving further details, e.g., thresholds for allowed (or not allowed) geometry changes. For the investigated *lexsyg research* reader the general sample geometry appears to be unchanged, and the sample arm positioning seems to be precise. Nevertheless, our experiments revealed that the sample carrier does not remain stable on the sample arm causing a drop or a rise in the signal intensity from IR-RF cycle to IR-RF cycle.

5.1. What type of movement?

The question remains what type of movement occurs. The technical design (cf. Fig. 7) allows the sample carrier to drift laterally up to 0.5 mm, depending on the diameter of the sample carrier. The drift is limited by the screws on the metal plate covering the heater. Another possibility is a rotation of the sample carrier, which is potentially unlimited. To investigate the type of movement, photos of marked sample carriers on the sample arm were taken between arm movements. These experiments were performed on the *lexsyg research* systems at the IRAMAT-CRP2A in Bordeaux (France) and at the Justus-Liebig-University of Giessen (Germany). The results indicate that the sample carrier is likely to rotate *and* drift (Fig. 11).

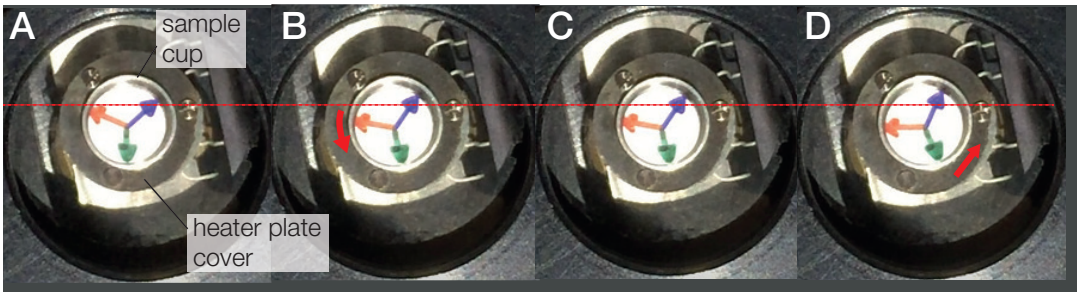

Figure 11. A set of four subsequent photos (A to D) taken of the sample arm holding a cup. The experiment was conducted with the *lexsyg research* reader 'Gauss' at the luminescence laboratory in Giessen. A paper with three arrows was placed on a standard sample cup. Red arrows indicate the movement of the sample carrier. Between each picture the sample arm was moved automatically by the reader. Between picture (A) and (B) the cup rotated slightly counterwise. No movement was observed from (B) to (C), while the cup slid upwards without rotation between (C) and (D).

5.2. Reasons for the movement

It is a tedious task to identify the reason for the movement beyond doubt, since the reasons may differ from reader to reader, and some of the systems might be not affected at all. For example: After its first weeks of operation, the system in Bordeaux suffered from a vibration of the sample arm. This issue was solved by a change of the drive chain. Such vibration can cause a drift of the sample carrier. Nevertheless, no vibration of the sample arm was observed for the *lexsyg research* readers in Giessen and Bordeaux in the course of these experiments.

Excluding this potential error source, it appears more likely that the drift and rotation of the sample carrier are favoured by a *combination* of two factors: (I) the radial movement of the sample arm (radial acceleration) and (II) a temperature-induced tension and bending of the metal plate covering the heating element. The heating element and the metal plate are made out of different materials (Andreas Richter, personal communication, March 2017). Differing thermal expansion coefficients force a faster expansion of the metal plate, which is fixed by the attachment screws. This setting is likely to cause a bending of the metal plate, producing a pivot point. If the sample arm starts the radial movement, the sliding friction is lowered, and the sample carrier can drift and/or rotate. In Bordeaux, the sample arm was removed from the reader for inspection and the bending of the covering metal plate has been confirmed.

The resulting sample carrier movement may appear small in absolute units ($\leqslant 0.5$ mm), but is significant concerning the typically measured grain size (4 µm up to 250 µm). Whether the observed effect correlates with the grains size has not been tested.

5.3. Impact

Our results proved an intensity change caused by the sample carrier movements. However, the final impact on the D_e cannot be easily quantified. It depends on the IR-RF curve shape of a sample and the position of the observed light level on the curve. In other words, the impact in absolute terms is higher if the observed signal is close to saturation. In Fig. 12 we try to provide an estimate of the impact of a particular relative change of intensity caused by the measurement equipment on the final D_e. The parameters for the shown IR-RF curve were obtained via curve fitting from the RF_{nat} curve shown in Fig. 1. Figure 12A simulates the impact of a 5 % intensity change for a normalised intensity of 0.84 (max. 1). Assuming that the unbiased D_e has an arbitrary value of 2935, an increase of the light level (no curvature change) would result in a D_e of 1908 (ca. -35 %) and 4414 (ca. $+50$ %) for a light level decrease, respectively. Figure 12B shows the relative impact on the D_e for five different levels of intensity changes (isolines).

The simulations demonstrate the curve shape caused leverage effect of a few percent of intensity variation on the final D_e. Thus, even minor intensity changes have a significant impact on the final D_e and should be avoided.

5.4. Correction approach

An important other question is whether and how the encountered effect can be corrected. An obvious solution would be a re-design by the manufacturer to maintain a stable sample geometry. Freiberg Instruments have already developed a new heating element without any covering metal plate. This re-design has been subject to preliminary tests in Freiberg (Germany) using a *lexsyg research* provided by the manufacturer. For the tests three different types of sample carriers: Al cups, stainless steel cups (henceforth VA) and Ni cups were placed on the re-designed sample arm. Photos were taken after each movement of the sample arm. No sample carrier movement was observed for Al cups and Ni cups. In contrast, VA cups (similar to the cups used in Bordeaux and Giessen) still showed a considerable movement (rotation and drift). Hence, the used VA sample carriers were re-polished to remove any irregularities in thickness, and the tests were repeated. However, the procedure could not reduce the sample carrier movement, which indicates that the used VA sample carriers suffer from distortion stress. To overcome this problem the production process of the carriers must be modified. According to Freiberg Instruments, future plans include stress relief annealing during the produc-

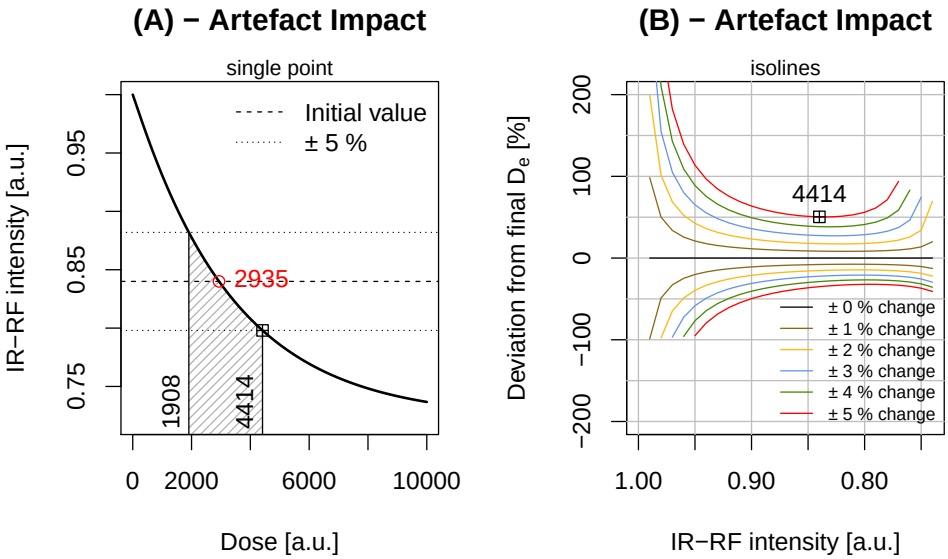

Figure 12. Impact simulation of light level changes on the final D_e. (A) The grey shaded area indicates the impact on the final D_e if the IR-RF intensity is increased (1908) or is decreased (4414) by 5 %. (B) Isolines showing the expected relative deviation from the 'unbiased' D_e for different percentages of light level change. The crossed rectangle in both curves marks a similar change of light level and its impact in both plots. Both figures based on curve parameters obtained via fitting from sample BDX16646 FG-KFS and are limited to them. For further details see main text.

tion process (Kay Dornich, personal communication, March 2017).[4]

Until these changes have been made, we tested a data post-processing approach. Three assumptions were made:

- The change in the luminescence intensity is caused by a focus change under the PMT, i.e. the emission is dominated by different grains (of the sample aliquots),
- the IR-RF signal shape is not significantly affected due to an averaging effect of the multiple grain aliquot,
- bleaching and irradiation are homogeneous over the area of the metal plate.

The net effect would be a change in detection sensitivity without a change in the IR-RF signal shape. These assumptions allow for a vertical sliding of the RF_{nat} curve instead of only a horizontal sliding as suggested previously (Frouin et al., 2017). In other words, to obtain the D_e of a sample the RF_{nat} curves were moved horizontally and vertically (x- and y-direction, but no rotation) until the best match with the RF_{reg} was found. The new position which was obtained by searching the global minimum for the squared residuals from RF_{nat} and RF_{reg} was taken as best fit of both curves.

We tested this approach with the curves from Fig. 1. For the red curve of samples BDX16646 (FG-KFS) this correction results in an apparent dose of 9 {$Q_{2.5}$: 7.2 ; $Q_{97.5}$: 108} Gy (red curves), instead of 49.5 {$Q_{2.5}$: 49.0 ; $Q_{97.5}$: 54} Gy (red curves). The results of the black curve RF_{nat} (Fig. 1 left plot) remained unchanged. Although the expected dose was 0 Gy, the inter-aliquot scatter was reduced markedly by ca. 80 %.

[4]Later tests carried out by Freiberg Instruments showed no sample carrier movement for the new setup even for VA cups. However, this could not further be verified before the manuscript was finished.

We further re-analysed the samples investigated by Frouin et al. (2017) and we found, except for sample BT706 (20.3 ± 3.5 ka instead of 28.2 ± 8.7 ka) no 'improvement' of the ages towards a better match with the independent age control. All other results remained similar within errors, but the coefficient of variation (inter-aliquot scatter) was reduced in 6 out of 9 cases by 3 % for sample FER3 up to 49 % for sample BT706. Thus, it appears that a correction by vertical sliding may partly help to reduce the inter-aliquot scatter and correct for the above-described signal intensity change. The remaining inter-aliquot scatter may be attributed to natural grain variation as suggested by Krbetschek et al. (2000) and supported by a study on single grains by Trautmann et al. (2000).

5.5. Further implications

Our results show the overall importance of a stable sample geometry for measuring IR-RF. We, therefore, recommend cross-checking results obtained with automatic systems and pay attention to effects described above.

Furthermore, the presented experiments are limited to IR-RF measurements only. However, there is no reason to believe that the movement of the sample carrier only affects IR-RF measurements. Therefore, we cross-checked optically stimulated luminescence (OSL) quartz calibration measurements carried out between 2015 and 2017 using Risø calibration quartz batch 90. In total, the results of six machines available at the IRAMAT-CRP2A were compared: Two *Risø TL/OSL DA20* (e.g., Bøtter-Jensen, 1997), two *lexsyg SMART* (Richter et al., 2015) and two *lexsyg research* readers; this includes the *lexsyg research* reader investigated in this study. We found no evidence for a higher coefficient of variation. Nevertheless, taking into account the small num-

ber of observations (total number of measured aliquots per system: 25 to 30) such an effect cannot be excluded. Therefore we recommend that each system is tested independently.

5.6. Limitations of this study

We investigated sample carrier movements on *lexsyg research* systems in Bordeaux, Giessen and (briefly) in Freiberg. On all tested systems, sample carrier movements were observed. However, for the system in Freiberg with the re-designed sample arm, the movement was limited to VA cups only. For the system in Giessen, the sample arm movement appeared to be slightly lower than for the system in Bordeaux. Nevertheless, the detailed IR-RF measurements presented here were only carried out on one system in Bordeaux. From re-analysed IR-RF measurements performed on the system in Giessen, we have no clear evidence for effects on the IR-RF signal itself. Furthermore, we did not investigate whether the sample carrier preparation (grain mounting: 'monolayer' vs. 'multilayer') might influence the observed change in signal intensity.

6. Conclusions

A non-systematic luminescence intensity change while measuring the IR-RF signal of K-feldspar was identified. The change leads to a higher inter-aliquot scatter in measured dose values. We identified a lateral shift (up to 0.5 mm) and/or a rotation of the sample carrier on the heater plate covering the heating element. We further conclude:

- Our experiments are limited to a particular *lexsyg research* reader installed at the IRAMAT-CRP2A.
- We observed sample carrier movements for *lexsyg research* readers at the luminescence laboratories in Bordeaux and Giessen. However, clear evidence for an effect on the IR-RF signal was observed for the reader in Bordeaux only.
- We tested a re-designed sample arm at Freiberg Instruments, which showed no sample carrier movement for Al and Ni cups, but still for VA cups. The movement of the latter is believed to be caused by distortion stress.
- The impact of the intensity change on a D_e is sample dependent and cannot be properly quantified. However, due to the stretched exponential curve shape, even minor intensity changes cause a significant impact on the D_e.
- We tested a data post-processing approach to correct for the unwanted IR-RF signal intensity change combining vertical and horizontal curve sliding. The method was capable of reducing the inter-aliquot scatter for the tested samples by 3 % up to 49 %. However, it remains unclear whether this approach is capable of fully correcting the observed change in signal intensity.
- No statistical evidence was found for a higher inter-aliquot scatter for OSL on the same reader, though further measurements are needed to confirm these results.

Finally, our results show that unwanted instrument effects are not always directly visible, but they are capable of considerably biasing measurement results.Thus, the increased complexity of the measurement systems demands a careful differentiation between system induced effects and sample properties.

Acknowledgements

Our manuscript benefited considerably from constructive input by Ashok Singhvi and Regina DeWitt. The authors further thank Guillaume Guérin for cross-checking the irradiation source calibration results. We thank Andreas Richter for his support while modifying the stack of the *lexsyg research* reader enabling the conducted experiments and for discussing the results. Rico Schweigel carried out the tests with the re-designed sample arm. The work of Sebastian Kreutzer is financed by a programme supported by the ANR - n° ANR-10-LABX-52. Madhav Krishna Murari is supported by the German Research Foundation (DFG A/C: 62201694).

Appendix

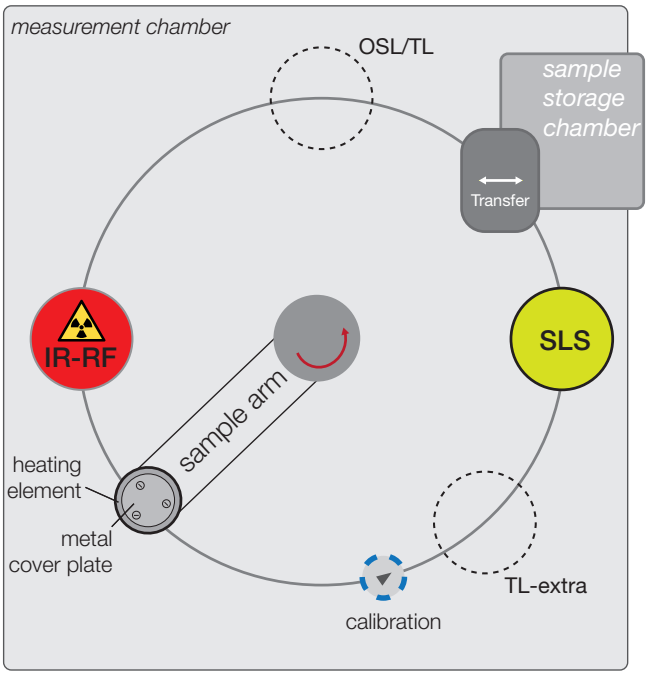

Figure 13. Technical drawing after Richter et al. (2013) showing the layout of the measurement chamber of a *lexsyg research* reader.

References

Adamiec, G., Heer, A., and Bluszcz, A. *Statistics of count numbers from a photomultiplier tube and its implications for error estimation*. Radiation Measurements, pp. 1–14, 2011.

Bøtter-Jensen, L. *Luminescence techniques: Instrumentation and methods*. Radiation Measurements, 27(5/6): 749–768, 1997.

Bray, H.E., Bailey, R.M., and Stokes, S. *Quantification of cross-irradiation and cross-illumination using a Risø TL/OSL DA-15 reader*. Radiation Measurements, 35(3): 275–280, 2002.

Buylaert, J.P., Jain, M., Murray, A.S., Thomsen, K.J., and Lapp, T. *IR-RF dating of sand-sized K-feldspar extracts: A test of accuracy*. Radiation Measurements, 47(9): 759–765, 2012.

Erfurt, G. *Radiolumineszenzspektroskopie und -dosimetrie an Feldspäten und synthetischen Luminophoren für die geochronometrische Anwendung*. PhD thesis, Technische Universität Bergakademie Freiberg, 2003.

Erfurt, G. and Krbetschek, M.R. *IRSAR - A single-aliquot regenerative-dose dating protocol applied to the infrared radiofluorescence (IR-RF) of coarse-grain K-feldspar*. Ancient TL, 21(1): 35–42, 2003.

Erfurt, G., Krbetschek, M.R., Bortolot, V.J., and Preusser, F. *A fully automated multi-spectral radioluminescence reading system for geochronometry and dosimetry*. Nuclear Instruments and Methods in Physics Research Section B: Beam Interactions with Materials and Atoms, 207(4): 487–499, 2003.

Frouin, M. *Les feldspaths comme support pour la datation par luminescence de gisements archéologiques et de séquences quaternaires d'Aquitaine*. PhD thesis, Université Bordeaux Montaigne, France, 2014.

Frouin, M., Huot, S., Mercier, N., Lahaye, C., and Lamothe, M. *The issue of laboratory bleaching in the infrared-radiofluorescence dating method*. Radiation Measurements, 81: 212–217, 2015.

Frouin, M., Huot, S., Kreutzer, S., Lahaye, C., Lamothe, M., Philippe, A., and Mercier, N. *An improved radiofluorescence single-aliquot regenerative dose protocol for K-feldspars*. Quaternary Geochronology, 38: 13–24, 2017.

Huot, S., Frouin, M., and Lamothe, M. *Evidence of shallow TL peak contributions in infrared radiofluorescence*. Radiation Measurements, 81: 237–241, 2015.

Kadereit, A. and Kreutzer, S. *Risø calibration quartz – a challenge for β-source calibration. An applied study with relevance for luminescence dating*. Measurement, 46(7): 2238–2250, 2013.

Krbetschek, M.R., Trautmann, T., Dietrich, A., and Stolz, W. *Radioluminescence dating of sediments: methodological aspects*. Radiation Measurements, 32(5-6): 493–498, 2000.

Kreutzer, S. *Lab report: IR-RF and should we care about the a-value?* German LED 2016, 2016-11-04 to 2016-11-06, Emmendingen, Germany, 2016.

Kreutzer, S., Schmidt, C., Fuchs, M.C., Dietze, M., Fischer, M., and Fuchs, M. *Introducing an R package for luminescence dating analysis*. Ancient TL, 30(1): 1–8, 2012.

Kreutzer, S., Hülle, D., Thomsen, K.J., Hilgers, A., Kadereit, A., and Fuchs, M. *Quantification of cross-bleaching during infrared (IR) light stimulation*. Ancient TL, 31(1): 1–10, 2013.

Kreutzer, S., Dietze, M., Burow, C., Fuchs, M.C., Schmidt, C., Fischer, M., and Friedrich, J. *Luminescence: Comprehensive Luminescence Dating Data Analysis*, 2017. URL https://CRAN.R-project.org/package=Luminescence. R package version 0.7.4.

Lomax, J., Kreutzer, S., and Fuchs, M. *Performance tests using the lexsyg luminescence reader*. Geochronometria, 41(4): 327–333, 2014.

Murray, A.S. and Wintle, A.G. *Luminescence dating of quartz using an improved single-aliquot regenerative-dose protocol*. Radiation Measurements, 32(1): 57–73, 2000.

Preusser, F., Degering, D., Fuchs, M., Hilgers, A., Kadereit, A., Klasen, N., Krbetschek, M.R., Richter, D., and Spencer, J.Q.G. *Luminescence dating: basics, methods and applications*. Eiszeitalter und Gegenwart (Quaternary Science Journal), 57(1-2): 95–149, 2008.

Richter, D., Pintaske, R., Dornich, K., and Krbetschek, M.R. *A novel beta source design for uniform irradiation in dosimetric applications*. Ancient TL, 30(2): 57–63, 2012.

Richter, D., Richter, A., and Dornich, K. *lexsyg — a new system for luminescence research*. Geochronometria, 40(4): 220–228, 2013.

Richter, D., Richter, A., and Dornich, K. *Lexsyg smart — a luminescence detection system for dosimetry, material research and dating application*. Geochronometria, 42(1): 202–209, 2015.

Schmidt, C., Kreutzer, S., Fattahi, M., Bailey, R.M., Zander, A., and Zöller, L. *On the luminescence signals of empty sample carriers*. Ancient TL, 29(2): 65–74, 2011.

Thomsen, K.J., Murray, A.S., Jain, M., and Bøtter-Jensen, L. *Laboratory fading rates of various luminescence signals from feldspar-rich sediment extracts*. Radiation Measurements, 43(9-10): 1474–1486, 2008.

Trautmann, .T, Krbetschek, M.R., Dietrich, A., and Stolz, W. *Feldspar radioluminescence: a new dating method and its physical background*. Journal of Luminescence, 85(1-3): 45–58, 1999.

Trautmann, T., Krbetschek, M.R., and Stolz, W. *A systematic study of the radioluminescence properties of single feldspar grains*. Radiation Measurements, 32(5-6): 685–690, 2000.

Wagner, G.A., Krbetschek, M.R., Degering, D., Bahain, J.-J., Shao, Q., Falguères, C., Voinchet, P., Dolo, J.M., Garcia, T., and Rightmire, G.P. *Radiometric dating of the type-site for Homo heidelbergensis at Mauer, Germany*. Proceedings of the National Academy of Sciences, 107(46): 19726–19730, 2010.

Wintle, A.G. *Anomalous Fading of Thermoluminescence in Mineral Samples*. Nature, 245: 143–144, 1973.

Reviewer

Ashok Singhvi, Regina DeWitt

Thesis Abstracts

Index

Nathan D. Brown	p. 31
Debra Colarossi	p. 32
Yujie Guo	p. 32
Gang Hu	p. 33
Amit Kumar Prasad	p. 34

Nathan D. Brown

Using luminescence signals from bedrock feldspars for low-temperature thermochronology

June 2017

University of California, Los Angeles, USA

Degree: Ph.D.

Supervisors: T. Mark Harrison, Edward J. Rhodes

Over the past several years, optically-stimulated luminescence signals (OSL) from quartz and infrared-stimulated luminescence (IRSL) from feldspar in bedrock have been investigated for their use in thermochronology. In this study, I propose using thermoluminescence (TL) from feldspar instead. Because TL is measured by gradually heating a sample, the luminescence emissions correspond to electron traps of increasing thermal stability. The primary goal of this dissertation is to describe how this signal can be optimally measured and interpreted to understand the recent thermal history of bedrock samples.

I first modified the laboratory luminescence reader to allow us to irradiate feldspar samples at a range of dose-rates, from 8.7×10^{-5} to 1.2×10^{-1} Gy/s to estimate the influence of dose-rate on the subsequent TL signals. Although less stable sites were not preferentially populated at higher dose-rates (an unexpected result), I did observe an increase in brightness at the lowest dose-rate, a result which may suggest that the dose-rate influences recombination or trapping competition probabilities. In natural TL signals, I observed the expected trend of greater site occupancy at lower measurement temperatures with higher dose-rates.

Next, I perform several experiments to relate the TL signal that I monitor to OSL and IRSL from feldspar. I propose that the TL signal preserves a more detailed structure of trapping stability than the optically-stimulated signals, which derive from the full range of TL stabilities. Moreover, preheating and phototransfer effects may redistribute trapped charge, potentially leading to inaccuracies in IRSL or post-IR IRSL thermochronology techniques.

I develop a novel method for determining the activation energy, effective frequency factor, and kinetic order values for natural and regenerative TL signals. This 'post-isothermal TL' method reveals that for the blue-green emission of the low-temperature TL peak, the apparent trap depth in measured bedrock K-feldspar samples increases to a depth of $\geq$1.9 eV as measurement temperature increases, at which point it reaches a plateau in some samples. If this plateau value is the true depth of the trap, the frequency factors are measured to decrease as measurement temperature increases, an observation consistent with the recent conception that feldspar luminescence (IRSL and TL) results from excited-state tunneling to randomly-distributed centers.

Three archived drill cores were sampled at depths corresponding to burial temperatures ranging from -4.1 to 60.2 °C. With higher ambient temperatures, there is a linear increase in the feldspar TL $T_{1/2}$ value (measurement temperature at half-maximum emission intensity) and a reduction in signal intensity. This behavior can be replicated by isothermal treatments in the laboratory. I interpret this behavior as reflecting the continuum of trap lifetimes present in feldspar TL, an observation that I substantiate with additive dose experiments and a numerical model.

I collected bedrock samples along vertical and longitudinal profiles within a glacial valley to investigate their thermal history. Using the relationship observed with the drill core samples, I successfully predict the ambient temperature of these samples from their $T_{1/2}$ values. By measuring the single-aliquot regenerative (SAR) equivalent dose (D_e) values at the natural $T_{1/2}$ positions, I estimated the maximum time that each sample has been at its current surface temperature. These ages correlate with periods of local glacial activity and offer insight into the erosional mechanisms involved, including post-glacial high-elevation plateau erosion: a key prediction of the glacial buzzsaw hypothesis.

Although a maximum age is useful, a more desirable solution is a continuous $T-t$ history. The final chapter pursues this goal with samples taken from a rapidly-uplifting Yucaipa Ridge tectonic block (YRB). I introduce a multiple-aliquot additive-dose (MAAD) measurement protocol that can be used to estimate the degree of dose saturation as a function of measurement temperature, $\frac{n}{N}(T)$. This MAAD TL $\frac{n}{N}(T)$ method capitalizes on the earlier observation of feldspar TL, that site stability increases with measurement temperature. Using the same kinetic model used to describe the drill core samples, I simulate two previously-proposed geologic cooling scenarios for the YRB and the model is found to be sensitive enough to discriminate between them. I then measure MAAD TL signals for several YRB samples, convert these to $\frac{n}{N}(T)$ functions, and use Monte Carlo simulations to invert for each sample's thermal history. Despite the vertical

relief being only about 0.4 km between the highest and lowest samples, the difference in trap saturation is significant, suggesting that this technique may be well suited to resolving Quaternary landscape evolution. I interpret the exhumation histories of these samples to reflect a combination of post-uplift relaxation of isotherms and a lagged erosional response in the form of fluvial downcutting.

Debra Colarossi

Developing luminescence chronometers to establish the timing of late Quaternary environmental changes in South Africa

January 2017

Department of Geography and Earth Sciences, Aberystwyth University, Aberystwyth, SY23 3DB, UK

Degree: Ph.D.

Supervisors: Prof Geoff Duller, Prof Stephen Tooth

The predominantly dryland climate of interior South Africa precludes the widespread preservation of organic proxy records. Various potential geoproxy records exist, but their exploitation requires accurately constrained chronologies. This study investigates the development of two luminescence chronometers, quartz OSL and K-feldspar post-IR IRSL. At four sites across the eastern interior (Moopetsi, Voordrag, St Paul's and Goedgedacht), these chronometers are used to constrain the timing of: (i) the late Quaternary initiation of deposition; (ii) intervening phases of erosion, deposition and pedogenesis; and (iii) the current deep erosional phase.

The value of using paired ages (i.e. determining quartz and K-feldspar ages from the same sample) becomes apparent, particularly at Voordrag where quartz OSL reaches saturation within the limit of radiocarbon dating. Paired chronologies show good agreement for younger samples ($<$24 ka) but systematic underestimation of quartz ages for older samples.

Investigation of the post-IR IRSL protocol showed that signal transfer between the Lx and Tx measurements caused systematic underestimation of older feldspar ages. Dose recovery tests showed that it was not possible to recover a large given dose (400 Gy) when using a small (5 Gy) test dose. Two solutions were investigated, specifically increasing the size of the test dose to 30 % of the De value and increasing the IR stimulation time. This led to the development of a modified post-IR IRSL protocol.

The derived quartz and K-feldspar single grain chronologies show that the initiation of deposition was not synchronous at the four study sites, and ranges from $\sim$153–65 ka. Intervening phases of erosion, deposition and pedogenesis remain difficult to constrain but broad inferences regarding climatic and geomorphic drivers can be made. The current phase of deep erosion appears to be linked to two periods of abrupt climate change, the 3.8–4.2 ka arid event and the Little Ice Age.

Yujie Guo

Luminescence dating of late Quaternary deposits in the Nihewan Basin, northern China: chronology and implications for Palaeolithic archaeology and environmental reconstructions

August 2016

School of Earth & Environmental Sciences, University of Wollongong, Wollongong, Australia

Degree: Ph.D.

Supervisors: Professor Richard G. Roberts (Principal Supervisor); Dr. Bo Li (Co-supervisor)

The Nihewan Basin is a key region to study Quaternary palaeoenvironmental, palaeontological and Palaeolithic histories in East Asia. Although many studies have been carried out over the last few decades, many questions remain unanswered. This thesis focuses on three of the most debated questions about the Nihewan Basin: 1) when and why did the Nihewan palaeo-lake disappear and the Sanggan River form?; 2) did the Middle Palaeolithic stage really exist in the Nihewan Basin?; 3) was the Upper Palaeolithic microblade technology developed from the local small-tool technology in the Nihewan Basin or was it imported from elsewhere? These questions are debated mainly due to the lack of firm chronological control for the late Quaternary stone artefact-bearing sediments in the basin. This thesis, therefore, aims to answer these questions from a chronological perspective, by studying six stone artefact-bearing lacustrine or fluvial sedimentary sections. My specific aims are to: 1) reveal the time of transition from the Nihewan palaeo-lake to the Sanggan River; 2) test the assignment of sites to the so-called Middle Palaeolithic in the Nihewan Basin based on their numerical chronologies; and 3) establish a chronological sequence for the small-tool and microblade technologies of the Upper Palaeolithic stage in the Nihewan Basin.

To achieve the first two aims, three Palaeolithic sitesMotianling (which captures the final stages of lacustrine sediment deposition), Queergou (representing lakeshore sediments) and Banjingzi (located on a fluvial terrace of the Sanggan River)have been selected for study. These sites have been assigned previously to the Middle Palaeolithic based mainly on stratigraphic correlations (at Motianling and Queergou) and uranium-series (U-series) age estimates (at Banjingzi), corresponding to a time period between about 30 and 140 thousand years (ka) ago. This time definition is the most commonly used criterion for assigning sites to the Middle Palaeolithic. However, the lithic assemblages at these sites are very different, and this might reflect the incorrect assignment of these three sites to the Middle Palaeolithic stage, given the lack of firm age control at each of them.

The sediment samples collected from the Motianling and Queergou sites were dated using the newly developed predose multi-elevated-temperature post-infrared IRSL (predose MET-pIRIR, or pMET-pIRIR) procedure for single aliquots composed of potassium feldspar (K-feldspar) grains, where the acronym IRSL refers to infrared (IR) stimulated

luminescence. The Banjingzi site was dated using the MET-pIRIR procedure applied to single grains of K-feldspar. I first tested and applied the pMET-pIRIR procedure using the lacustrine and fluvial sediments in the Nihewan Basin. The IRSL ages for the cultural layers at Motianling, Queergou and Banjingzi are 315 ± 13 ka, 268 ± 13 ka and 86 ±4 ka, respectively, suggesting that the Motianling and Queergou sites should be assigned to the Lower Palaeolithic on chronological grounds, while the age of Banjingzi is consistent with its Middle Palaeolithic attribution. The ages obtained for these sites also indicate that the Sanggan River formed between about 270 and 86 ka ago, but details of the process of demise of the Nihewan palaeo-lake and the formation of the Sanggan River, and the factors responsible for these events, need to be further investigated in the future.

Xibaimaying has been considered as the latest small-tool site in the Nihewan Basin, based on the U-series ages of about 15 and 18 ka on animal bones. To address the third aim, I redated this site using well-established optically stimulated luminescence (OSL) dating methods for single grains of quartz. The resulting OSL ages indicate that the cultural layer was deposited 46 ± 3 ka ago, during marine isotope stage (MIS) 3 - more than 20 millennia earlier than previously thought and also older than the earliest primitive microliths found at the site of Zhiyu, which has a calibrated ^{14}C age of ∼31–39 ka cal BP (where BP means before present: AD 1950 by correction), and the earliest typical microliths known from the site of Youfang (dated by OSL to ∼26–29 ka). These new ages for human occupation of Xibaimaying remove support for the existing, commonly held concept of parallel development of the small-tool and microblade industries in the Nihewan Basin during the Upper Palaeolithic. However, reliable age estimates from additional sites are needed to confidently infer the nature of the chronological relationship between these two Upper Palaeolithic industries and the associated toolmakers.

Two additional microblade sites, Erdaoliang and Dadiyuan, were also dated as part of this study, to further contribute to the Palaeolithic chronological framework for the Nihewan Basin. Both sites were dated using conventional OSL dating methods for single aliquots and single grains of quartz. The OSL ages indicate that the cultural layers at Erdaoliang and Dadiyuan were deposited 24.1 ± 1.8 and 8.9 ± 0.5 ka ago, respectively.

The thesis concludes with a generalised Palaeolithic chronological framework for the Nihewan Basin, extending from ∼1.95 million years (Ma) ago to ∼7.0 ka ago, based on the luminescence chronologies for the sites dated in this study and on the numerical chronologies developed for other sites in the basin. Suggestions are also made for possible future lines of enquiry, to resolve outstanding questions about the history of human occupation and environmental change in northern China

Gang Hu

Optically stimulated luminescence dating of glacial sediments in the Laohugou Valley, western Qilianshan and the Basongcuo Catchment, eastern Nyainquentanglha

May 2014

Institute of Tibetan Plateau Research, Chinese Academy of Sciences, Beijing, China

Degree: Ph.D.
Supervisor: Chaolu Yi

The Tibetan Plateau is often referred to as the Third pole of the world, with 1/3 of the mountain glaciers outside the polar regions. Widely distributed landforms and sediments produced by Quaternary glaciations offer us an opportunity to understand glacier changes associated with climatic change. However, insufficient chronological data of glacial deposits limit our understanding of this process. Optically stimulated luminescence (OSL) has been applied widely in dating of Quaternary sediments in the areas where organic material for ^{14}C dating is lacking. However, partial bleaching is a common problem for dating glacial sediment and can lead to age overestimation.

In this study, Quaternary glaciations in the Laohugou Valley of the western Qilianshan and the Basongcuo Catchment of Eastern Nyainquentanglha were identified by field survey. Eight samples from the Laohugou Valley and 39 samples from the Basongcuo Catchment were collected from the glacial sediments for OSL dating, respectively. The fractions of coarse-, medium-, fine-grained quartz grain and polymineral fine grain were dated. The results show that the OSL signals of all the sediments are dominated by the fast component and that the thermal transfer effect is very low, suggesting the quartz is suitable for OSL dating. The fine-grained quartz is better bleached than the medium grain in glacial sediment of the Basongcuo Catchment. Some of the fine grains might come from aeolian dust in local area. The post-IR IRSL ages of the polymineral fine grains are much older than those of quartz grains, suggesting feldspar is poorly bleached. Using small aliquot and minimum age model, we can gain reliable OSL ages for the glacial sediments.

The OSL dates show that the glaciers advanced during the global LGM and re-advanced or kept in the Late Glacial in the Laohugou valley. The outwash terrace was formed at 10 ± 1.7 ka and 0.5 ± 0.7 ka, suggesting extensive glacial retreat in that time. The moraines in the Basongcuo Catchment could be assigned to four stages. The ages of Stage-I, -II and -III occurred between 0.2–1.3 ka, ∼7.5 ka and 10–13 ka, respectively. The glacier displayed several short-time advances during Stage-IV, which lasted from ∼30 to ∼16 ka.

The OSL dates show that the glacier advance in the Laohugou valley of the western Qilianshan was consistent with the glacier advance of the eastern Qilianshan. Considering the annual precipitation increases notably from west to east, we argue that the temperature mainly contributed to the glacier advance. The OSL dates of the glacial sediments

in the Basongcuo Catchment, Eastern Nyainquentanglha are consistent with those in the surrounding area. Comparing the ages of glacier advances with the insolation, effective moisture and speleothem records from Dongge-Hulu cave, we argue that the glacier advances in the Basongcuo Catchment were also controlled by temperature.

Those who are interested in this thesis can ask the Dr Gang Hu (hugang@itpcas.ac.cn) or Dr. Chaolu Yi (clyi@itpcas.ac.cn) for provision.

Amit Kumar Prasad

Understanding defect related luminescence processes in wide bandgap materials using low temperature multi-spectroscopic techniques

January 2017

Center for Nuclear Technologies, Technical University of Denmark, Risø Campus, Roskilde 4000

Degree: Ph.D.

Supervisors: Dr. Mayank Jain (main supervisor) and Dr. Torben Lapp (co-supervisor)

Feldspar is a dominant, naturally occurring mineral that comprises about ∼60 % of the Earths crust. It is widely used in optically stimulated luminescence (OSL) dating of sediments to obtain chronologies of past events as old as ∼0.5 Ma, and thus, plays a crucial role in understanding Quaternary climate changes, landscape development and human evolution and dispersal. Optical properties of feldspar originate from a) a wide band gap (∼7.7 eV), b) crystal defects (impurity atoms and distortions) that create localized energy states within the bandgap, and c) conduction band and the low-mobility band tail states, which play a role in charge transport. Despite a rapid progress in the infra-red stimulated luminescence (IRSL) dating technique using feldspar, a clear understanding of luminescence process is still lacking. A better understanding of feldspar as a physical system is expected to lead to its improved exploitation as a luminescence chronometer. My Ph.D. investigates the nature of luminescence generating defects and processes in feldspar, and tests whether the intra-defect relaxation transitions may be successfully used to improve the dating technique. It includes mapping the energy states of defects individually and characterizing their emission process, understanding the dynamics of the excited-state relaxation and tunneling, and defect interactions with the crystal lattice and the band tail states. The experiments were carried out using the Risø station for CryOgenic LUminescence Research (COLUR) and a high sensitive spectrometer attached to the Risø TL/OSL reader. The key findings of my Ph.D. research are summarize as follows:

1) I discovered the excitation-energy dependent emission (a red edge effect) in the green-orange emission in feldspar, and demonstrated that this effect arises from interaction of a deep lying defect with the band tail states. This effect can be used to measure the band-tail width through relatively simple spectroscopic (photoluminescence) measurements.

2) My studies on Fe^{3+} show that its deep red emission varies with site dependence of Fe^{3+} even within a single sample. Furthermore, it is observed that there exists an excitation-energy dependence of the main radiative transition ($^4T_1 \rightarrow {}^6A_1$) in Fe^{3+}; this is possibly related to spin-lattice interaction.

3) I explored a model analogue system for feldspar called YPO_4:Ce,Sm, in order to understand IRSL produced by excited-state tunneling. For the first time, a precise mapping of the energy levels of the metastable Sm^{2+} was carried out, and the temperature-dependent relaxation lifetime of Sm^{2+} excited state was determined using the defects internal radiative-transition. It was then demonstrated that OSL decay curves resulting from optically induced, sub-conduction band electron transfer ($Sm^{2+} \rightarrow Ce^{4+}$) can be adequately described using the prevalent mathematical model of excited-state tunneling.

4) Finally, inspired by the results of YPO_4:Ce,Sm, I discovered a Stokes-shifted, infra-red photoluminescence (IRPL) signal arising from the principal trap in feldspar (excitation ∼ 1.4 eV (885 nm), emission: ∼ 1.3 eV (950 nm)). Current methods of OSL rely on transfer of electrons from the principal trap to holes located elsewhere in the lattice; this is by default a destructive readout of dosimetric information. Furthermore, OSL (or IRSL) suffer from sensitivity changes because of competition in the recombination process, leading to possible uncertainties in the dose measurement. In contrast to IRSL, the IRPL signal arises from intra-defect excitation and the subsequent radiative relaxation within the principle trap (i.e. the trap giving rise to IRSL). IRPL is a non-destructive readout technique and the lifetime of the excited state relaxation is estimated to be ∼40 µs at 7K and ∼29 µs at 295 K. The IRPL signal increases with dose and the preliminary dating investigations indicate that this signal contains an athermal non-fading component, likely arising from the trapped electrons that do not have a nearby hole center.

There are two important technique developments in my thesis. Firstly, based on the model of the red edge effect, a simple method is proposed for estimation of the width of the band tail states in feldspar. Secondly, it is shown that the new IRPL signal can be used for non-destructive probing of dosimetric information in the principal trap. The IRPL technique is likely to provide a) a robust understanding of the behavior of electron trapping centers in feldspar, b) a possibility of selective probe of non-fading electrons without using any thermal assistance, and c) precise measurements of luminescence from very small volumes by repeated readout. These possibilities open new windows for development of robust dating methods as well as advanced imaging techniques. I envision that the IRPL signal will significantly impact the field of optical dating.

A PDF of this thesis can be downloaded from: https://www.researchgate.net/profile/Amit_Prasad10 or http://orbit.dtu.dk

Bibliography

Compiled by Sebastien Huot

From 1st December 2016 to 14th May 2017

Various geological applications

- aeolian

Buró, B., Sipos, G., Lóki, J., Andrási, B., Félegyházi, E., Négyesi, G., 2016. Assessing Late Pleistocene and Holocene phases of aeolian activity on the Nyírség alluvial fan, Hungary. Quaternary International 425, 183-195, http://dx.doi.org/10.1016/j.quaint.2016.01.007.

Colgan, P.M., Amidon, W.H., Thurkettle, S.A., 2017. Inland dunes on the abandoned bed of Glacial Lake Chicago indicate eolian activity during the Pleistocene-Holocene transition, southwestern Michigan, USA. Quaternary Research 87, 66-81, http://dx.doi.org/10.1017/qua.2016.13.

Erginal, A.E., Kıyak, N.G., Selim, H.H., Bozcu, M., Öztürk, M.Z., Ekinci, Y.L., Demirci, A., Elmas, E.K., Öztürk, T., Çakır, Ç., Karabıyıkoğlu, M., 2017. Eolianite and coquinite as evidence of MIS 6 and 5, NW Black Sea coast, Turkey. Aeolian Research 25, 1-9, http://dx.doi.org/http://dx.doi.org/10.1016/j.aeolia.2017.01.004.

Gliganic, L.A., Cohen, T.J., Slack, M., Feathers, J.K., 2016. Sediment mixing in aeolian sandsheets identified and quantified using single-grain optically stimulated luminescence. Quaternary Geochronology 32, 53-66, http://dx.doi.org/10.1016/j.quageo.2015.12.006.

Hirsch, F., Spröte, R., Fischer, T., Forman, S.L., Raab, T., Bens, O., Schneider, A., Hüttl, R.F., 2017. Late Quaternary aeolian dynamics, pedostratigraphy and soil formation in the North European Lowlands – new findings from the Baruther ice-marginal valley. Die Erde 148, 58-73, http://dx.doi.org/10.12854/erde-148-30.

Li, Y., Tsukamoto, S., Hu, K., Frechen, M., 2017. Quartz OSL and K-feldspar post-IR IRSL dating of sand accumulation in the Lower Liao Plain (Liaoning, NE China). Geochronometria 44, 1-15, http://dx.doi.org/10.1515/geochr-2015-0051.

Liu, X.-J., Xiao, G., E, C., Li, X., Lai, Z., Yu, L., Wang, Z., 2017. Accumulation and erosion of aeolian sediments in the northeastern Qinghai-Tibetan Plateau and implications for provenance to the Chinese Loess Plateau. Journal of Asian Earth Sciences 135, 166-174, http://dx.doi.org/http://dx.doi.org/10.1016/j.jseaes.2016.12.034.

Munroe, J.S., Gorin, A.L., Stone, N.N., Amidon, W.H., 2017. Properties, age, and significance of dunes near Snow Water Lake, Elko County, Nevada. Quaternary Research 87, 24-36, http://dx.doi.org/10.1017/qua.2016.5.

Munyikwa, K., Rittenour, T.M., Feathers, J.K., 2017. Temporal constraints for the Late Wisconsinan deglaciation of western Canada using eolian dune luminescence chronologies from Alberta. Palaeogeography, Palaeoclimatology, Palaeoecology 470, 147-165, http://dx.doi.org/http://dx.doi.org/10.1016/j.palaeo.2016.12.034.

Roettig, C.B., Kolb, T., Wolf, D., Baumgart, P., Richter, C., Schleicher, A., Zöller, L., Faust, D., 2017. Complexity of Quaternary aeolian dynamics (Canary Islands). Palaeogeography, Palaeoclimatology, Palaeoecology 472, 146-162, http://dx.doi.org/http://dx.doi.org/10.1016/j.palaeo.2017.01.039.

Telfer, M.W., Hesse, P.P., Perez-Fernandez, M., Bailey, R.M., Bajkan, S., Lancaster, N., 2017. Morphodynamics, boundary conditions and pattern evolution within a vegetated linear dunefield. Geomorphology 290, 85-100, http://dx.doi.org/10.1016/j.geomorph.2017.03.024.

- alluvial fan

Singh, A.K., Jaiswal, M.K., Pattanaik, J.K., Dev, M., 2016. Luminescence chronology of alluvial fan in North Bengal, India: Implications to tectonics and climate. Geochronometria 43, 102-112, http://dx.doi.org/10.1515/geochr-2015-0037.

- bioclastic

Sharma, K., Bhatt, N., Shukla, A.D., Cheong, D.-K., Singhvi, A.K., 2017. Optical dating of late Quaternary carbonate sequences of Saurashtra, western India. Quaternary Research 87, 133-150, http://dx.doi.org/10.1017/qua.2016.12.

- cave

Cai, Y., Qiang, X., Wang, X., Jin, C., Wang, Y., Zhang, Y., Trinkaus, E., An, Z., 2017. The age of human remains and associated fauna from Zhiren Cave in Guangxi, southern China. Quaternary International 434, Part A, 84-91, http://dx.doi.org/10.1016/j.quaint.2015.12.088.

Epure, L., Muntean, V., Constantin, S., Moldovan, O.T., 2017. Ecophysiological groups of bacteria from cave sediments as potential indicators of paleoclimate. Quaternary International 432, Part A, 20-32, http://dx.doi.org/10.1016/j.quaint.2015.04.016.

Munroe, J.S., Perzan, Z.M., Amidon, W.H., 2016. Cave sediments constrain the latest Pleistocene advance of the Laurentide Ice Sheet in the Champlain Valley, Vermont, USA. Journal of Quaternary Science 31, 893-904, http://dx.doi.org/10.1002/jqs.2913.

- coastal

Bitinas, A., Mažeika, J., Buynevich, I.V., Damušytė, A., Molodkov, A., Grigienė, A., 2017. Constraints of Radiocarbon Dating in Southeastern Baltic Lagoons: Assessing the Vital Effects, in: Harff, J., Furmańczyk, K., von Storch, H. (Eds.), Coastline Changes of the Baltic Sea from South to East: Past and Future Projection. Springer International Publishing, Cham, pp. 137-171.

Gao, L., Long, H., Shen, J., Yu, G., Yin, Y., 2016. High-resolution OSL dating of a coastal sediment sequence from the South Yellow Sea. Geochronometria 43, 143-154, http://dx.doi.org/10.1515/geochr-2015-0044.

Lipar, M., Webb, J.A., Cupper, M.L., Wang, N., 2017. Aeolianite, calcrete/microbialite and karst in southwestern Australia as indicators of Middle to Late Quaternary palaeoclimates. Palaeogeography, Palaeoclimatology, Palaeoecology 470, 11-29, http://dx.doi.org/http://dx.doi.org/10.1016/j.palaeo.2016.12.019.

Milana, J.P., Guedes, C.C.F., Buso, V.V., 2017. The coastal ridge sequence at Rio Grande do Sul: A new geoarchive for past climate events of the Atlantic coast of southern Brazil since the mid Holocene. Quaternary International 438, Part A, 187-199, http://dx.doi.org/10.1016/j.quaint.2016.11.029.

Oliver, T.S.N., Donaldson, P., Sharples, C., Roach, M., Woodroffe, C.D., 2017. Punctuated progradation of the Seven Mile Beach Holocene barrier system, southeastern Tasmania. Marine Geology 386, 76-87, http://dx.doi.org/10.1016/j.margeo.2017.02.014.

Oliver, T.S.N., Tamura, T., Hudson, J.P., Woodroffe, C.D., 2017. Integrating millennial and interdecadal shoreline changes: Morpho-sedimentary investigation of two prograded barriers in southeastern Australia. Geomorphology 288, 129-147, http://dx.doi.org/10.1016/j.geomorph.2017.03.019.

Proborukmi, M.S., Urban, B., Frechen, M., Grube, A., Rolf, C., 2017. Late Pliocene–Pleistocene record of the Garding-2 research drill core, Northwest Germany. Zeitschrift der Deutschen Gesellschaft für Geowissenschaften 168, 141-167, http://dx.doi.org/10.1127/zdgg/2017/0103.

Shtienberg, G., Dix, J.K., Roskin, J., Waldmann, N., Bookman, R., Bialik, O.M., Porat, N., Taha, N., Sivan, D., 2017. New perspectives on coastal landscape reconstruction during the Late Quaternary: A test case from central Israel. Palaeogeography, Palaeoclimatology, Palaeoecology 468, 503-519, http://dx.doi.org/http://dx.doi.org/10.1016/j.palaeo.2016.12.045.

Vilumaa, K., Tõnisson, H., Sugita, S., Buynevich, I.V., Kont, A., Muru, M., Preusser, F., Bjursäter, S., Vaasma, T., Vandel, E., Molodkov, A., Järvelill, J.I., 2016. Past extreme events recorded in the internal architecture of coastal formations in the Baltic Sea Region. Journal of Coastal Research 75, 775-779, http://dx.doi.org/10.2112/SI75-156.1.

- colluvial

Henkner, J., Ahlrichs, J.J., Downey, S., Fuchs, M., James, B.R., Knopf, T., Scholten, T., Teuber, S., Kühn, P., 2017. Archaeopedology and chronostratigraphy of colluvial deposits as a proxy for regional land use history (Baar, southwest Germany). CATENA 155, 93-113, http://dx.doi.org/http://dx.doi.org/10.1016/j.catena.2017.03.005.

Kühn, P., Lehndorff, E., Fuchs, M., 2017. Lateglacial to Holocene pedogenesis and formation of colluvial deposits in a loess landscape of Central Europe (Wetterau, Germany). CATENA 154, 118-135, http://dx.doi.org/http://dx.doi.org/10.1016/j.catena.2017.02.015.

- estuary

Avnaim-Katav, S., Almogi-Labin, A., Agnon, A., Porat, N., Sivan, D., 2017. Holocene hydrological events and human induced environmental changes reflected in a southeastern Mediterranean fluvial archive. Palaeogeography, Palaeoclimatology, Palaeoecology 468, 263-275, http://dx.doi.org/http://dx.doi.org/10.1016/j.palaeo.2016.12.021.

Das, A., Prizomwala, S.P., Makwana, N., Thakkar, M.G., 2017. Late Pleistocene-Holocene climate and sea level changes inferred based on the tidal terrace sequence, Kachchh, Western India. Palaeogeography, Palaeoclimatology, Palaeoecology 473, 82-93, http://dx.doi.org/http://dx.doi.org/10.1016/j.palaeo.2017.02.026.

- fault

Grützner, C., Carson, E., Walker, R.T., Rhodes, E.J., Mukambayev, A., Mackenzie, D., Elliott, J.R., Campbell, G., Abdrakhmatov, K., 2017. Assessing the activity of faults in continental interiors: Palaeoseismic insights from SE Kazakhstan. Earth and Planetary Science Letters 459, 93-104, http://dx.doi.org/10.1016/j.epsl.2016.11.025.

Malik, J.N., Gadhavi, M.S., Kothyari, G.C., Satuluri, S., 2017. Paleo-earthquake signatures from the South Wagad Fault (SWF), Wagad Island, Kachchh, Gujarat, western India: A potential seismic hazard. Journal of Structural Geology 95, 142-159, http://dx.doi.org/10.1016/j.jsg.2016.12.011.

Rizza, M., Ritz, J.F., Prentice, C., Vassallo, R., Braucher, R., Larroque, C., Arzhannikova, A., Arzhannikov, S., Mahan, S., Massault, M., Michelot, J.L., Todbileg, M., 2015. Earthquake Geology of the Bulnay Fault (Mongolia). Bulletin of the Seismological Society of America 105, 72-93, http://dx.doi.org/10.1785/0120140119.

Wang, D., Yin, G.-M., Wang, X.-L., Liu, C.-R., Han, F., Du, J.-H., 2016. OSL dating of the late Quaternary slip rate on the Gyaring co Fault in central Tibet. Geochronometria 43, 162-173, http://dx.doi.org/10.1515/geochr-2015-0040.

Zhang, H., He, Z., Ma, B., Long, J., Liang, K., Wang, J., 2017. The vertical slip rate of the Sertengshan piedmont fault, Inner Mongolia, China. Journal of Asian Earth Sciences 143, 95-108, http://dx.doi.org/http://doi.org/10.1016/j.jseaes.2017.04.014.

- fluvial

Bartz, M., Rixhon, G., Kehl, M., El Ouahabi, M., Klasen, N., Brill, D., Weniger, G.-C., Mikdad, A., Brückner, H., 2017. Unravelling fluvial deposition and pedogenesis in ephemeral stream deposits in the vicinity of the prehistoric rock shelter of Ifri n'Ammar (NE Morocco) during the last 100 ka. CATENA 152, 115-134, http://dx.doi.org/http://dx.doi.org/10.1016/j.catena.2016.12.007.

Bejjit, L., Haddad, M., Belaabed, R., Charroud, M., Benkdad, A., Bounakhla, M., Huot, S., Falguères, C., Lamothe, M., 2017. Développement de la méthode de datation par luminescence (TL/OSL) au Maroc. L'Anthropologie 121, 25-34, http://dx.doi.org/10.1016/j.anthro.2017.03.002.

Chang, Q., Lai, Z., An, F., Wang, H., Lei, Y., Han, F., 2017. Chronology for terraces of the Nalinggele River in the north Qinghai-Tibet Plateau and implications for salt lake resource formation in the Qaidam Basin. Quaternary International 430, Part B, 12-20, http://dx.doi.org/10.1016/j.quaint.2016.02.022.

Croke, J., Thompson, C., Denham, R., Haines, H., Sharma, A., Pietsch, T., 2016. Reconstructing a millennial-scale record of flooding in a single valley setting: the 2011 flood-affected Lockyer Valley, south-east Queensland, Australia. Journal of Quaternary Science 31, 936-952, http://dx.doi.org/10.1002/jqs.2919.

Cunha, P.P., Martins, A.A., Buylaert, J.-P., Murray, A.S., Raposo, L., Mozzi, P., Stokes, M., 2017. New data on the chronology of the Vale do Forno sedimentary sequence (Lower Tejo River terrace staircase) and its relevance as a fluvial archive of the Middle Pleistocene in western Iberia. Quaternary Science Reviews 166, 204-226, http://dx.doi.org/10.1016/j.quascirev.2016.11.001.

Delile, H., Schmitt, L., Jacob-Rousseau, N., Grosprêtre, L., Privolt, G., Preusser, F., 2016. Headwater valley response to climate and land use changes during the Little Ice Age in the Massif Central (Yzeron basin, France). Geomorphology 257, 179-197, http://dx.doi.org/10.1016/j.geomorph.2016.01.010.

Fu, X., Li, S.-H., Li, B., Fu, B., 2017. A fluvial terrace record of late Quaternary folding rate of the Anjihai anticline in the northern piedmont of Tian Shan, China. Geomorphology 278, 91-104, http://dx.doi.org/10.1016/j.geomorph.2016.10.034.

Gao, H., Li, Z., Pan, B., Liu, F., Liu, X., 2016. Fluvial responses to late Quaternary climate change in the Shiyang River drainage system, western China. Geomorphology 258, 82-94, http://dx.doi.org/10.1016/j.geomorph.2016.01.018.

Ghosh, R., Sehgal, R.K., Srivastava, P., Shukla, U.K., Nanda, A.C., Singh, D.S., 2016. Discovery of Elephas cf. namadicus from the late Pleistocene strata of Marginal Ganga Plain. Journal of the Geological Society of India 88, 559-568, http://dx.doi.org/10.1007/s12594-016-0521-7.

Grimley, D.A., Anders, A.M., Bettis Iii, E.A., Bates, B.L., Wang, J.J., Butler, S.K., Huot, S., 2017. Using magnetic fly ash to identify post-settlement alluvium and its record of atmospheric pollution, central USA. Anthropocene 17, 84-98, http://dx.doi.org/10.1016/j.ancene.2017.02.001.

He, X., Zhang, X., He, Z., Jia, L., Ye, P., Zhao, J., 2017. Late Quaternary alluvial fan terraces: Langshan, Inner Mongolia, China. Geomorphology 286, 34-44, http://dx.doi.org/10.1016/j.geomorph.2017.03.003.

Hu, X., Pan, B., Fan, Y., Wang, J., Hu, Z., Cao, B., Li, Q., Geng, H., 2017. Folded fluvial terraces in a young, actively deforming intramontane basin between the Yumu Shan and the Qilian Shan mountains, NE Tibet. Lithosphere, http://dx.doi.org/10.1130/l614.1.

Kemp, J., Pietsch, T., Gontz, A., Olley, J., 2017. Lacustrine-fluvial interactions in Australia's Riverine Plains. Quaternary Science Reviews 166, 352-362, http://dx.doi.org/10.1016/j.quascirev.2017.02.015.

Kothyari, G.C., Kandregula, R.S., Luirei, K., 2017. Morphotectonic records of neotectonic activity in the vicinity of North Almora Thrust Zone, Central Kumaun Himalaya. Geomorphology 285, 272-286, http://dx.doi.org/http://dx.doi.org/10.1016/j.geomorph.2017.02.021.

Kumar, A., Srivastava, P., 2017. The role of climate and tectonics in aggradation and incision of the Indus River in the Ladakh Himalaya during the late Quaternary. Quaternary Research 87, 363-385, http://dx.doi.org/10.1017/qua.2017.19.

Larkin, Z.T., Tooth, S., Ralph, T.J., Duller, G.A.T., McCarthy, T., Keen-Zebert, A., Humphries, M.S., 2017. Timescales, mechanisms, and controls of incisional avulsions in floodplain wetlands: Insights from the Tshwane River, semiarid South Africa. Geomorphology 283, 158-172, http://dx.doi.org/10.1016/j.geomorph.2017.01.021.

Lawrence, D., Philip, G., Wilkinson, K., Buylaert, J.P., Murray, A.S., Thompson, W., Wilkinson, T.J., 2017. Regional power and local ecologies: Accumulated population trends and human impacts in the northern Fertile Crescent. Quaternary International 437, Part B, 60-81, http://dx.doi.org/10.1016/j.quaint.2015.06.026.

Meister, J., Krause, J., Müller-Neuhof, B., Portillo, M., Reimann, T., Schütt, B., 2017. Desert agricultural systems at EBA Jawa (Jordan): Integrating archaeological and paleoenvironmental records. Quaternary International 434, Part B, 33-50, http://dx.doi.org/10.1016/j.quaint.2015.12.086.

Morais, E.S.d., Santos, M.L.d., Cremon, É.H., Stevaux, J.C., 2016. Floodplain evolution in a confluence zone: Paraná and Ivaí rivers, Brazil. Geomorphology 257, 1-9, http://dx.doi.org/10.1016/j.geomorph.2015.12.017.

Morriss, M.C., Wegmann, K.W., 2017. Geomorphology of the Burnt River, eastern Oregon, USA: Topographic adjustments to tectonic and dynamic deformation. Geomorphology 278, 43-59, http://dx.doi.org/10.1016/j.geomorph.2016.09.015.

Oldknow, C.J., Hooke, J.M., 2017. Alluvial terrace development and changing landscape connectivity in the Great Karoo, South Africa. Insights from the Wilgerbosch River catchment, Sneeuberg. Geomorphology 288, 12-38, http://dx.doi.org/10.1016/j.geomorph.2017.03.009.

Panin, A., Adamiec, G., Buylaert, J.-P., Matlakhova, E., Moska, P., Novenko, E., 2017. Two Late Pleistocene climate-driven incision/aggradation rhythms in the middle Dnieper River basin, west-central Russian Plain. Quaternary Science Reviews 166, 266-288, http://dx.doi.org/10.1016/j.quascirev.2016.12.002.

Preusser, F., May, J.-H., Eschbach, D., Trauerstein, M., Schmitt, L., 2016. Infrared stimulated luminescence dating of 19th century fluvial deposits from the upper Rhine River. Geochronometria 43, 131-142, http://dx.doi.org/10.1515/geochr-2015-0045.

Pupim, F.d.N., Assine, M.L., Sawakuchi, A.O., 2017. Late Quaternary Cuiabá megafan, Brazilian Pantanal: Channel patterns and paleoenvironmental changes. Quaternary International 438, Part A, 108-125, http://dx.doi.org/10.1016/j.quaint.2017.01.013.

Ramisch, A., Bens, O., Buylaert, J.-P., Eden, M., Heine, K., Hürkamp, K., Schwindt, D., Völkel, J., 2017. Fluvial landscape development in the southwestern Kalahari during the Holocene – Chronology and provenance of fluvial deposits in the Molopo Canyon. Geomorphology 281, 94-107, http://dx.doi.org/http://dx.doi.org/10.1016/j.geomorph.2016.12.021.

Rixhon, G., Briant, R.M., Cordier, S., Duval, M., Jones, A., Scholz, D., 2017. Revealing the pace of river landscape evolution during the Quaternary: recent developments in numerical dating methods. Quaternary Science Reviews 166, 91-113, http://dx.doi.org/10.1016/j.quascirev.2016.08.016.

Sharma, S., Bartarya, S.K., Marh, B.S., 2016. The role of pre-existing topography in the evolution of post-glacial fluvial landforms in the middle Satluj valley, north-western Himalaya, India. Quaternary International 425, 399-415, http://dx.doi.org/10.1016/j.quaint.2016.08.015.

Sharma, S., Shukla, A.D., Bartarya, S.K., Marh, B.S., Juyal, N., 2017. The Holocene floods and their affinity to climatic variability in the western Himalaya, India. Geomorphology 290, 317-334, http://dx.doi.org/10.1016/j.geomorph.2017.04.030.

Srivastava, P., Kumar, A., Chaudhary, S., Meena, N., Sundriyal, Y.P., Rawat, S., Rana, N., Perumal, R.J., Bisht, P., Sharma, D., Agnihotri, R., Bagri, D.S., Juyal, N., Wasson, R.J., Ziegler, A.D., 2017. Paleofloods records in Himalaya. Geomorphology 284, 17-30, http://dx.doi.org/http://dx.doi.org/10.1016/j.geomorph.2016.12.011.

Stokes, M., Mather, A.E., Belfoul, M., Faik, F., Bouzid, S., Geach, M.R., Cunha, P.P., Boulton, S.J., Thiel, C., 2017. Controls on dryland mountain landscape development along the NW Saharan desert margin: Insights from Quaternary river terrace sequences (Dadès River, south-central High Atlas, Morocco). Quaternary Science Reviews 166, 363-379, http://dx.doi.org/10.1016/j.quascirev.2017.04.017.

Sun, X., Yi, S., Lu, H., Zhang, W., 2017. TT-OSL and post-IR IRSL dating of the Dali Man site in central China. Quaternary International 434, Part A, 99-106, http://dx.doi.org/10.1016/j.quaint.2015.05.027.

Vespremeanu-Stroe, A., Zăinescu, F., Preoteasa, L., Tătui, F., Rotaru, S., Morhange, C., Stoica, M., Hanganu, J., Timar-Gabor, A., Cârdan, I., Piotrowska, N., 2017. Holocene evolution of the Danube delta: An integral reconstruction and a revised chronology. Marine Geology 388, 38-61, http://dx.doi.org/10.1016/j.margeo.2017.04.002.

Vignon, V., Mugnier, J.L., Vassallo, R., Srivastava, P., Malik, M.A., Jayangondaperumal, R., Jouanne, F., Buoncristiani, J.F., Carcaillet, J., Replumaz, A., Jomard, H., 2017. Sedimentation close to the active Medlicott Wadia Thrust (Western Himalaya): How to estimate climatic base level changes and tectonics. Geomorphology 284, 175-190, http://dx.doi.org/http://dx.doi.org/10.1016/j.geomorph.2016.07.040.

Yan, Y., Zhou, J., He, Z., Sun, Q., Fei, J., Zhou, X., Zhao, K., Yang, L., Long, H., Zheng, H., 2017. Evolution of Luyang Lake since the last 34,000 years: Climatic changes and anthropogenic impacts. Quaternary International 440, 90-98, http://dx.doi.org/http://dx.doi.org/10.1016/j.quaint.2016.06.009.

Zink, A.J.C., Porto, E., Fouache, E., Rante, R., 2017. Paléocours du delta du Zerafshan (oasis de Boukhara, Ouzbékistan) : premières datations par luminescence. L'Anthropologie 121, 46-54, http://dx.doi.org/10.1016/j.anthro.2017.03.013.

- glacial

Bisht, P., Nawaz Ali, S., Rana, N., Singh, S., Poonam, Sundriyal, Y.P., Bagri, D.S., Juyal, N., 2017. Pattern of Holocene glaciation in the monsoon-dominated Kosa Valley, central Himalaya, Uttarakhand, India. Geomorphology 284, 130-141, http://dx.doi.org/http://dx.doi.org/10.1016/j.geomorph.2016.11.023.

Buechi, M.W., Lowick, S.E., Anselmetti, F.S., 2017. Luminescence dating of glaciolacustrine silt in overdeepened basin fills beyond the last interglacial. Quaternary Geochronology 37, 55-67, http://dx.doi.org/10.1016/j.quageo.2016.09.009.

Evans, D.J.A., Bateman, M.D., Roberts, D.H., Medialdea, A., Hayes, L., Duller, G.A.T., Fabel, D., Clark, C.D., 2017. Glacial Lake Pickering: stratigraphy and chronology of a proglacial lake dammed by the North Sea Lobe of the British–Irish Ice Sheet. Journal of Quaternary Science 32, 295-310, http://dx.doi.org/10.1002/jqs.2833.

Kenzler, M., Tsukamoto, S., Meng, S., Frechen, M., Hüneke, H., 2017. New age constraints from the SW Baltic Sea area – implications for Scandinavian Ice Sheet dynamics and palaeo-environmental conditions during MIS 3 and early MIS 2. Boreas 46, 34-52, http://dx.doi.org/10.1111/bor.12206.

Lamsters, K., Kalińska-Nartiša, E., Zelčs, V., Alexanderson, H., 2017. New luminescence ages reveal Early to Middle Weichselian deposits in central Latvia. Geological Quarterly 61, 480-490, http://dx.doi.org/10.7306/gq.1349.

Schaetzl, R.J., Lepper, K., Thomas, S.E., Grove, L., Treiber, E., Farmer, A., Fillmore, A., Lee, J., Dickerson, B., Alme, K., 2017. Kame deltas provide evidence for a new glacial lake and suggest early glacial retreat from central Lower Michigan, USA. Geomorphology 280, 167-178, http://dx.doi.org/http://dx.doi.org/10.1016/j.geomorph.2016.11.013.

Smedley, R.K., Scourse, J.D., Small, D., Hiemstra, J.F., Duller, G.A.T., Bateman, M.D., Burke, M.J., Chiverrell, R.C., Clark, C.D., Davies, S.M., Fabel, D., Gheorghiu, D.M., McCarroll, D., Medialdea, A., Xu, S., 2017. New age constraints for the limit of the British–Irish Ice Sheet on the Isles of Scilly. Journal of Quaternary Science 32, 48-62, http://dx.doi.org/10.1002/jqs.2922.

Trauerstein, M., Lowick, S.E., Preusser, F., Veit, H., 2017. Testing the suitability of dim sedimentary quartz from northern Switzerland for OSL burial dose estimation. Geochronometria 44, 66-76, http://dx.doi.org/10.1515/geochr-2015-0058.

- lacustrine

Barrett, S., Starnberger, R., Tjallingii, R., Brauer, A., Spötl, C., 2017. The sedimentary history of the inner-alpine Inn Valley, Austria: extending the Baumkirchen type section further back in time with new drilling. Journal of Quaternary Science 32, 63-79, http://dx.doi.org/10.1002/jqs.2924.

Fu, X., Cohen, T.J., Arnold, L.J., 2017. Extending the record of lacustrine phases beyond the last interglacial for Lake Eyre in central Australia using luminescence dating. Quaternary Science Reviews 162, 88-110, http://dx.doi.org/10.1016/j.quascirev.2017.03.002.

Li, G., Duan, Y., Huang, X., Buylaert, J.-P., Peng, W., Madsen, D.B., Rao, Z., She, L., Xie, H., Chen, J., Chen, F., 2017. The luminescence dating chronology of a deep core from Bosten Lake (NW China) in arid central Asia reveals lake evolution over the last 220 ka. Boreas 46, 264-281, http://dx.doi.org/10.1111/bor.12209.

Li, G., Li, F., Jin, M., She, L., Duan, Y., Madsen, D., Wang, L., Chen, F., 2017. Late Quaternary lake evolution in the Gaxun Nur basin, central Gobi Desert, China, based on quartz OSL and K-feldspar pIRIR dating of paleoshorelines. Journal of Quaternary Science 32, 347-361, http://dx.doi.org/10.1002/jqs.2928.

Long, H., Shen, J., 2017. Sandy beach ridges from Xingkai Lake (NE Asia): Timing and response to palaeoclimate. Quaternary International 430, Part B, 21-31, http://dx.doi.org/10.1016/j.quaint.2015.11.009.

Onken, J., Forman, S., 2017. Terminal Pleistocene to early Holocene volcanic eruptions at Zuni Salt Lake, west-central New Mexico, USA. Bulletin of Volcanology 79, 10, http://dx.doi.org/10.1007/s00445-016-1089-1.

- loess

Babeesh, C., Achyuthan, H., Jaiswal, M.K., Lone, A., 2017. Late Quaternary loess-like paleosols and pedocomplexes, geochemistry, provenance and source area weathering, Manasbal, Kashmir Valley, India. Geomorphology 284, 191-205, http://dx.doi.org/http://dx.doi.org/10.1016/j.geomorph.2017.01.004.

Bate, S., Stevens, T., Buylaert, J.-P., Marković, S.B., Roos, P., Tasić, N., 2017. Pottery versus sediment: Optically stimulated luminescence dating of the Neolithic Vinča culture, Serbia. Quaternary International 429, Part A, 45-53, http://dx.doi.org/10.1016/j.quaint.2014.09.042.

Klasen, N., Loibl, C., Rethemeyer, J., Lehmkuhl, F., 2017. Testing feldspar and quartz luminescence dating of sandy loess sediments from the Doroshivtsy site (Ukraine) against radiocarbon dating. Quaternary International 432, Part A, 13-19, http://dx.doi.org/http://dx.doi.org/10.1016/j.quaint.2015.05.036.

Lauer, T., Frechen, M., Vlaminck, S., Kehl, M., Lehndorff, E., Shahriari, A., Khormali, F., 2017. Luminescence-chronology of the loess palaeosol sequence Toshan, Northern Iran – A highly resolved

climate archive for the last glacial–interglacial cycle. Quaternary International 429, Part B, 3-12, http://dx.doi.org/10.1016/j.quaint.2015.03.045.

Lauer, T., Vlaminck, S., Frechen, M., Rolf, C., Kehl, M., Sharifi, J., Lehndorff, E., Khormali, F., 2017. The Agh Band loess-palaeosol sequence – A terrestrial archive for climatic shifts during the last and penultimate glacial–interglacial cycles in a semiarid region in northern Iran. Quaternary International 429, Part B, 13-30, http://dx.doi.org/10.1016/j.quaint.2016.01.062.

Stauch, G., Schulte, P., Ramisch, A., Hartmann, K., Hülle, D., Lockot, G., Diekmann, B., Nottebaum, V., Müller, C., Wünnemann, B., Yan, D., Lehmkuhl, F., 2017. Landscape and climate on the northern Tibetan Plateau during the late Quaternary. Geomorphology 286, 78-92, http://dx.doi.org/10.1016/j.geomorph.2017.03.008.

Sun, X., Lu, H., Wang, S., Yi, L., Li, Y., Bahain, J.J., Voinchet, P., Hu, X., Zeng, L., Zhang, W., Zhuo, H., 2017. Early human settlements in the southern Qinling Mountains, central China. Quaternary Science Reviews 164, 168-186, http://dx.doi.org/http://doi.org/10.1016/j.quascirev.2017.04.005.

Sun, X., Yi, S., Lu, H., Zhang, W., 2017. TT-OSL and post-IR IRSL dating of the Dali Man site in central China. Quaternary International 434, Part A, 99-106, http://dx.doi.org/10.1016/j.quaint.2015.05.027.

Wen, X., Chen, M., Feng, W., Huang, C., 2017. Mid-late Holocene climatic changes recorded by loess deposits in the eastern margin of the Tibetan Plateau: Implication for human migrations. Quaternary International 441, Part A, 77-88, http://dx.doi.org/10.1016/j.quaint.2016.11.046.

Zech, M., Kreutzer, S., Zech, R., Goslar, T., Meszner, S., McIntyre, C., Häggi, C., Eglinton, T., Faust, D., Fuchs, M., 2017. Comparative 14C and OSL dating of loess-paleosol sequences to evaluate post-depositional contamination of n-alkane biomarkers. Quaternary Research 87, 180-189, http://dx.doi.org/10.1017/qua.2016.7.

Zeng, L., Lu, H., Yi, S., Stevens, T., Xu, Z., Zhuo, H., Yu, K., Zhang, H., 2017. Long-term Pleistocene aridification and possible linkage to high-latitude forcing: New evidence from grain size and magnetic susceptibility proxies from loess-paleosol record in northeastern China. CATENA 154, 21-32, http://dx.doi.org/http://dx.doi.org/10.1016/j.catena.2017.02.020.

- marine

Armitage, S.J., Pinder, R.C., 2017. Testing the applicability of optically stimulated luminescence dating to Ocean Drilling Program cores. Quaternary Geochronology 39, 124-130, http://dx.doi.org/http://doi.org/10.1016/j.quageo.2017.02.008.

Balescu, S., Weisrock, A., Huot, S., Lamothe, M., Ghaleb, B., Ouammou, A., Rousseau, L., Abdessadok, S., 2017. Les hauts niveaux marins interglaciaires pléistocènes enregistrés dans la région d'Agadir : bilan des données chronologiques. L'Anthropologie 121, 102-111, http://dx.doi.org/10.1016/j.anthro.2017.03.010.

Gao, L., Long, H., Shen, J., Yu, G., Liao, M., Yin, Y., 2017. Optical dating of Holocene tidal deposits from the southwestern coast of the South Yellow Sea using different grain-size quartz fractions. Journal of Asian Earth Sciences 135, 155-165, http://dx.doi.org/10.1016/j.jseaes.2016.12.036.

Karkani, A., Evelpidou, N., Vacchi, M., Morhange, C., Tsukamoto, S., Frechen, M., Maroukian, H., 2017. Tracking shoreline evolution in central Cyclades (Greece) using beachrocks. Marine Geology 388, 25-37, http://dx.doi.org/10.1016/j.margeo.2017.04.009.

Lamothe, M., 2017. La contribution de la luminescence à la datation des hauts niveaux marins du Pléistocène. L'Anthropologie 121, 19-24, http://dx.doi.org/10.1016/j.anthro.2017.03.014.

Neudorf, C.M., Smith, N., Lepofsky, D., Toniello, G., Lian, O.B., 2017. Between a rock and a soft place: Using optical ages to date ancient clam gardens on the Pacific Northwest. PLOS ONE 12, e0171775, http://dx.doi.org/10.1371/journal.pone.0171775.

Oakley, D.O.S., Kaufman, D.S., Gardner, T.W., Fisher, D.M., VanderLeest, R.A., 2017. Quaternary marine terrace chronology, North Canterbury, New Zealand, using amino acid racemization and infrared-stimulated luminescence. Quaternary Research 87, 151-167, http://dx.doi.org/10.1017/qua.2016.9.

Scarelli, F.M., Sawakuchi, A.O., Barboza, E.G., Cantelli, L., Gabbianelli, G., 2016. Quartz OSL dating of Pre- and Post-Little Ice Age beach ridges in Ravenna coastal plain northwest Adriatic Sea (Emilia-Romagna, Italy). Gravel 14, 1-10.

- soil

Breuning-Madsen, H., Kristensen, J.Å., Awadzi, T.W., Murray, A.S., 2017. Early cultivation and bioturbation cause high long-term soil erosion rates in tropical forests: OSL based evidence from Ghana. CATENA 151, 130-136, http://dx.doi.org/http://dx.doi.org/10.1016/j.catena.2016.12.002.

- tephra

Zens, J., Zeeden, C., Römer, W., Fuchs, M., Klasen, N., Lehmkuhl, F., 2017. The Eltville Tephra (Western Europe) age revised: Integrating stratigraphic and dating information from different Last Glacial loess localities. Palaeogeography, Palaeoclimatology, Palaeoecology 466, 240-251, http://dx.doi.org/10.1016/j.palaeo.2016.11.033.

- travertine

Meyer, M.C., Aldenderfer, M.S., Wang, Z., Hoffmann, D.L., Dahl, J.A., Degering, D., Haas, W.R., Schlütz, F., 2017. Permanent human occupation of the central Tibetan Plateau in the early Holocene. Science 355, 64-67, http://dx.doi.org/10.1126/science.aag0357.

- volcanic

Onken, J., Forman, S., 2017. Terminal Pleistocene to early Holocene volcanic eruptions at Zuni Salt Lake, west-central New Mexico, USA. Bulletin of Volcanology 79, 10, http://dx.doi.org/10.1007/s00445-016-1089-1.

Sears, D.W.G., Sears, H., Sehlke, A., Hughes, S.S., 2017. Induced thermoluminescence as a method for dating recent volcanism: Eastern Snake River Plain, Idaho, USA. Journal of Geophysical Research: Solid Earth 122, 906-922, http://dx.doi.org/10.1002/2016JB013596.

Toktamış, D., Toktamış, H., Yazıcı, A.N., 2017. Thermoluminescence behavior of basaltic rocks collected in southeastern region of Turkey. Applied Radiation and Isotopes 121, 109-115, http://dx.doi.org/http://dx.doi.org/10.1016/j.apradiso.2016.12.051.

Archaeology applications

Aidona, E., Polymeris, G.S., Camps, P., Kondopoulou, D., Ioannidis, N., Raptis, K., 2017. Archaeomagnetic versus luminescence methods: the case of an Early Byzantine ceramic workshop in Thessaloniki, Greece. Archaeological and Anthropological Sciences, 1-17, http://dx.doi.org/10.1007/s12520-017-0494-5.

Al Khasawneh, S., Murray, A.S., Bourke, S., Bonatz, D., 2017. Testing feldspar luminescence dating of young archaeological heated materials using potshards from Pella (Tell Tabqat Fahl) in the Jordan valley. Geochronometria 44, 98-110, http://dx.doi.org/10.1515/geochr-2015-0056.

al Khasawneh, S., Murray, A.S., Gebel, H.G., Bonatz, D., 2016. First application of OSL dating to a chalcolithic well structure in Qulbān Banī Murra, Jordan. Mediterranean Archaeology and Archaeometry 16, 127-134, http://dx.doi.org/10.5281/zenodo.160962.

Ao, H., Liu, C.-R., Roberts, A.P., Zhang, P., Xu, X., 2017. An updated age for the Xujiayao hominin from the Nihewan Basin, North China: Implications for Middle Pleistocene human evolution in East Asia. Journal of Human Evolution 106, 54-65, http://dx.doi.org/http://dx.doi.org/10.1016/j.jhevol.2017.01.014.

Athanassas, C., García Sanjuán, L., Theodorakopoulou, K., Jain, M., Sohbati, R., Guerin, G., Lozano Rodríguez, J.A., 2016. Testing the potential of optically stimulated luminescence (OSL) for the dating of the Antequera megaliths (Málaga, Spain): Assessing the results of the first round of sampling. Menga. Revista de prehistoria de andalucía 07, 157-164.

Bate, S., Stevens, T., Buylaert, J.-P., Marković, S.B., Roos, P., Tasić, N., 2017. Pottery versus sediment: Optically stimulated luminescence dating of the Neolithic Vinča culture, Serbia. Quaternary International 429, Part A, 45-53, http://dx.doi.org/10.1016/j.quaint.2014.09.042.

Bobak, D., Łanczont, M., Mroczek, P., Połtowicz-Bobak, M., Nowak, A., Kufel–Diakowska, B., Kusiak, J., Standzikowski, K., 2017. Magdalenian settlement on the edge of the loess island: A case study from the northern foreland of the Carpathians (SE Poland). Quaternary International 438, Part B, 158-173, http://dx.doi.org/10.1016/j.quaint.2017.04.034.

Dunseth, Z.C., Junge, A., Lomax, J., Boaretto, E., Finkelstein, I., Fuchs, M., Shahack-Gross, R., 2017. Dating archaeological sites in an arid environment: A multi-method case study in the Negev Highlands, Israel. Journal of Arid Environments 144, 156-169, http://dx.doi.org/10.1016/j.jaridenv.2017.05.006.

Duval, M., 2016. Comments on "ESR dating of the Majuangou and Banshan Paleolithic sites in the Nihewan Basin, North China" by Liu et al. (2014). Journal of Human Evolution 90, 198-202, http://dx.doi.org/10.1016/j.jhevol.2015.04.010.

Duval, M., Arnold, L.J., Guilarte, V., Demuro, M., Santonja, M., Pérez-González, A., 2017. Electron spin resonance dating of optically bleached quartz grains from the Middle Palaeolithic site of Cuesta de la Bajada (Spain) using the multiple centres approach. Quaternary Geochronology 37, 82-96, http://dx.doi.org/10.1016/j.quageo.2016.09.006.

Feathers, J.K., 2017. A response to some unwarranted criticism of single-grain dating: Comments on Thomsen et al., Quaternary Geochronology 31 (2016), 77–96. Quaternary Geochronology 37, 108-115, http://dx.doi.org/10.1016/j.quageo.2016.11.005.

Froese, D., Stiller, M., Heintzman, P.D., Reyes, A.V., Zazula, G.D., Soares, A.E.R., Meyer, M., Hall, E., Jensen, B.J.L., Arnold, L.J., MacPhee, R.D.E., Shapiro, B., 2017. Fossil and genomic evidence constrains the timing of bison arrival in North America. Proceedings of the National Academy of Sciences 114, 3457-3462, http://dx.doi.org/10.1073/pnas.1620754114.

Frouin, M., Guérin, G., Lahaye, C., Mercier, N., Huot, S., Aldeias, V., Bruxelles, L., Chiotti, L., Dibble, H.L., Goldberg, P., Madelaine, S., McPherron, S.J.P., Sandgathe, D., Steele, T.E., Turq, A., 2017. New luminescence dating results based on polymineral fine grains from the Middle and Upper Palaeolithic site of La Ferrassie (Dordogne, SW France). Quaternary Geochronology 39, 131-141, http://dx.doi.org/http://doi.org/10.1016/j.quageo.2017.02.009.

Ghosh, R., Sehgal, R.K., Srivastava, P., Shukla, U.K., Nanda, A.C., Singh, D.S., 2016. Discovery of Elephas cf. namadicus from the late Pleistocene strata of Marginal Ganga Plain. Journal of the Geological Society of India 88, 559-568, http://dx.doi.org/10.1007/s12594-016-0521-7.

Guérin, G., Frouin, M., Tuquoi, J., Thomsen, K.J., Goldberg, P., Aldeias, V., Lahaye, C., Mercier, N., Guibert, P., Jain, M., Sandgathe, D., McPherron, S.J.P., Turq, A., Dibble, H.L., 2017. The complementarity of luminescence dating methods illustrated on the Mousterian sequence of the Roc de Marsal: A series of reindeer-dominated, Quina Mousterian layers dated to MIS 3. Quaternary International 433, Part B, 102-115, http://dx.doi.org/10.1016/j.quaint.2016.02.063.

Guérin, G., Valladas, H., Joron, J.-L., Mercier, N., Reyss, J.-L., Zaidner, Y., 2017. Apports de la datation par la luminescence des sites du Proche-Orient et résultats préliminaires du site de Nesher Ramla (Israël). L'Anthropologie 121, 35-45, http://dx.doi.org/10.1016/j.anthro.2017.03.003.

Guo, Y.-J., Li, B., Zhang, J.-F., Yuan, B.-Y., Xie, F., Roberts, R.G., 2017. New ages for the Upper Palaeolithic site of Xibaimaying in the Nihewan Basin, northern China: implications for small-tool and microblade industries in north-east Asia during Marine Isotope Stages 2 and 3. Journal of Quaternary Science 32, 540-552, http://dx.doi.org/10.1002/jqs.2949.

Henkner, J., Ahlrichs, J.J., Downey, S., Fuchs, M., James, B.R., Knopf, T., Scholten, T., Teuber, S., Kühn, P., 2017. Archaeopedology and chronostratigraphy of colluvial deposits as a proxy for regional land use history (Baar, southwest Germany). CATENA 155, 93-113, http://dx.doi.org/http://dx.doi.org/10.1016/j.catena.2017.03.005.

Holen, S.R., Deméré, T.A., Fisher, D.C., Fullagar, R., Paces, J.B., Jefferson, G.T., Beeton, J.M., Cerutti, R.A., Rountrey, A.N., Vescera, L., Holen, K.A., 2017. A 130,000-year-old archaeological site in southern California, USA. Nature 544, 479-483, http://dx.doi.org/10.1038/nature22065.

Jacobs, Z., Li, B., Farr, L., Hill, E., Hunt, C., Jones, S., Rabett, R., Reynolds, T., Roberts, R.G., Simpson, D., Barker, G., 2017. The chronostratigraphy of the Haua Fteah cave (Cyrenaica, northeast Libya) — Optical dating of early human occupation during Marine Isotope Stages 4, 5 and 6. Journal of Human Evolution 105, 69-88, http://dx.doi.org/http://doi.org/10.1016/j.jhevol.2017.01.008.

Jacobs, Z., Roberts, R.G., 2017. Single-grain OSL chronologies for the Still Bay and Howieson's Poort industries and the transition between them: Further analyses and statistical modelling. Journal of Human Evolution 107, 1-13, http://dx.doi.org/http://dx.doi.org/10.1016/j.jhevol.2017.02.004.

Jennings, R.P., Parton, A., Clark-Balzan, L., White, T.S., Groucutt, H.S., Breeze, P.S., Parker, A.G., Drake, N.A., Petraglia, M.D., 2016. Human occupation of the northern Arabian interior during early Marine Isotope Stage 3. Journal of Quaternary Science 31, 953-966, http://dx.doi.org/10.1002/jqs.2920.

Kinnaird, T., Bolòs, J., Turner, A., Turner, S., 2017. Optically-stimulated luminescence profiling and dating of historic agricultural terraces in Catalonia (Spain). Journal of Archaeological Science 78, 66-77, http://dx.doi.org/10.1016/j.jas.2016.11.003.

Lebrun, B., Tribolo, C., Chevrier, B., Lespez, L., Rasse, M., Camara, A., Mercier, N., Huysecom, É., 2017. Chronologie du Paléolithique ouest africain : premières datations OSL de la Vallée de la Falémé (Sénégal). L'Anthropologie 121, 1-8, http://dx.doi.org/10.1016/j.anthro.2017.03.001.

Li, Z.-Y., Wu, X.-J., Zhou, L.-P., Liu, W., Gao, X., Nian, X.-M., Trinkaus, E., 2017. Late Pleistocene archaic human crania from Xuchang, China. Science 355, 969-972, http://dx.doi.org/10.1126/science.aal2482.

Liritzis, I., Zacharias, N., Al-Otaibi, F., Iliopoulos, I., Katagas, C., Shaltout, M., 2016. Chronology of construction and occupational phases of Nawamis tombs, Sinai based on OSL dating. Geochronometria 43, 121-130, http://dx.doi.org/10.1515/geochr-2015-0041.

Meyer, M.C., Aldenderfer, M.S., Wang, Z., Hoffmann, D.L., Dahl, J.A., Degering, D., Haas, W.R., Schlütz, F., 2017. Permanent human occupation of the central Tibetan Plateau in the early Holocene. Science 355, 64-67, http://dx.doi.org/10.1126/science.aag0357.

Moore, C.R., West, A., LeCompte, M.A., Brooks, M.J., Daniel Jr, I.R., Goodyear, A.C., Ferguson, T.A., Ivester, A.H., Feathers, J.K., Kennett, J.P., Tankersley, K.B., Adedeji, A.V., Bunch, T.E., 2017. Widespread platinum anomaly documented at the Younger Dryas onset in North American sedimentary sequences. Scientific Reports 7, 44031, http://dx.doi.org/10.1038/srep44031.

Neudorf, C.M., Smith, N., Lepofsky, D., Toniello, G., Lian, O.B., 2017. Between a rock and a soft place: Using optical ages to date ancient clam gardens on the Pacific Northwest. PLOS ONE 12, e0171775, http://dx.doi.org/10.1371/journal.pone.0171775.

Nian, X., Li, F., Chen, F., Zhang, W., Zhao, Y., Zhou, J., Gao, X., 2016. Optically stimulated luminescence ages for human occupation during the penultimate glaciation in the western Loess Plateau of China. Journal of Quaternary Science 31, 928-935, http://dx.doi.org/10.1002/jqs.2917.

Pailoplee, S., Won-In, K., Chaisuwan, B., Charusiri, P., 2016. Thermoluminescence and optically stimulated luminescence dating of bricks from the Thung Tuk archaeological site, Southern Thailand. Songklanakarin Journal of Science and Technology 38, 699-705, http://dx.doi.org/10.14456/sjst-psu.2016.88.

Richter, D., Grün, R., Joannes-Boyau, R., Steele, T.E., Amani, F., Rué, M., Fernandes, P., Raynal, J.-P., Geraads, D., Ben-Ncer, A., Hublin, J.-J., McPherron, S.P., 2017. The age of the hominin fossils from Jebel Irhoud, Morocco, and the origins of the Middle Stone Age. Nature 546, 293-296, http://dx.doi.org/10.1038/nature22335.

Richter, D., Klinger, P., Schmidt, C., van den Bogaard, P., Zöller, L., 2017. New chronometric age estimates for the context of the Neanderthal from Wannen-Ochtendung (Germany) by TL and argon dating. Journal of Archaeological Science: Reports 14, 127-136, http://dx.doi.org/10.1016/j.jasrep.2017.05.032.

Richter, D., McPherron, S.P., Dibble, H., Goldberg, P., Sandgathe, D.S., 2017. Additional chronometric data for the small flake assemblages ('Asinipodian') from Pech de l'Azé IV (France) and a comparison with similar assemblages at the nearby site of Roc de Marsal, 148. in: Wojtczak, D., Al Najiar, M., Jagher, R., Elsuede, H., Wegmüller, F., Otte, M. (Eds.), Vocation préhistoire. Hommage à Jean-Marie Le Tensorer. Etudes et recherches archéologiques de l'Université de Liège (ERAUL), pp. 323-335.

Scerri, E.M.L., Blinkhorn, J., Niang, K., Bateman, M.D., Groucutt, H.S., 2017. Persistence of Middle Stone Age technology to the Pleistocene/Holocene transition supports a complex hominin evolutionary scenario in West Africa. Journal of Archaeological Science: Reports 11, 639-646, http://dx.doi.org/http://dx.doi.org/10.1016/j.jasrep.2017.01.003.

Sun, Y., Chongyi, E., Lai, Z., Hou, G., 2017. Luminescence dating of prehistoric hearths in Northeast Qinghai Lake and its paleoclimatic implication. Archaeological and Anthropological Sciences, 1-10, http://dx.doi.org/10.1007/s12520-017-0472-y.

Terradillos-Bernal, M., Díez Fernández-Lomana, J.C., Jordá Pardo, J.-F., Benito-Calvo, A., Clemente, I., Marcos-Sáiz, F.J., 2017. San Quirce (Palencia, Spain). A Neanderthal open air campsite with short term-occupation patterns. Quaternary International 435, Part A, 115-128, http://dx.doi.org/http://dx.doi.org/10.1016/j.quaint.2015.09.082.

Thomsen, K.J., Murray, A.S., Buylaert, J.-P., Jain, M., Hansen, J.H., Aubry, T., Guérin, G., 2017. Reply to: "A response to some unwarranted criticisms of single-grain dating" by J.K. Feathers. Quaternary Geochronology 37, 8-14, http://dx.doi.org/10.1016/j.quageo.2016.10.007.

Tribolo, C., Asrat, A., Bahain, J.-J., Chapon, C., Douville, E., Fragnol, C., Hernandez, M., Hovers, E., Leplongeon, A., Martin, L., Pleurdeau, D., Pearson, O., Puaud, S., Assefa, Z., 2017. Across the Gap: Geochronological and Sedimentological Analyses from the Late Pleistocene-Holocene Sequence of Goda Buticha, Southeastern Ethiopia. PLOS ONE 12, e0169418, http://dx.doi.org/10.1371/journal.pone.0169418.

Tribolo, C., Mercier, N., Valladas, H., Lefrais, Y., Miller, C.E., Parkington, J., Porraz, G., 2016. Chronology of the Pleistocene deposits at Elands Bay Cave (South Africa) based on charcoals, burnt lithics, and sedimentary quartz and feldspar grains. Southern African Humanities 29, 129-152.

Urbanová, P., Delaval, E., Lanos, P., Guibert, P., Dufresne, P., Ney, C., Thernot, R., Mellinand, P., 2016. Multi-method dating of Grimaldi castle foundations in Antibes, France. ArchéoSciences - Revue d'archéométrie 40, 17-33, http://dx.doi.org/10.4000/archeosciences.4702.

Urbanová, P., Guibert, P., 2017. Methodological study on single grain OSL dating of mortars: Comparison of five reference archaeological sites. Geochronometria 44, 77-97, http://dx.doi.org/10.1515/geochr-2015-0050.

Veth, P., Ward, I., Manne, T., Ulm, S., Ditchfield, K., Dortch, J., Hook, F., Petchey, F., Hogg, A., Questiaux, D., Demuro, M., Arnold, L., Spooner, N., Levchenko, V., Skippington, J., Byrne, C., Basgall, M., Zeanah, D., Belton, D., Helmholz, P., Bajkan, S., Bailey, R., Placzek, C., Kendrick, P., 2017. Early human occupation of a maritime desert, Barrow Island, North-West Australia. Quaternary Science Reviews 168, 19-29, http://dx.doi.org/10.1016/j.quascirev.2017.05.002.

Weeks, L., Cable, C., Franke, K., Newton, C., Karacic, S., Roberts, J., Stepanov, I., David-Cuny, H., Price, D., Bukhash, R.M., Radwan, M.B., Zein, H., 2017. Recent archaeological research at Saruq al-Hadid, Dubai, UAE. Arabian Archaeology and Epigraphy 28, 31-60, http://dx.doi.org/10.1111/aae.12082.

Westaway, M.C., Olley, J., Grün, R., 2017. At least 17,000 years of coexistence: Modern humans and megafauna at the Willandra Lakes, South-Eastern Australia. Quaternary Science Reviews 157, 206-211, http://dx.doi.org/http://dx.doi.org/10.1016/j.quascirev.2016.11.031.

Wright, D.K., Thompson, J.C., Schilt, F., Cohen, A.S., Choi, J.-H., Mercader, J., Nightingale, S., Miller, C.E., Mentzer, S.M., Walde, D., Welling, M., Gomani-Chindebvu, E., 2017. Approaches to Middle Stone Age landscape archaeology in tropical Africa. Journal of Archaeological Science 77, 64-77, http://dx.doi.org/http://dx.doi.org/10.1016/j.jas.2016.01.014.

Yu, L., An, P., Lai, Z., 2016. Different implications of OSL and radiocarbon ages in archaeological sites in the Qaidam Basin, Qinghai-Tibetan Plateau. Geochronometria 43, 188-200, http://dx.doi.org/10.1515/geochr-2015-0048.

Zink, A.J.C., Porto, E., Fouache, E., Rante, R., 2017. Paléocours du delta du Zerafshan (oasis de Boukhara, Ouzbékistan) : premières datations par luminescence. L'Anthropologie 121, 46-54, http://dx.doi.org/10.1016/j.anthro.2017.03.013.

Various ESR applications

Ao, H., Liu, C.-R., Roberts, A.P., Zhang, P., Xu, X., 2017. An updated age for the Xujiayao hominin from the Nihewan Basin, North China: Implications for Middle Pleistocene human evolution in East Asia. Journal of Human Evolution 106, 54-65, http://dx.doi.org/http://dx.doi.org/10.1016/j.jhevol.2017.01.014.

Bitinas, A., Mažeika, J., Buynevich, I.V., Damušytė, A., Molodkov, A., Grigienė, A., 2017. Constraints of Radiocarbon Dating in Southeastern Baltic Lagoons: Assessing the Vital Effects, in: Harff, J., Furmańczyk, K., von Storch, H. (Eds.), Coastline Changes of the Baltic Sea from South to East: Past and Future Projection. Springer International Publishing, Cham, pp. 137-171.

Duval, M., 2016. Comments on "ESR dating of the Majuangou and Banshan Paleolithic sites in the Nihewan Basin, North China" by Liu et al. (2014). Journal of Human Evolution 90, 198-202, http://dx.doi.org/10.1016/j.jhevol.2015.04.010.

Duval, M., Arnold, L.J., Guilarte, V., Demuro, M., Santonja, M., Pérez-González, A., 2017. Electron spin resonance dating of optically bleached quartz grains from the Middle Palaeolithic site of Cuesta de la Bajada (Spain) using the multiple centres approach. Quaternary Geochronology 37, 82-96, http://dx.doi.org/10.1016/j.quageo.2016.09.006.

Fujiwara, T., Toyoda, S., Uchida, A., Nishido, H., Ishibashi, J.-I., 2016. The alpha effectiveness of the dating ESR signal in barite: possible dependence with age. Geochronometria 43, 174-178, http://dx.doi.org/10.1515/geochr-2015-0043.

Richard, M., Falguères, C., Pons-Branchu, E., Ghaleb, B., Valladas, H., Mercier, N., Richter, D., Bahain, J.-J., Conard, N.J., 2017. Datation par les méthodes ESR/U-Th combinées de sites du Pléistocène supérieur : méthodologie et application en contexte karstique. L'Anthropologie 121, 63-72, http://dx.doi.org/10.1016/j.anthro.2017.03.006.

Richter, D., Grün, R., Joannes-Boyau, R., Steele, T.E., Amani, F., Rué, M., Fernandes, P., Raynal, J.-P., Geraads, D., Ben-Ncer, A., Hublin, J.-J., McPherron, S.P., 2017. The age of the hominin fossils from Jebel Irhoud, Morocco, and the origins of the Middle Stone Age. Nature 546, 293-296, http://dx.doi.org/10.1038/nature22335.

Rixhon, G., Briant, R.M., Cordier, S., Duval, M., Jones, A., Scholz, D., 2017. Revealing the pace of river landscape evolution during the Quaternary: recent developments in numerical dating methods. Quaternary Science Reviews 166, 91-113, http://dx.doi.org/10.1016/j.quascirev.2016.08.016.

Şahiner, E., Meriç, N., Polymeris, G.S., 2017. Thermally assisted OSL application for equivalent dose estimation; comparison of multiple equivalent dose values as well as saturation levels determined by luminescence and ESR techniques for a sedimentary sample collected from a fault gouge. Nuclear Instruments and Methods in Physics Research Section B: Beam Interactions with Materials and Atoms 392, 21-30, http://dx.doi.org/10.1016/j.nimb.2016.12.001.

Sharma, K., Bhatt, N., Shukla, A.D., Cheong, D.-K., Singhvi, A.K., 2017. Optical dating of late Quaternary carbonate sequences of Saurashtra, western India. Quaternary Research 87, 133-150, http://dx.doi.org/10.1017/qua.2016.12.

Shimada, A., Takada, M., Toyoda, S., 2016. Electron spin resonance signals of quartz in present-day river bed sediments and possible source rocks in the Kizu River basin, Western Japan. Geochronometria 43, 155-161, http://dx.doi.org/10.1515/geochr-2015-0039.

Vaccaro, G., Panzeri, L., Paleari, S., Martini, M., Fasoli, M., 2017. EPR investigation of the role of germanium centers in the production of the 110°C thermoluminescence peak in quartz. Quaternary Geochronology 39, 99-104, http://dx.doi.org/http://doi.org/10.1016/j.quageo.2017.02.005.

Basic research

Angeli, V., Polymeris, G.S., Sfampa, I.K., Tsirliganis, N.C., Kitis, G., 2017. Component resolved bleaching study in natural calcium fluoride using CW-OSL, LM-OSL and residual TL glow curves after bleaching. Applied Radiation and Isotopes 122, 89-95, http://dx.doi.org/http://doi.org/10.1016/j.apradiso.2017.01.014.

Brown, N.D., Rhodes, E.J., 2017. Thermoluminescence measurements of trap depth in alkali feldspars extracted from bedrock samples. Radiation Measurements 96, 53-61, http://dx.doi.org/10.1016/j.radmeas.2016.11.011.

Chen, R., Lawless, J.L., Pagonis, V., 2017. Thermoluminescence associated with two-electron traps. Radiation Measurements 99, 10-17, http://dx.doi.org/http://dx.doi.org/10.1016/j.radmeas.2017.03.002.

Combès, B., Philippe, A., 2017. Bayesian analysis of individual and systematic multiplicative errors for estimating ages with stratigraphic constraints in optically stimulated luminescence dating. Quaternary Geochronology 39, 24-34, http://dx.doi.org/http://doi.org/10.1016/j.quageo.2017.02.003.

Friedrich, J., Pagonis, V., Chen, R., Kreutzer, S., Schmidt, C., 2017. Quartz radiofluorescence: a modelling approach. Journal of Luminescence 186, 318-325, http://dx.doi.org/http://dx.doi.org/10.1016/j.jlumin.2017.02.039.

Frouin, M., Huot, S., Kreutzer, S., Lahaye, C., Lamothe, M., Philippe, A., Mercier, N., 2017. An improved radiofluorescence single-aliquot regenerative dose protocol for K-feldspars. Quaternary Geochronology 38, 13-24, http://dx.doi.org/10.1016/j.quageo.2016.11.004.

Hunter, P.G., Spooner, N.A., 2017. Investigation of the role of the production process on the luminescence of sea salt products. Geochronometria 44, 121-128, http://dx.doi.org/10.1515/geochr-2015-0055.

Kazakis, N.A., Tsetine, A.T., Kitis, G., Tsirliganis, N.C., 2017. A SAR protocol for heat-sensitive materials exhibiting sensitization (SARHS) for the estimation of the equivalent dose. Radiation Measurements 99, 1-9, http://dx.doi.org/http://dx.doi.org/10.1016/j.radmeas.2017.02.011.

Kitis, G., Pagonis, V., 2017. New expressions for half life, peak maximum temperature, activation energy and kinetic order of a thermoluminescence glow peak based on the Lambert W function. Radiation Measurements 97, 28-34, http://dx.doi.org/http://dx.doi.org/10.1016/j.radmeas.2016.12.013.

Kitis, G., Pagonis, V., Tzamarias, S.E., 2017. The influence of competition effects on the initial rise method during thermal stimulation of luminescence: A simulation study. Radiation Measurements 100, 27-36, http://dx.doi.org/10.1016/j.radmeas.2017.03.047.

Korovkin, M.V., Ananyeva, L.G., 2017. Effect of irradiation and thermal annealing on quartz materials luminescence. IOP Conference Series: Materials Science and Engineering 168, 012033.

Liu, J., Murray, A., Sohbati, R., Jain, M., 2016. The effect of test dose and first IR stimulation temperature on post-IR IRSL measurements of rock slices. Geochronometria 43, 179-187, http://dx.doi.org/10.1515/geochr-2015-0049.

Madcour, W.E., El-Kolaly, M.A., Afifi, S.Y., 2017. Thermoluminescence properties of local feldspar from Gattar mountain area. Arab Journal of Nuclear Science and Applications 50, 59-66.

Mercier, N., 2017. Vers une approche nouvelle de la dosimétrie : implications pour les méthodes de datation par luminescence et résonance paramagnétique électronique. L'Anthropologie 121, 9-18, http://dx.doi.org/10.1016/j.anthro.2017.03.005.

Muñoz-Salinas, E., Castillo, M., Arce, J.L., 2017. OSL signal resetting in young deposits determined with a pulsed photon-stimulated luminescence (PPSL) unit. Boreas 46, 325-337, http://dx.doi.org/10.1111/bor.12215.

Oniya, E.O., Polymeris, G.S., Jibiri, N.N., Tsirliganis, N.C., Babalola, I.A., Kitis, G., 2017. Pure thermal sensitisation and pre-dose effect of OSL in both unfired and annealed quartz samples. Nuclear Instruments and Methods in Physics Research Section B: Beam Interactions with Materials and Atoms 400, 1-10, http://dx.doi.org/http://doi.org/10.1016/j.nimb.2017.03.156.

Ortega, F., Santiago, M., Martinez, N., Marcazzó, J., Molina, P., Caselli, E., 2017. On the analysis of glow curves with the general order kinetics: Reliability of the computed trap parameters. Journal of Luminescence 184, 38-43, http://dx.doi.org/http://dx.doi.org/10.1016/j.jlumin.2016.11.034.

Polymeris, G.S., Pagonis, V., Kitis, G., 2017. Thermoluminescence glow curves in preheated feldspar samples: An interpretation based on random defect distributions. Radiation Measurements 97, 20-27, http://dx.doi.org/http://dx.doi.org/10.1016/j.radmeas.2016.12.012.

Şahiner, E., Meriç, N., Polymeris, G.S., 2017. Thermally assisted OSL application for equivalent dose estimation; comparison of multiple equivalent dose values as well as saturation levels determined by luminescence and ESR techniques for a sedimentary sample collected from a fault gouge. Nuclear Instruments and Methods in Physics Research Section B: Beam Interactions with Materials and Atoms 392, 21-30, http://dx.doi.org/10.1016/j.nimb.2016.12.001.

Sohbati, R., Murray, A., Lindvold, L., Buylaert, J.-P., Jain, M., 2017. Optimization of laboratory illumination in optical dating. Quaternary Geochronology 39, 105-111, http://dx.doi.org/http://doi.org/10.1016/j.quageo.2017.02.010.

Strebler, D., Burow, C., Brill, D., Brückner, H., 2017. Using R for TL dating. Quaternary Geochronology 37, 97-107, http://dx.doi.org/10.1016/j.quageo.2016.09.001.

Tang, S.-L., Li, S.-H., 2017. Low temperature thermochronology using thermoluminescence signals from K-feldspar. Geochronometria 44, 112-120, http://dx.doi.org/10.1515/geochr-2015-0057.

Trauerstein, M., Lowick, S.E., Preusser, F., Veit, H., 2017. Testing the suitability of dim sedimentary quartz from northern Switzerland for OSL burial dose estimation. Geochronometria 44, 66-76, http://dx.doi.org/10.1515/geochr-2015-0058.

Vaccaro, G., Panzeri, L., Paleari, S., Martini, M., Fasoli, M., 2017. EPR investigation of the role of germanium centers in the production of the 110°C thermoluminescence peak in quartz. Quaternary Geochronology 39, 99-104, http://dx.doi.org/http://doi.org/10.1016/j.quageo.2017.02.005.

Dose rate issues

Armitage, S.J., Pinder, R.C., 2017. Testing the applicability of optically stimulated luminescence dating to Ocean Drilling Program cores. Quaternary Geochronology 39, 124-130, http://dx.doi.org/http://doi.org/10.1016/j.quageo.2017.02.008.

Mercier, N., 2017. Vers une approche nouvelle de la dosimétrie : implications pour les méthodes de datation par luminescence et résonance paramagnétique électronique. L'Anthropologie 121, 9-18, http://dx.doi.org/10.1016/j.anthro.2017.03.005.

Meyer, M.C., Aldenderfer, M.S., Wang, Z., Hoffmann, D.L., Dahl, J.A., Degering, D., Haas, W.R., Schlütz, F., 2017. Permanent human occupation of the central Tibetan Plateau in the early Holocene. Science 355, 64-67, http://dx.doi.org/10.1126/science.aag0357.

Richard, M., Falguères, C., Pons-Branchu, E., Ghaleb, B., Valladas, H., Mercier, N., Richter, D., Bahain, J.-J., Conard, N.J., 2017. Datation par les méthodes ESR/U-Th combinées de sites du Pléistocène supérieur : méthodologie et application en contexte karstique. L'Anthropologie 121, 63-72, http://dx.doi.org/10.1016/j.anthro.2017.03.006.

Urbanová, P., Guibert, P., 2017. Methodological study on single grain OSL dating of mortars: Comparison of five reference archaeological sites. Geochronometria 44, 77-97, http://dx.doi.org/10.1515/geochr-2015-0050.

Dosimetry

Angeli, V., Polymeris, G.S., Sfampa, I.K., Tsirliganis, N.C., Kitis, G., 2017. Component resolved bleaching study in natural calcium fluoride using CW-OSL, LM-OSL and residual TL glow curves after bleaching. Applied Radiation and Isotopes 122, 89-95, http://dx.doi.org/http://doi.org/10.1016/j.apradiso.2017.01.014.

Kalita, J.M., Chithambo, M.L., 2017. On the sensitivity of thermally and optically stimulated luminescence of α-Al2O3:C and α-Al2O3:C,Mg. Radiation Measurements 99, 18-24, http://dx.doi.org/http://dx.doi.org/10.1016/j.radmeas.2017.03.006.

Nyirenda, A.N., Chithambo, M.L., 2017. The influence of radiation-induced defects on thermoluminescence and optically stimulated luminescence of α-Al2O3:C. Nuclear Instruments and Methods in Physics Research Section B: Beam Interactions with Materials and Atoms 397, 92-100, http://dx.doi.org/http://dx.doi.org/10.1016/j.nimb.2017.02.077.

Instruments

Hong, D.-G., Kim, M.-J., 2017. Development and Performance Testing of a Time-resolved OSL Measurement System. Journal of Radiation Protection and Research 42, 69-76, http://dx.doi.org/10.14407/jrpr.2017.42.1.69.

Portable system

Muñoz-Salinas, E., Castillo, M., Arce, J.L., 2017. OSL signal resetting in young deposits determined with a pulsed photon-stimulated luminescence (PPSL) unit. Boreas 46, 325-337, http://dx.doi.org/10.1111/bor.12215.

Review

Horowitz, Y.S., Eliyahu, I., Oster, L., 2016. Kinetic simulations of thermoluminescence dose response: long overdue confrontation with the effects of ionisation density. Radiation Protection Dosimetry 172, 524-540, http://dx.doi.org/10.1093/rpd/ncv495.

Le Pape, L., 2017. Application of EPR in Studies of Archaeological Samples, in: Webb, G.A. (Ed.), Modern Magnetic Resonance. Springer International Publishing, Cham, pp. 1-25.

Wintle, A.G., Adamiec, G., 2017. Optically stimulated luminescence signals from quartz: A review. Radiation Measurements 98, 10-33, http://dx.doi.org/http://dx.doi.org/10.1016/j.radmeas.2017.02.003.

LED CAPE TOWN 2017

RHODES UNIVERSITY
Where leaders learn

LED 2017
11-15 SEPT 2017
SOUTHERN SUN CAPE SUN HOTEL
23 STRAND STREET ,CT, 8000

CONFERENCE CHAIRMAN : **MAKAIKO CHITHAMBO** • COORDINATOR : **XOLELWA MBUYEPHI** • WEBSITE : **WWW.LED2017.COM**

15TH INTERNATIONAL CONFERENCE ON LUMINESCENCE AND ELECTRON SPIN RESONANCE DATING

WELCOME TO LED 2017 IN CAPE TOWN, SOUTH AFRICA

We are pleased to invite you to the 15th International Con-ference on Luminescence and Electron Spin Resonance Dating (LED2017) to be held in Cape Town, South Africa, in September 2017. The LED series of meetings are held every three years and provide a forum for discussion of new developments on stimulated luminescence and its applications with emphasis on retrospective dosimetry. The conference in Cape Town will be hosted by Rhodes University and will be the latest in a well-established series going back nearly 40 years with the last three held in Canada (2014), Poland (2011) and China (2008).

TOPICS

1. Basic Physical Processes and Materials' Characteristics
2. Instrumentation and procedures
3. Advances in equivalent dose determination
4. Advances in dose rate determination
5. Innovative dating approaches
6. Applications in Earth and Planetary Sciences
7. Applications in Archaeology
8. ESR: advances and applications

SCIENTIFIC ADVISORY COMMITTEE

Christina Ankjærgaard, Wageningen University, Netherlands
Andrzej Bluszcz, Politechnika Śląska, Poland
Makaiko Chithambo, Rhodes University, South Africa
Geoff Duller, Aberystwyth University, UK
Mauro Fasoli, Università di Milano-Bicocca, Italy
Rainer Grün, Griffith University, Australia
Bo Li, University of Wollongong, Australia
George Polymeris, Ankara University, Turkey
Frank Preusser, University of Freiburg, Germany
Mathieu Duval, Griffith University, Australia

LOCAL SUPPORT TEAM

Makaiko Chithambo, Rhodes University, South Africa, Chairman
Mutsa Chinyamakobvu, Rhodes University, South Africa
Angel Nyirenda, Rhodes University, South Africa
Schadrack Nsengiyumva, Rhodes University, South Africa
Sunil Thomas, Rhodes University, South Africa
Mary Evans, University of the Witwatersrand, South Africa
Ebenezer Oniya, Adekunle Ajasin University, Nigeria
Folorunso Ogundare, University of Ibadan, Nigeria

IMPORTANT DATES

ABSTRACT SUBMISSION DEADLINE
1 APRIL 2017

NOTIFICATION OF ACCEPTANCE
31 MAY 2017

EARLY REGISTRATION DEADLINE
30 JUNE 2017

WORKSHOP
10 SEPTEMBER 2017

CONFERENCE
11-15 SEPTEMBER 2017

POST CONFERENCE TRIP
15-17 SEPTEMBER 2017

PAYMENT DEADLINE FOR EARLY REGISTRATION
30 JUNE 2017

PAYMENT DEADLINE FOR LATE REGISTRATION
15 AUGUST 2017

MANUSCRIPT SUBMISSION DEADLINE
31 JANUARY 2018

CONFERENCE CHAIRMAN
Makaiko L. Chithambo

Department of Physics and Electronics
Rhodes University, PO BOX 94
Grahamstown 6140, South Africa
Tel: 046 603 8450
Fax: 046 622 5049
Email: m.chithambo@ru.ac.za

Ancient TL

ISSN 0735-1348

Aims and Scope

Ancient TL is a journal devoted to Luminescence dating, Electron Spin Resonance (ESR) dating, and related techniques. It aims to publish papers dealing with experimental and theoretical results in this field, with a minimum of delay between submission and publication. Ancient TL also publishes a current bibliography, thesis abstracts, letters, and miscellaneous information, e.g., announcements for meetings.

Frequency

Two issues per annum in June and December

Submission of articles to Ancient TL

Ancient TL has a reviewing system in which direct dialogue is encouraged between reviewers and authors. For instructions to authors and information on how to submit to Ancient TL, please visit the website at:
http://www.ecu.edu/cs-cas/physics/ancient-timeline/ancient-tl1.cfm

Journal Enquiries

For enquiries please contact the editor:
Regina DeWitt, Department of Physics, East Carolina University, Howell Science Complex, 1000 E. 5th Street, Greenville, NC 27858, USA; Tel: +252-328-4980; Fax: +252-328-0753 (dewittr@ecu.edu)

Subscriptions to Ancient TL

Ancient TL Vol. 32 No.2 December 2014 was the last issue to be published in print. Past and current issues are available for download free of charge from the Ancient TL website:
http://www.ecu.edu/cs-cas/physics/ancient-timeline/ancient-tl5.cfm